# DAMAGE TOLERANCE IN PRESSURIZED FUSELAGES
11th Plantema Memorial Lecture

T. Swift*

The fatigue and damage tolerance capability of pressurized fuselage structure is extremely sensitive to stress level, geometrical design, and material choice. Considerable improvements have been made in designing fuselage structure to sustain large, obviously detectable damage. The historical evolution of these improvements is discussed. Consideration is given to the difficulties and current concerns associated with in-service, noninspectable, multisite damage within a damage tolerance philosophy that depends upon inspection. Recommendations are given related to operating stress level, design detail, and material choice required for long service life and large damage capability of minimum-gauge pressurized structure.

## INTRODUCTION

Aircraft structural fatigue, a phenomenon that has been with us since a propeller shaft fatigue failure delayed the first flight of the Wright Brothers' airplane at Kitty Hawk (1), is still a problem today. This is not, I believe, because we as fatigue specialists in industry, research establishments, universities, regulatory authorities, and airlines are ignoring the problem. Indeed, when one considers the magnitude of literary effort describing research on the subject since the word fatigue was first coined by the French engineer Poncelet in 1839, it is difficult to believe we have not yet completely solved the problem.

In the Ninth Plantema Memorial Lecture, John Mann (2) provided an incredible history of fatigue failures and mentioned that in Europe, more than 150 years ago, a number of engineers recognized that fractures of some mechanical components were due to repeated loadings. In 1969, 136 years later, Professor Jaap Schijve stated in his introduction to the Second

* Douglas Aircraft Company, McDonnell Douglas Corporation,
Long Beach, California

Plantema Memorial Lecture, "Fatigue in aircraft structures is a problem for which quantitative and generally accepted solutions are not available as yet." I believe we have made considerable progress since 1969 with the introduction of damage tolerance principles in the regulatory requirements, but the overall problem is not yet solved. Even since the last ICAF meeting in 1985, lives have been lost as a consequence of fatigue failures in the air transportation system.

In the introduction to the Fourth Plantema Memorial Lecture, Professor Gassner (3) made a perceptive observation: "Increasing demands for economy and safety in highly utilized structures under random loading necessitate a fatigue life to failure only slightly in excess of service life. This presupposes reliable calculation and experimental procedures for both fatigue life prediction and fatigue life substantiation." There are two important aspects to this statement. The first is the balance between economics and safety. All of us who are experienced in air transportation are aware that unless we design for the highest structural efficiency the system will be uneconomical to operate. As distasteful as this may seem to the safety idealist, it is a fact of life that the system must be economically viable. On the other hand, although we recognize it is impossible to completely eliminate risk, we must do our utmost to keep it to an acceptably low level.

The second important point made by Professor Gassner was the necessity of providing a fatigue life only slightly in excess of service life in order to achieve a balance between economy and safety. The fact is that even though a fatigue life goal may be initially established for an aircraft type, the current economic environment is dictating that aircraft remain in service far beyond this initial life goal. This is illustrated in Table 1, which gives the initial life goals and current high time for some commercial transport aircraft. A number of these aircraft are currently flying well beyond their initial life goals. However, this is not being achieved with completely crack-free airplanes. Fatigue is a random variable. Even though service life goals are initially specified and the best analytical methods, backed by full-scale testing, are employed, fatigue cracking may still occur to some extent in a fleet of aircraft. Safety in these cases is being maintained by the diligent combined efforts of the manufacturers, regulatory authorities, and the operators through inspection programs that depend upon the degree of damage tolerance inherent in the structure in the case of the aging fleet and designed into the structure for future aircraft. Some of these inspections are part of the initial maintenance program, some are required by airworthiness directives, and others have been initiated through supplemental inspection programs.

As we strive to design efficient structures to meet the current and future economic needs of the air transportation system, a careful balance between durability and damage tolerance is needed for safety. This approach is not universally agreed upon. A school of thought exists which holds that durability is not a safety issue and is only required to preclude frequent nuisance repairs for economic reasons. This school of thought relies completely on damage tolerance for safety, which in turn relies on in-service inspection. However, it is possible for a number of small cracks, each not easily inspected, to suddenly join together and form a long critical crack. Sophisticated nondestructive inspection techniques exist to find this type of cracking, but they are not considered economically feasible in service. It is believed, therefore, that the structure should be designed and tested so that multiple-site cracking cannot occur within the projected life of the aircraft. In the opinion of this author, this is a durability issue and is therefore required for safety. If at the end of the initially projected lifetime it is judged that the aircraft service life should be extended, then a reassessment may be necessary in the case of multiple-site damage. Even though the aircraft may have been designed using fail-safe multiple-load-path principles, there is a possibility that fail-safety may be degraded with increased usage because of multiple-site cracking. Under these circumstances, it is believed the life may be extended only by careful reassessment of critical structural areas such as skin splices. In the case of multiple-site damage, this can only be successfully achieved by continued testing of a high-time aircraft or by destructive teardown inspection of a high-time aircraft in critical splice areas.

This author believes that the continued efforts of the entire fatigue and fracture community to develop analytical and test methodology have considerably increased the level of safety. However, it appears that inadvertent incidents have been responsible for the greatest loss of life in structurally related accidents in recent years. These include fatigue propagation following maintenance-induced damage, fatigue cracking induced earlier than anticipated because of corrosion, and early fatigue cracking caused by poor repairs. Thus, irrespective of how well we can predict fatigue life, be it only slightly more than design service life as stated by Professor Gassner, we must try to design into the structure as much inherent capability for sustaining easily detectable damage as is economically feasible since in-service inspection currently appears to be the weak link in a damage tolerance philosophy. This can be achieved by maintaining operating and limit stress levels at a reasonable level, careful consideration of structural geometry, and the use of the most damage-resistant materials.

This paper will utilize the transport aircraft pressurized fuselage as an example to illustrate how important stress level, material, and geometrical details are in designing for tolerance to large readily detectable damage. A number of pressurized fuselage design features will be considered starting with the Comet I design and progressing to current designs that incorporate considerable damage tolerance capability.

Apologies are expressed for renewed discussion of the Comet I accidents, but the subsequent investigations are a credit to the manufacturer and the authorities involved. Because of this investigation, in the opinion of this author, the fatigue and damage tolerance capability of the current commercial fleet has considerably improved over early pressurized aircraft. Evidence of this fact exists in that a number of fleets are currently operating at double their initially anticipated design life goals.

## EARLY EXPERIENCE WITH PRESSURIZED CABINS

On January 10, 1954, a Comet I aircraft (registration number G-ALYP) known as Yoke Peter (Figure 1) disintegrated in the air at approximately 30,000 feet and crashed into the Mediterranean Sea off the island of Elba. The aircraft was on a flight from Rome to London. At the time of the accident, the aircraft had flown 3,680 hours and had experienced 1,286 pressurized flights.

Design of the Comet commenced in September 1946. The first prototype flew on July 27, 1949. BOAC started proving flights in April 1951. Yoke Peter first flew on January 9, 1951, and was granted a certificate of registration on September 18, 1951. The aircraft was delivered to BOAC on March 2, 1952, after accumulating 339 flight hours (4). Yoke Peter was the first high-altitude jet-propelled passenger aircraft in the world to enter scheduled service. It was advancing the state of the art in a number of areas, not the least of which was that its cabin pressure was almost double that of any other pressurized transport aircraft in operation at the time.

After the Elba accident, the Comets were removed from service on January 11, 1954. A number of modifications were made to the fleet to rectify some of the items that may have caused the accident. Service was resumed on March 23, 1954. On April 8, 1954, only 16 days after resumption of service, another Comet aircraft, known as Yoke Yoke, disintegrated in the air at approximately 35,000 feet and crashed into the sea off Naples. This aircraft was on a flight from Rome to Cairo. At the time of the crash, the aircraft had flown 2,703 hours and had experienced 903 pressurized flights. The loss of the Comets created probably more discussion than any other accident in the air transportation system. Some of us may believe this to be old history by now, but from a pressurized fuselage design standpoint these accidents became a valuable learning experience, and the entire industry gained considerable benefit from the subsequent investigation. They pointed out to aircraft designers throughout the world a very strong message that attention to stress level, geometry, and material choice was of prime importance in the design of pressurized fuselages. It is a fact that we learn more from failures than successes, and it is believed worthwhile to keep repeating these historical events to ourselves. This fact became obvious after the F-111 failure in 1969, which started a virtual revolution in the development of fracture technology in the United States.

After the loss of Yoke Yoke, BOAC immediately suspended all services. On April 12, 1954, the chairman of the Air Registration Board withdrew the certificate of airworthiness. The minister of supply instructed Sir Arnold Hall, director of the Royal Aircraft Establishment (RAE), to complete an investigation into the cause of the accidents. On April 18, 1954, Sir Arnold decided that a repeated loading test of the pressure cabin was needed. It was decided to conduct the test in a tank under water to minimize damage in the event of failure. In early June 1954, the test started on Yoke Uncle, an aircraft removed from service. This particular aircraft had already accumulated 1,231 pressurized flights prior to the test. After 1,826 more test pressurizations, for a total of 3,057, a failure occurred in the pressure cabin. The cabin cyclic pressure was 8.25 psi, but a proof cycle of 1.33P was applied at approximately 1,000 pressure cycle intervals. It was during the application of one of these proof cycles that the failure in the cabin occurred. Examination of the failure provided evidence of fatigue. The failure origin on Yoke Uncle was at the aft lower corner of the forward escape hatch, as shown in Figure 2. Further investigation of Yoke Peter structure recovered from the sea near Elba confirmed that the primary cause of failure was pressure cabin rupture due to fatigue. The origin in this case was at the right-hand aft corner of the rear automatic direction finding (ADF) window on top of the aircraft, as shown in Figure 3.

Yoke Uncle was repaired and the fuselage skin was fitted with strain gages at a number of escape hatch and window cutout corners. At a cabin pressure of 8.25 psi with inertia loading representing 1.3 g, the stress distribution on the outside of the skin at the lower aft corner of the forward escape hatch was as shown in Figure 2 (5). The stress distribution at the left rear corner of the forward ADF window was as shown in Figure 3 for the same loading condition. The highest stresses were recorded at the upper forward corner of the right hand window between frames 24 and 25, as shown in Figure 4. The peak stress here was 45.7 ksi, which represented 70 percent of the ultimate strength capability of the DTD 546 skin material. The stresses illustrated by Figures 2, 3, and 4 were recorded on the outside of the skin and no attempt was made to measure internal stresses. The highest stresses were recorded at the angle $\theta$ shown in Figures 2, 3, and 4.

If one considers an element ABCD, inclined at angle $\theta$, the element would be curved as shown in Figures 2, 3, and 4 because of fuselage curvature. Even though the edge of the window or door may be internally supported by stiffening elements, it is a fact, based on this author's experience, that out-of-plane bending causes the inside principal stress to be between 1.26 and 2.03 times higher than the measured outside stress. This fact was discovered by full-scale testing in the early 1970s, as reported by Stone (6) during the Seventh ICAF Symposium. This out-of-plane bending is not normally considered in a coarse-grid, two-dimensional, finite-element analysis, but could very well explain why door jamb and window corners crack in service as frequently as they do. This is easily verified when one considers the number of door jamb patches that exist in commercial fleets of aircraft in current service. As previously mentioned, we have not solved the problems yet, but we learn on every full-scale test we conduct. It will be appreciated that the out-of-plane bending problem would not have been discovered without detailed investigation following cracking problems on a full-scale aircraft fatigue test specimen.

If one carefully reviews the stress distributions on the outside of the skin, as shown in Figures 2, 3, and 4, it becomes apparent that at the rivet holes they are not in themselves sufficiently high to have caused failure in 1,286 cycles in the case of Yoke Peter and 3,057 cycles in the case of Yoke Uncle. However, considering the out-of-plane bending described here, it becomes apparent that the stresses on the inside may easily be high enough to cause failure in that time. Take for example the failure of Yoke Peter at the aft ADF window right aft corner. If we assume the identical stress distribution as was measured at the forward ADF window left aft corner and use the factors of 1.26 and 2.03 previously described, we can plot a band of possible internal stress distributions in the corner of the window. This band is illustrated in Figure 5. Curve A represents measured stresses (5). Curves B and D are factored by 1.26 and 2.03, respectively. Curve C represents an average. Curve EF, to the left of Figure 5, represents an Sn curve obtained by testing specimens with nonfilled holes. These Sn data were also described by Stone (6). It is felt that open-hole Sn data are representative for 1/8-inch-diameter rivets, since rivets this small do not swell in the hole sufficiently to help the fatigue life. The spread in expected life is shown in Figure 5. If one considers the center of the first rivet in from the edge of the skin and doubler, the expected lives would be 100, 1,500, and 6,300 cycles for the maximum, mean, and minimum stresses, respectively. Since Yoke Peter failed in 1,286 cycles, it can be seen that the early failures may be attributable to high stresses caused by induced secondary bending effects due to shell curvature, which appears to have been unknown at the time of the Comet design as mentioned by Stone (6). This was also the case on testing a large pressurized shell in the early 1970s. As can be seen from the measured stress distribution, it is advantageous to keep the rivets as far away from the cutout edge as is practicable, thus reducing the gross stress at the first row of fasteners. Increasing the thickness of the doublers will, of course, reduce the stresses, but one needs to be extremely cautious here. In the testing described by Stone (6), one door jamb corner was increased in thickness by a factor of two, but the ratio of outside stress to inside stress increased from 1.58 to 2.03. This indicates that the stresses are not a linear function of skin and doubler thickness.

It is evident that both stress level and geometry played an important role in early fatigue cracking in the Comet fuselage. However, other factors related to Comet geometry are also worth mentioning.

The configuration of the basic Comet pressure shell was as shown in Figure 6a. There were no crack-stopper straps to provide continuity of the frame outer flange across the stringer cutout in the frame. The cutout, shown in Figure 6b, creates a very high stress concentration at the first fastener, A. In the case of Yoke Peter, evidence of fatigue was found at one of these fasteners in the vicinity of the right-hand rear corner of the rear ADF window at the attachment of frame 17 to the skin and doubler. This location, illustrated by Figures 3 and 6c, was thought to be the failure origin of Yoke Peter (7). The fastener at this location was a countersunk bolt, as shown in Figure 6c. The countersink had created a knife-edge condition in both the skin and outside doubler. Thus, the early fatigue failure was caused by high gross stresses combined with a local geometrical feature, creating high bearing stresses at a hole where the countersink was knife-edged. It is now well known that knife-edged holes in aluminum are undesirable from a fatigue standpoint. Once the fatigue crack was initiated, its propagation went undetected until fast fracture took place. Evidently the combination of high gross stress, material fracture toughness, and geometric design detail in the pressurized shell were such that crack arrest did not occur.

## Comet Residual Strength Capability

From a lessons-learned standpoint, it is advantageous to study the Comet pressurized shell general damage tolerance capability. The basic fuselage skin material was 0.028-inch-thick DTD 546 in minimum-gauge areas. Fracture toughness data for this material do not appear to be generally available. However, D. Williams (8) was instrumental in having a number of residual strength tests performed on a Comet I cabin to support a crack arresting theory he had described (9). One such test provided sufficient information to determine the plane stress fracture toughness for the DTD 546 material. The fuselage was fitted with aluminum straps 1.2 inches wide by 0.128 inch thick at 21-inch centers as shown in Figure 7. A saw cut 6.5 inches long was made in the 0.028-inch-thick skin with one end (A) just touching strap No. 1, as shown in Figure 7. Cyclic pressure was applied between 0 and 8.25 psi to propagate the crack. After 21 cycles, during which time crack tip B had propagated an additional 1.75 inches, fast fracture occurred and the crack was arrested at strap No. 2. The cracking configuration, illustrated in Figure 7, was analyzed using a displacement compatibility approach, similar to that outlined in Reference 10, to obtain the effects of stiffening on the crack tip stress intensity factor. The plane stress fracture toughness Kc obtained from this test was 93.95 ksi $\sqrt{\text{in.}}$ using Equation 1:

$$K_c = \sigma_h \sqrt{\pi a}\, \beta \beta_B \tag{1}$$

Where $\sigma_h$ is an average uniform hoop stress across the bay obtained from Equation 2. This equation, developed by Flugge (11), accounts for the circumferential and axial stiffening material.

$$\sigma_h = \frac{t_x PR + \nu\left(t_\phi - t\right) PR/2}{\left(1-\nu^2\right) t_\phi t_x + \nu^2 t\left(t_\phi + t_x - t\right)} \tag{2}$$

Where $t_x = t + A_L/S$
$t_\phi = t + A_F/L$
$t$ = skin thickness
$A_L$ = longeron area
$A_F$ = frame area
$S$ = longeron spacing
$L$ = frame spacing
$P$ = internal cabin pressure
$R$ = shell radius
$\nu$ = Poisson's ratio

The term $\beta$, obtained from the displacement compatibility analysis, is shown plotted in Figure 7b and accounts for the stiffening effect of the riveted strap taking rivet flexibility into consideration. The term $\beta_B$ accounts for bulging at the crack tip due to pressure and shell radius. An expression for the term $\beta_B$, developed in Appendix 1 based on the test result by Williams (8), is given by Equation 3:

$$\beta_B = 1 + 5(L/2) / R\left[\frac{1}{2}(1 + \mathrm{Cos}\ 2\pi x/L) + F/2(1 - \mathrm{Cos}\ 2\pi x/L)\right] \quad (3)$$

Where L = distance between stiffeners
R = shell radius
F = proportion of bulging at the stiffeners compared to full bulging between stiffeners
x = distance from center of bay to crack tip

Observations during residual strength tests on curved panels have led this author to conclude that when a crack tip is halfway between frames spaced about 20 inches apart, the crack tip bulging will be unaffected by stiffeners. However, as the crack tip approaches the stiffener the bulging is reduced (12). Where stiffening includes a substantial frame member reinforced by a crack stopper strap, the bulging is completely damped out. For a lighter stiffener, however, this bulging may not be completely damped out at the stiffener. In the case of a strap alone, as in the Williams tests, it appears that bulging was not completely damped out at the strap. This information can be obtained from the crack lengths at fast fracture and arrest assuming the displacement compatibility analysis is properly accounting for load transfer into the stiffening elements. An expression was developed by Kuhn (13) for the effects of bulging in unstiffened pressurized shells. This author has found that Kuhn's expression correlates with stiffened panel tests when the crack tip is midway between frames. The resulting bulge equation, assuming full bulge midway between frames damping out to some proportion of full bulge F at the stiffener, may be expressed as Equation 3.

The term F in Equation 3 was determined to be 0.4266 for the Williams test configuration. Other parameters are given in Figure 7a. A residual strength diagram for the Williams test is shown in Figure 7c.

Using the information gained from the Williams test, combined with a displacement compatibility analysis for the Comet I type frame/skin combination, it is possible to investigate a number of skin cracking configurations. The proportion of crack tip bulging at the frame was assumed to be the same as obtained from the Williams test. Figure 8 illustrates the result for a one-bay crack midway between frames where the crack is running toward the notch in the frame. The average hoop stress determined by Equation 2 at a cabin pressure of 8.25 psi was 14.42 ksi. Curve ABC represents the residual strength from a skin fracture viewpoint. The stress level corresponding to point B provides the allowable residual strength, assuming the frame remains intact. However, as the skin crack approaches the frame, the load transferred into the frame causes considerable frame bending because the frame neutral axis is offset from the skin line given by C. Assuming about 2 inches of skin material is effective as frame bending material, the allowable from a frame strength standpoint is given by curve DE. However, as the crack tip approaches this effective frame bending material, a considerable reduction in frame bending capability occurs coupled with a large increase in moment arm C as the frame neutral axis moves farther away from the skin line. This results in a drastic reduction in the allowable gross strength, from a frame bending standpoint, shown by curve FGH. Thus, as the crack tip passes through the effective skin region, depicted by the shaded area in Figure 8, the residual strength from a frame strength standpoint experiences a rapid reduction as illustrated by curve JKGH. The residual strength is therefore represented by point K, where failure would be precipitated by frame failure. Therefore, a full one-bay crack cannot be tolerated.

Assuming a skin crack started at a frame midway between the notches and propagated in a straight line into two adjacent bays with the center frame intact, the residual strength diagram would be as shown in Figure 9. At the average hoop stress of 14.42 ksi, fast fracture would be expected at A and the crack would be arrested at B. The allowable gross average stress would be given at the intersection of the center frame strength allowable curve and the skin fracture curve depicted by the point C. For this case, the capability to sustain large damage appears feasible.

If a skin crack started at the first attachment near the notch, in a location similar to the suspected failure origin of Yoke Peter (Figure 6c), and propagated into two adjacent bays, the residual strength diagram would be similar to that shown in Figure 10. From a frame bending standpoint, it can be seen that the allowable gross strength at the notch is low compared to the allowable from a skin fracture standpoint. In this case, the cracked skin is ineffective in providing frame bending material, which results in reduced bending inertia and increased moment arm C. On failure of the center frame, the configuration will be converted to that illustrated in Figure 11 for a two-bay crack with a broken frame where the crack is propagating toward the notch in the frame. In this case, fast fracture will occur at point A on the skin fracture curve, and the crack will not be arrested. Even if the frame remains intact, the residual strength from a skin fracture standpoint (point B on the skin fracture curve) is below the applied stress, so the crack will not be arrested. The outer frame strength allowable, assuming the skin is effective as frame bending material, is shown by curve CD. However, as in the case of the one-bay crack, as the crack tip approaches this effective material and continues past the frame, the allowable from a frame strength standpoint is reduced to curve FE.

Finally, for the case of a two-bay crack with the center frame broken but with the crack heading midway between the notches, the residual strength is illustrated in Figure 12. It can be seen that fast fracture will occur at A and the crack will be arrested at B.

The residual strength curves for several cracking configurations for structure similar to Comet I minimum-gauge construction are illustrated in Figures 8 through 12 and can be summarized as follows. If the crack is propagating along a line midway between frame notches, the combination of skin fracture toughness, gross stress level, and frame geometry provides adequate residual strength for both one- and two-bay crack configurations. However, the most likely cracking configuration is with a crack adjacent to the notch because of the high stress concentration caused by the notch. Neither one- or two-bay cracks can be tolerated when the crack path is along a line passing through the notches. From a large detectable damage viewpoint, the notch in the frame appears to be the weak link in this design concept. This notch, which allows the longitudinal stringer to pass through the frame, was typical of early unpressurized fuselage designs. For example, the DC-2 and DC-3 typical fuselage construction is as shown in Figure 13.

## EARLY DOUGLAS PRESSURIZED AIRCRAFT

The first Douglas pressurized transport aircraft was the DC-6, which received its type certificate on 23 June 1947. This was followed by the DC-6A and B on 11 April 1951, the DC-7 on 12 November 1953, the DC-7B on 25 May 1955, and the DC-7C on 15 May 1956. Cabin pressure for these aircraft was much lower than the Comet. For example, DC-6 and DC-6B low-altitude aircraft operated with 8,000-foot cabins at 20,000 feet. For these aircraft, the maximum nominal differential pressure was 4.16 psi. In the case of the higher altitude DC-6B and DC-7 aircraft, the cabin and aircraft altitudes were 8,000 and 25,000 feet respectively. In this case, the maximum nominal differential pressure was 5.46 psi.

A number of interesting incidents related to cabin residual strength occurred on these early pressurized aircraft, which are worth mentioning here. On 22 August 1950, a propeller blade from the No. 3 engine failed on a DC-6 aircraft flying at 21,000 feet from Los Angeles to Chicago. The cabin differential pressure was 4.16 psi. The blade struck the fuselage edgewise and left the other side flatwise. The resulting damage was a hole about 250 square feet in size (Figure 14a). A safe emergency landing was made in Denver. A similar incident occurred on 5 March 1957, when an entire propeller assembly left No. 1 engine of a DC-7 flying at 14,000 feet from New York to San Francisco. The propeller assembly "sawed' its way through the cabin. All three blades made separate, long cuts at distinct, longitudinally spaced intervals. The final damage amounted to an opening of about 80 square feet (Figure 14b). The cabin differential pressure at the time of the incident was 5.1 psi. This aircraft made an uneventful landing in Memphis, Tennessee. A propeller failure of this type had occurred on the ground with the cabin unpressurized. In this case, the extent of longitudinal damage was confined to a narrow sawcut-like slot in the lower fuselage (Figure 15a). Thus, it can be appreciated that cabin pressure, causing hoop tension in the skin, is the primary damage driver.

In the DC-6/DC-7 minimum-gauge construction (Figure 15b), frame members were not shear-clipped to the skin between stringers. Transfer of pressure-induced radial loading from the skin to the frame was via a flexible load path through the frame-to-longeron attachments. However, these frames were effective in reducing hoop tension in the skin and, at the low pressures experienced in the DC-6 and DC-7 series aircraft, were effective in arresting longitudinal cracking.

A number of interesting facts arise when one compares the Comet losses to the two propeller blade incidents just described. The minimum gauge of the Comet's DTD 546 skin was 0.028 inch, with a shell radius of 61.5 inches and a nominal cabin operating pressure of 8.25 psi The fracture toughness of this material was 93.95 ksi $\sqrt{\text{in.}}$ obtained from the previously described tests by Williams. The minimum gauge of the DC-6/DC-7 skin (7075-T6) was 0.025 inch, with a shell radius of 62.5 inches and a nominal cabin operating pressure of 4.16 and 5.46 psi for the DC-6 and DC-7, respectively. The fracture toughness for this material was about 60 ksi $\sqrt{\text{in.}}$. A comparison of the residual strength capability may be approximately obtained by neglecting the effects of frames and considering the effective critical damage index, l, for the unstiffened shells; i.e.,

$$l = 2/\pi[K_c t/(PR)]^2 \qquad (4)$$

Where $K_c$ = plane stress fracture toughness
$t$ = skin thickness
$P$ = nominal cabin pressure
$R$ = shell radius

The resulting figures are 8.557, 10.595, and 6.15 for the Comet, DC-6, and DC-7 respectively. It can be seen that both aircraft series are in the same general area since the DC-6 and DC-7 numbers are on both sides of the Comet value. However, in 1955 the 0.025-inch skins were replaced with 0.032-inch skins for the DC-6B high-altitude aircraft (25,000 feet) after fuselage No. 644 and after fuselage No. 651 for DC-7 aircraft. This increased the effective critical damage index from 6.15 to 10.08. Of course, it should be remembered that these numbers are not intended to indicate true critical crack lengths. They are only useful for comparative purposes. This, therefore, does not explain the outcome of Comet versus the propeller blade incidents. However, using the method described in Reference 14, the destructive energy release of compressed air during the failure process in the case of the Comet is approximately 2.64 times higher than that for the propeller incident for the DC-6 and 1.58 times higher for the DC-7 because of higher differential pressure caused by a difference in altitude at the time of the incident; e.g., 30,000 feet for Comet Yoke Peter near Elba, 35,000 feet for Comet Yoke Yoke near Naples, 21,000 feet for the DC-6 near Denver, and 14,000 feet for the DC-7 near Memphis. These facts could explain the difference in outcome.

## FIRST DOUGLAS HIGH-ALTITUDE AIRCRAFT

The first Douglas high-altitude jet transport aircraft was the DC-8. Development started a little after the Comet accidents at a time when cabin designers were expressing concern about high-altitude pressure. The DC-8 entered service in May 1959 with an original design service goal of 50,000 hours and 25,000 landings. As mentioned earlier, we learn more from failures than successes, and the aircraft industry as a whole gained considerable benefit from the Comet investigation. Indeed the DC-8 development program in particular gained much from this experience. It pointed out that considerable attention to detail design was needed to provide long life together with improved residual strength capability in pressurized cabins designed for high-altitude flight.

The DC-8 development test program included many longitudinal and transverse splice fatigue specimens. These tests were followed by more than 30 development tests of large curved components and by a full-scale forward fuselage fatigue test to verify the structural integrity of the design from a pressurization standpoint. The component development tests included two different test philosophies and involved testing large (6 by 10 feet) full-scale curved stiffened panels. The first series of tests was known as water cycle tests based on the concept illustrated in Figure 16. Both fatigue and crack propagation tests were performed in this water cycle fixture. The second series of tests was conducted using an air tank. This concept consisted of a steel tank made in two sections connected by a 10-foot-long aluminum section representing the fuselage structure. The short end of the steel tank was free to move axially to ensure the same axial pressure load that would exist in the fuselage. An opening at the top of the simulated fuselage structure was used for mounting the 6- by 10-foot development test panels. The total volume of the tank was 8,870 cubic feet, which closely approximated the 10,000-cubic-foot occupied volume of the DC-8. The overall concept was to perform fatigue tests in the water cycle fixture to develop and propagate fatigue cracks and then transfer the panels to the air tank fixture for residual strength testing. The air tank fixture is illustrated in Figure 17. A view of the inside of the tank, showing loosely attached safety bolts, is presented in Figure 18. A circular saw arrangement was sometimes used on the air tank panels to extend the skin damage. A typical panel from this series of tests is shown in Figure 19. The panels were intended to cover various areas of the aircraft, as shown in Figure 20.

The objective of these tests, from a residual strength standpoint, was to demonstrate the ability to safely sustain a full one-bay crack between adjacent frames without explosive decompression. The number of pressure cycles applied to these panels ranged from 92,500 for early development tests to over 1 million pressure cycles for later verification testing. Nominal cabin pressure for the DC-8 aircraft was 8.77 psi. Cyclic tests were performed conservatively in most cases with a maximum pressure of 15.4 psi and a minimum pressure of 3.1 psi to account for the effects of skin shear stresses. This series of tests established the minimum-gauge configuration for the DC-8 fuselage, as shown in Figure 21. Skin material was 0.05-inch-thick 2014-T6 aluminum alloy. Frames at 20-inch centers were 7075-T6 with 6-4 titanium crack stopper straps 0.025 inch thick. For skin panel thicknesses greater than 0.05 and less than 0.071 inch, 2014-T6 material was used. However, the titanium crack stopper proved to be unnecessary for the damage size considered with these skin thicknesses. For skin thicknesses greater than 0.071 inch, 7075-T6 was used.

The minimum-gauge design concept was further verified by a full-scale forward fuselage fatigue test equivalent to 140,000 pressurized flights, which was conducted in a water tank (Figure 22). The specimen is shown in the water tank in Figure 23. Maximum cabin pressure used for the test was 9.3 psi (nominal cabin pressure was 8.77 psi). Inertial bending in the fuselage was simulated by loading the cargo and passenger floors and nose gear. The test was completed with no fatigue cracking in the minimum-gauge section.

Following fatigue testing, the residual strength of the shell was substantiated by wedge penetration to simulate foreign object damage. This type of damage may be expected from turbine disintegration. Tests were performed at six locations on the fuselage (Figure 24). The fuselage was pressurized to 9.27 psi to simulate internal cabin pressure and aerosuction. Inertial loading was applied to the passenger and cargo floors and the nose gear to simulate a fail-safe condition. A nitrogen pressure gun with a 15-inch-wide steel blade was used to penetrate the shell and various stiffening elements. Figures 25 and 26 show the results of test No. 5, where the damage included a completely severed frame and crack stopper, longeron, and two bays of skin. Figure 26 shows how the 0.05-inch-thick skin crack turned at 90 degrees. This cracking configuration, known as "flapping," resulted in controlled decompression, which sometimes occurs from longitudinal cracks in thin sheet structures.

## DC-9 SERIES AIRCRAFT FUSELAGE MINIMUM-GAUGE DEVELOPMENT

The development of the DC-9 fuselage minimum-gauge structure gained considerably from all the testing previously performed on the DC-8. The original design service life goal for the DC-9 was 30,000 hours and 40,000 landings. To justify these goals, a substantial component fatigue test program was conducted. The program included tests of large curved development panels in a water cycle machine similar to the one shown in Figure 16. Panels included minimum-gauge construction and window belt areas. Skin splices were included in these panels. In order to accommodate the effects of skin shear combined with pressure at the splices, the cyclic pressure was increased to 9.6 psi compared to the nominal cabin pressure of 7.46 psi. This created an extremely conservative test for many other areas of the panels, including skin bending at the skin-to-frame shear clip connection and at the concentration caused by the cutout in the shear clip to allow continuity of the axial stiffeners. Over 300,000 cycles were applied to many of these panels. Natural fatigue cracks and sawcuts in the skin were propagated to obtain crack growth rates. These tests were followed by residual strength tests to verify the damage tolerance capability of the minimum-gauge construction. This construction is illustrated in Figure 27. At the nominal cabin pressure of 7.46 psi, the PR/t hoop skin stress is 9,820 psi. Average hoop stress across the bay between frames is 7,980 psi based on Equation 2. This stress, which is low compared to other aircraft in the commercial fleet, gives the DC-9 the potential for an extremely long life. As with the DC-8, the objective during DC-9 development was to demonstrate the aircraft's ability to safely sustain a full one-bay skin crack between adjacent frames without explosive decompression. Much greater capability than this, however, was demonstrated by the development test program.

The minimum-gauge construction of the DC-9 fuselage was further verified by a forward fuselage test almost identical to that described for the DC-8. A total of 120,600 simulated flights were applied, including inertial loading of the passenger and cargo floors and the nose gear. Cabin pressure was 8.06 psi to include the effects of aerosuction.

## EARLY FRACTURE MECHANICS DEVELOPMENT

Analytical development in fracture mechanics technology was initiated at Douglas on the Supersonic Transport program in the early 1960s. This methodology included a crack arresting program based on the redundant force analysis of stiffened panels. The development, based on work by Christensen and Denke (15), was summarized at the ICAF Symposium in Rome in 1963 (16). The concept included the following residual strength equation:

$$\sigma_R = \sigma_{tu} / \left[ R_{ct}\sqrt{1 + l_c\left(1/R_\sigma{}^2 - 1\right)} \right] \tag{5}$$

Where $\sigma_{tu}$ = ultimate strength of skin material
$l$ = critical crack length defined as 0.975L
$L$ = frame spacing
$R_\sigma$ = notch resistance factor
$R_{ct}$ = the ratio of crack tip stress in the unstiffened panel to that in the stiffened panel at a given crack length

The notch resistance factor was determined by residual strength testing and was approximately 0.58 and 0.52 for 2014-T6 and 7075-T6 sheet material, respectively. The term $R_{ct}$ was determined by a finite-element analysis known as the lumped-parameter analysis. A typical idealization is shown in Figure 28a. It can be seen that the stiffening element is represented by a single idealized bar, which picks up axial load as the crack propagates. The crack is simulated by disconnecting reactions one at a time. The term $R_{ct}$, resulting from this analysis, is a function of the thickness of the shear panel $t_{csp}$, established to simulate the flexibility of the fastening system and the area of the stiffener. A typical residual strength diagram, based on a critical crack length equal to 97.5 percent of the frame spacing, is shown parametrically in Figure 28b.

## DC-10 FUSELAGE MINIMUM-GAUGE DEVELOPMENT

DC-10 development started in early 1967. The design service life goal was 60,000 hours and 42,000 landings. It was recognized early that considerable attention to detail geometry, material choice, and operating stress level would be required in the fuselage to meet these goals, particularly since radial load due to pressure was more than three times that of the DC-6 and 1.58 times higher than the DC-8. With this in mind, an early fuselage fatigue development test program was initiated. Some of these tests are illustrated in Figure 29.

Considerable attention was paid to those design details that appeared many times throughout the structure. Typical examples are longitudinal and circumferential splices, longeron-to-frame joints, and the frame-to-skin shear clip cutouts previously described. Each of the cutout details occurs approximately 15,000 times in the DC-10 fuselage. For this reason, considerable effort was made to ensure that problems due to fatigue would not occur at these details.

At the longeron-to-frame connection, a radial load is applied from the skin to the frame outer flange. This load is caused by radial displacement of the skin due to cabin pressure reacted by frames that resist this radial growth. The resulting load causes local bending in the longeron. This local bending is intensified by overall longeron bending due to pressure reacted at the frame. In addition to stresses caused by these two effects, a further stress $\sigma_x$ is applied by axial pressure loads and fuselage bending. At one period during the development phase, consideration was given to removing the frame-to-skin shear clips at the crown of the fuselage since skin shear transfer to the frame is low. During testing of large curved panels under axial loads and pressure, the longeron-to-frame connection load was measured by a pair of small load cells, as shown in Figure 30. Measurements were taken with the shear clip both intact and removed. A considerable increase in load is indicated when the shear clip is removed. This load is also affected by axial stress $\sigma_x$. Load is reduced with increasing axial stress because of Poisson's ratio effects caused by skin biaxial stresses. Curved panel fatigue testing indicated that a considerable improvement in fatigue life could be gained by the addition of a small reinforcement washer to distribute this radial load and thereby reduce local bending stresses in the longeron flange. As a result of these tests, it was also decided to include the shear clips even in areas of low shear transfer. However, the longeron-to-frame connection is a fatigue sensitive area. Should fatigue cracking cause failure of a longeron, the skin will be overloaded locally. Eventually, fatigue cracking may occur in the skin above the broken longeron. In this case, the skin crack would propagate into both adjacent bays, as indicated in Figure 31a. Thus, for circumferential skin cracks it appeared feasible to assume that a two-bay skin crack with a broken central longeron might occur. Therefore, a design goal was established to be able to sustain limit load with a broken stiffener and a two-bay circumferential skin crack.

Early development testing indicated that skin stresses in the vicinity of the shear clip cutout were higher than gross applied stresses. As mentioned earlier, this cutout creates a high stress concentration factor in the skin. Hoop stresses due to cabin pressure are generally lower at the frame, but in some locations skin stresses are increased by frame bending. It is reasonable to assume, therefore, that if a skin crack occurred at the first fastener in the shear clip (Figure 31b), the crack could possibly propagate into both adjacent skin bays. For this reason, a goal was established to sustain a full two-bay longitudinal skin crack. Thus, the design goal for DC-10 fuselage skin damage tolerance capability was as shown in Figure 32. This goal is compared to the design goals to meet FAR 25, which were used for earlier aircraft. The damage tolerance design goals for all these aircraft were exceeded, as indicated by Figures 25 and 26 for the DC-8, for example.

Further Analytical Development

It was recognized that improvements in fracture mechanics analytical capability were needed to parametrically evaluate a number of candidate structural configurations and materials. As mentioned earlier, some capability already existed, and methods to determine residual strength in the presence of skin cracks in stiffened structures had been developed, as indicated by Equation 5. However, the finite-element analysis described in Figure 28a had not included the ability to simulate the combined effectivity of the frame/crack stopper combination. Early testing on stiffened flat panels had indicated considerable frame bending in the presence of longitudinal skin cracks (Figure 33a). In addition, the stresses in the frame/crack stopper combination could not be estimated using simple beam theory. That is, the crack stopper frame combination did not follow MC/I distributions. The main reason for this was the differences in flexibility of the load path between the skin and crack stopper and the crack stopper and frame. In the case of the circumferential crack, tests of curved stiffened panels under axial loads and pressure had indicated considerable bending in the crack arresting stiffeners as shown by Figure 33b. At this point it was decided to improve the finite-element analysis capability to account for these additional effects. The resulting idealization is illustrated in Figures 34 and 35 for the circumferential and longitudinal crack cases, respectively.

Consider the idealization for the circumferential crack illustrated by Figure 34. The panel was divided into a number of bars and shear panels. The bars carried axial load only and the shear panels carried only shear loads. Loads were applied at the top of the panel, and load reactions at the bottom were disconnected one at a time to simulate the propagating crack. The crack tip stress was defined by the stress in the last bar adjacent to the simulated crack, as shown in Figure 34. The stiffening elements were represented by additional lumped bars connected to the main panel by a series of shear panels. The stiffness of these shear panels was chosen to simulate the stiffness of the fastening system between skin and stiffening elements. Both stiffened and unstiffened panels were analyzed, and the effect of stiffening was obtained by taking the ratio between crack tip stresses in the unstiffened and stiffened panels. In the early days of the DC-10 development, this ratio was expressed as $R_{ct}$ and used in Equation 5 to obtain residual strength. This analytical method is adequately explained in References 17 and 18. However, as development progressed, the concept of crack tip stress intensity factor was gaining popularity. Residual strength from a skin fracture standpoint was being expressed as:

$$\sigma_R = K_c / \left(\beta\sqrt{\pi a}\right) \qquad (6)$$

Where $K_c$ = plane stress fracture toughness

$$\beta = \frac{\text{crack tip stress in stiffened panel}}{\text{crack tip stress in unstiffened panel}}$$

The term $\beta$ is the reciprocal of $R_{ct}$, the term used in earlier literature. The stiffened-panel analysis also gave stiffener stresses as a function of crack length.

## Candidate Materials for DC-10 Minimum Gauge

A number of candidate alloys were considered for fuselage skin material. The high-strength alloy 7075-T6 had been used for the DC-6 and DC-7. This alloy had also been used on the DC-8 where increased thicknesses were required to react skin shear loads. These increased thicknesses resulted in low PR/t stresses in areas where 7075-T6 was used. The DC-8 and DC-9 minimum-gauge material was 2014-T6, which had higher fracture toughness than 7075-T6. Because of its successful use on the DC-8 and DC-9, it became a candidate for DC-10. In the late 1960s, 7075-T73 had been developed primarily as a stress-corrosion-resistant alloy. This alloy has found extensive use in forgings to offset many stress corrosion failures experienced in the

7079-T6 alloy previously used. However, 7075-T73 provided considerably higher fracture toughness than 7075-T6 or 2014-T6. For this reason it became a candidate in sheet form for minimum-gauge material in the DC-10. Another serious contender was, of course, the old faithful 2024-T3, which had been used on the DC-3.

These candidate alloys were initially evaluated by residual strength analysis using the lumped-parameter finite-element approach. Cracking scenarios considered included the two-bay circumferential skin crack with a broken central longeron. All four candidate alloys and a number of stiffener configurations and areas were considered. The plane stress fracture toughness for these candidate alloys was assumed to be 158 ksi $\sqrt{\text{in.}}$ for 2024-T3, 90 ksi $\sqrt{\text{in.}}$ for 7075-T73, 70 ksi $\sqrt{\text{in.}}$ for 2014-T6, and 63.5 ksi $\sqrt{\text{in.}}$ for 7075-T6. Figure 36 shows the results of this analysis for two sizes of "hat" section longerons. A limit gross stress level of 34 ksi had been established as a goal from previous experience. This stress included the effects of internal cabin pressure and fuselage bending. The goal was to meet the extent of damage established at 34 ksi but not to pay a weight penalty. The residual strength diagrams shown in Figure 36 reflect skin fracture criteria as well as stiffener strength criteria. The stiffener material used was 7075-T6 extrusion. The residual strength for the two-bay crack condition was established at the intersection of the skin fracture curve and the stiffener strength curve curve for cases C and D of Figure 36a. However, for cases A and B of Figure 36a and cases A, B, and C of Figure 36b, the residual strength is limited by skin fracture criteria at the peaks of the curves, as indicated. It can be seen for both longeron sizes that the goal of 34 ksi could only be achieved with 2024-T3 material.

Two candidate stiffening configurations as well as the four candidate skin materials were used to evaluate longitudinal cracks. There was considerable discussion as to whether or not the separate titanium crack stopper straps, previously used on the DC-8, were really essential. The minimum frame size had already been established from a fuselage general instability requirement. Finite-element analysis using the lumped-parameter method produced the skin fracture residual strength curves shown in Figure 37. The effects of bulging due to curvature and pressure, $\beta_{B,}$ are depicted by the dotted lines in the figure. An equation similar to Equation 3 was used to calculate $\beta_{B.}$ However, bulging was assumed to be completely damped out by the substantial frame section. This assumption was verified later by curved panel testing. The bulge equation used here is given by Equation 3 in Reference 12. A 20-ksi design limit principal stress had been established as a goal for the longitudinal crack case based on the maximum hoop tension stress midway between frames at nominal cabin pressure plus aerodynamic suction together with a limit shear stress. The hoop tension midway between frames is 82 percent of the PR/t stress. This stress level is conservative on two counts. First, the average stress across the bay is much lower than the maximum between frames. Second, the effects of shear in the presence of longitudinal cracking is not transferred to the frames. It can be seen in Figure 37a, for the configuration that included a titanium crack stopper strap, that the peak of the residual strength curve for the two-bay crack case is higher than the design stress for 2024-T3, 7075-T73, and 2014-T6. However, when the crack stopper is not used, only 2024-T3 is adequate. Based on these results, 2014-T6 and 7075-T6 were removed as candidates in the subsequent test program.

## Development Test Program for Large Damage Simulation

A development test program was initiated to validate analytical methodology and to study a number of geometrical combinations for large damage tolerance capability. Figure 38a shows one of a series of uniaxially loaded stiffened flat panels, 120 inches wide by 75 inches deep, used for evaluating longitudinal cracks. Configurations for this series included frames with and without crack stoppers made from the two remaining candidate alloys, 2024-T3 and 7075-T73. Figure 38b shows two of a series of 60-inch-wide, uniaxially loaded stiffened panels used to simulate large circumferential skin and axial stiffener damage. Figure 38c shows one of a series of large curved stiffened panels tested under pressure and axial load to simulate both longitudinal and circumferential damage. These panels were used to evaluate crack tip bulging caused by pressure and curvature. A number of configurations were included. Each panel contained typical longitudinal and circumferential skin splices and longeron splices. These panels were tested in a unique vacuum machine designed in such a way that internal inspection could be performed while cyclic pressure and axial loads were applied. This was achieved by lowering a vacuum chamber, fitted with a pressurized seal, onto the panel. The chamber was evacuated causing atmospheric pressure applied from the underside. Axial loads were applied by hydraulic jacks at the ends of the panels. Prior to performing residual strength tests, the equivalent of at least three lifetimes of fatigue loading was applied to these panels. The objective here was to include the possible effects of multisite fatigue damage ahead of the simulated primary cracks. More than 383,000 pressure cycles, representing at least nine lifetimes, were applied to one panel. Each of the three panel types illustrated by Figure 38, were tested to failure. Figures 39a and 39b show typical examples of flat panels tested to failure to evaluate longitudinal and circumferential damage. Figure 39c shows a typical curved panel after failure from a longitudinal crack.

Other curved panels containing circumferential cracks were also loaded to failure.

Longitudinal Crack Results

The benefits of the titanium crack stopper straps can be seen by comparing the test results of two flat panels made from 7075-T73 skin and 7075-T6 frames. Figure 40a shows the results for a panel with no crack stoppers. In this case, a 3-inch sawcut was made in the skin over a frame near the shear clip cutout. Cyclic load was applied to propagate the crack to a predetermined length, and then static load was applied up to a gross stress of 17.0 ksi. This was repeated several times. Eventually, fast fracture occurred at a half-crack length of 17.5 inches, and the crack was arrested at a half-crack length of 19.63 inches. Cyclic load was again applied to further propagate the crack. Static load was then applied incrementally. The panel failed at a gross stress of 18.1 ksi with a half-crack length of 20.97 inches. Analysis based on the lumped-parameter finite-element approach and a plane stress fracture toughness of 92.76 ksi $\sqrt{\text{in.}}$ (determined from fast fracture) produced the residual strength curve shown in Figure 40a. The diagram shows that skin fracture and center frame strength criteria are about the same and are below the design stress goal of 20.0 ksi. As can be seen, very good correlation was obtained with the finite-element analysis.

A second panel, with titanium crack stopper straps located at the frames, was tested. In this case, a 4-inch-long sawcut was made in the skin over a crack stopper strap. Constant-amplitude cyclic loading was applied to give a gross stress of 15.0 ksi with $R = 0.05$. After 13,125 cycles, a small crack initiated in the center crack stopper strap under the skin crack. The strap was almost completely failed at 27,991 cycles. The primary objective of this test was to determine the effectiveness of the outer crack stopper straps in reducing the crack tip stress intensity factor when the skin crack was about 40 inches long. It can be seen from Figure 40a that, with identical frame sections, the strength of the panel would be limited by center frame strength. The center frame was therefore reinforced by adding a short angle to the outer cap. Static load was applied at various crack lengths, and fast fracture eventually occurred at 20.14 ksi with a half-crack length of 10.285 inches. The crack was arrested at both adjacent frames. Cycling was continued to extend the crack, and the panel was then loaded statically in increments to failure. The gross stress at failure was 25.12 ksi with a half-crack length of 20.06 inches. As before, lumped-parameter finite-element analysis resulted in the residual strength diagram shown by Figure 40b. The panel strength in this case was limited by outer crack stopper strength, as indicated. This was validated by removing a section of the crack stopper for tension testing. This test indicated that the use of a crack stopper strap was of considerable benefit. In fact, the peak of the skin fracture curve was increased from about 18.5 ksi for the panel without crack stopper straps to about 30 ksi for the panel with crack stoppers. This is illustrated by comparing points A and B of Figures 40a and 40b, respectively. The finite-element analysis in this case correlated exactly with the test since the point at which crack arrest occurred and the gross strength based on outer crack stopper strength were predicted exactly. The results of the test on the panel with crack stopper straps indicated that 7075-T73 skin would provide adequate skin fracture toughness for the longitudinal crack case. The strength with a two-bay crack was well over the 20-ksi goal and, in fact, the panel strength was limited by stiffener strength, which is unaffected by skin material fracture toughness.

The importance of geometric detail is illustrated in Figure 41, which shows the results of a test on one of the flat panels just described. A sawcut was made in the skin over a frame without crack stoppers and propagated to a predetermined length, when static load was applied incrementally. Fast fracture of the crack occurred at a gross stress of 19.124 ksi. The crack was arrested at adjacent frames as shown in Figure 41a. During fast fracture, the shear clip failed (as shown in Figures 41a and 41b) because of extremely high frame bending moment M and direct load P caused by transfer of the load from the cracked sheet. However, the main frame member remained intact, as shown by Figure 41c. Had the frame design been similar to Figure 41d, center frame failure would have precipitated complete failure of the panel. The frame design described in Figures 41b and 41c is therefore considered far superior to that shown in Figure 41d.

A number of residual strength tests were performed on curved panels using the vacuum test machine illustrated in Figure 38d. The results of some of this testing are illustrated in Figure 42. In each case, cyclic pressure and axial loading were applied for a minimum of two lifetimes prior to residual strength testing. One panel was fatigue-tested to more than nine lifetimes prior to residual strength testing. The objective here was to account for the possible effects of small multisite damage that might have been present ahead of the primary crack tips. As in the case of flat panels, after fatigue cycling, sawcuts were made in the skin near the shear clip cutout and propagated under cyclic loading to predetermined lengths. The area of the cutout was the most critical from a residual strength standpoint. Residual strength tests for the longitudinal crack were performed under simulated cabin pressure loads only, since axial tension stress increases residual strength when applied to a curved panel under pressure (see Figure 42 of Reference 17). Results of the more significant tests are shown in Figure 42 of this paper. The most significant result from a design goal standpoint was obtained during test No. 4. A simulated cabin pressure of 14.59 psi was applied to a panel containing a 34.98-inch-long skin crack with both the center frame and crack stopper failed. The maximum hoop tension stress at midbay for this pressure is approximately 20 ksi. Note that the design goal of 20 ksi was based on 82 percent of PR/t stress at 9.1 psi combined with limit shear stress for a 40-inch-long crack with only the center crack stopper failed. It can easily be seen from the plots of $K/(\sigma \sqrt{\pi a})$ in Figure 42 that a 35-inch-long skin crack with both center crack stopper and frame failed (represented by point B) is more than twice as critical as a 40-inch-long skin crack with the center frame intact (represented by point A). Thus, the design goal was far exceeded by this test.

The conclusions resulting from finite-element analysis, supported by both flat panel and curved panel testing, were as follows:

1. The use of titanium crack stoppers would considerably increase the residual strength from a skin fracture standpoint.

2. The use of 2024-T3 skin would exceed the design goals by a considerable margin from a fracture toughness standpoint.

3. The residual strength capability would be limited by stiffener strength criteria.

The final conclusion is illustrated in Figure 43, which shows the residual strength limited by center frame strength at point C. This is followed closely by the outer crack stopper failure criterion at point B. The residual strength from a skin fracture standpoint is shown by point A. It must be remembered that the average gross hoop stress across the bay due to cabin pressure is much lower than the 20-ksi goal. For the panels illustrated in Figures 42 and 43, this average stress, given by Equation 2, is 1181.8P where P is the pressure differential. For a nominal cabin pressure of 8.6 psi, this average stress is 10.163 ksi, which, as can be seen by the curve in Figure 43, provides ample margin even for the stiffener strength criterion. However, there are locations in the pressure cabin where frame bending occurs because of the transfer of payload into the shell. These effects must be added during the stress analysis for the fail-safe conditions. It is evident from a longitudinal crack standpoint that the use of 2024-T3 skin will provide a fracture toughness well in excess of the requirements. In fact, for this specific case, some degradation in skin fracture toughness can be tolerated since stiffening element strength is critical.

Circumferential Crack Results

A number of panels were tested to demonstrate the residual strength for the two-bay circumferential crack with a broken central longeron (Figure 32). The results of these tests are also included in Reference 18. The test setup is shown in Figure 38b. Prior to residual strength testing on panels, one longeron was completely sawed through, and a crack starter slot with sharpened ends was cut in the skin directly over the longeron cut. The skin cracks were propagated to predetermined lengths under constant amplitude stress levels to determine the effects of stiffening on crack growth rates. Higher loads were then applied statically in increments to simulate fail-safe loads. The primary purpose of these tests was to determine if these cracks tended to cause a fast fracture in the skin, and, if such a tendency existed, if the longerons were adequate as natural crack stoppers. In most cases, two tests were performed on each panel. The results of these tests for the two remaining candidate skin alloys, 2024-T3 and 7075-T73, are shown in Figure 44. Test configurations included both "hat" and "tee" section longerons. It can be seen that the goal of 34-ksi gross stress from cabin pressure and fuselage bending can only be achieved with 2024-T3 skin material. With this material, the goal was achieved with considerable margin. As indicated in Figure 44, three of the panels were not tested to failure after exceeding the 34-ksi goal. It was decided to extend the damage for these panels to three bays of skin with two broken longerons. These results are shown on the right side of Figure 44.

In the case of the circumferential crack with a broken central longeron, the margin for skin fracture toughness over stiffener strength is not as apparent as for the longitudinal crack case. Figure 45, which shows the results of analysis and testing for a 2024-T3 panel containing a two-bay skin crack with a broken central longeron, illustrates this point. The results of this test and analysis are complicated and are described in more detail in Reference 19. The 60-inch-wide test panel was made from 0.071-inch-thick 2024-T3 sheet, stiffened by extruded "hat" section longerons at 8-inch spacing, each with a gross area of 0.5471 square inch. A sawcut was made in the central longeron and adjacent skin and propagated under cyclic loading to obtain crack growth rate data. At an average half-crack length of 7.57 inches, static load was applied in increments to verify the capability of the panel in the presence of a two-bay crack with a broken central longeron.

Slow stable growth of the skin crack occurred, as shown in Figure 45. As can be seen, this growth extended beyond the intact stiffeners. Failure of the panel occurred at a gross stress of 39.7 ksi with an average half-crack length of 9.88 inches. Failure of the panel was precipitated when the skin-to-outer-stiffener rivets failed over the entire length of the panel. Elastic analysis of this panel failure, using a displacement compatibility approach as described in Reference 10, is illustrated in Figure 45. Skin plane stress fracture toughness used was 197.87 ksi $\sqrt{\text{in.}}$ obtained from fast fracture of a similar panel. Three failure criteria, illustrated by dotted lines, are described in Figure 45. These include skin fracture, stiffener strength, and first rivet failure criteria represented by points A, B, and C, respectively. Gross failure stresses represented by these three points were 53.6, 32.5, and 11.5 ksi, as shown in the Figure 45 table. Elastic analysis therefore illustrated that the first rivets adjacent to the crack in the intact crack arresting stiffeners should have failed when a gross stress of 11.5 ksi was applied to the panel. Failure, however, occurred at 39.7 ksi. The elastic analysis predicted that skin fracture strength was far in excess of both stiffener strength and first rivet strength. This elastic analysis, however, was completely inadequate in predicting failure stress at a panel gross stress as high as that applied. In fact, the first rivet yielded, reducing the effectivity of the intact stiffeners. This in turn increased crack tip stress intensity factor and reduced allowable gross stress from a skin fracture standpoint.

The computer program that provided the elastic analysis was modified, as described in Reference 10, to include the nonlinear deformation characteristics of the rivets based on the model shown in Figure 45. This model was developed from test data for specimens tested back-to-back as shown to cancel out bending effects. An elastic solution was generated based on the initial slope of the fastener displacement curve. Each resulting fastener load was compared to the trielastic model shown in Figure 45. The flexibility matrix of the rivet system was then regenerated based on the appropriate slope of this model. A new solution was obtained representative of the rivet flexibilities by the model. The crack tip stress intensity factor obtained from the first solution was compared to that obtained from the second solution. This procedure was repeated until the difference in stress intensity factors between the current and previous solutions had damped out to a low number. The resulting analysis is briefly described by the solid line curves on Figure 45. Skin fracture, stiffener strength, and first rivet failure criteria, at a half-crack length of 9.88 inches, is described by points A′, B′, and C′, respectively. The gross stress levels represented by these points, listed in the Figure 45 table, are 41.25, 44.9, and 39.5 ksi, respectively. It can be seen that the panel gross stress at failure, precipitated by first rivet failure, is within 0.5 percent of the actual failure stress. The skin fracture criterion is the second most important and is only 1.75 ksi higher than the rivet criterion, which suggests that, if the skin fracture toughness had been a little lower than 197.87 ksi $\sqrt{in.}$, the panel failure would have been precipitated by skin fracture rather than rivet failure.

The failure process, described in more detail in Reference 19, is as follows: Gross stress is applied to the panel and the skin crack extends stably following the R curve illustrated in Figure 45. At a gross stress of 39.7 ksi (39.5 ksi predicted by analysis) the first rivet adjacent to the crack fails after exceeding the failure displacement described by the model in Figure 45. As this rivet yields, the skin fracture strength of the panel is reduced from a gross stress of 53.6 ksi down to 41.25 ksi, described by points A and A′, respectively. At the same time, the strength of the panel from a stiffener strength criterion increases from 32.5 to 44.9 ksi, described by points B and B′, respectively. At 39.7 ksi, the first rivet fails and causes point A′, the skin fracture residual strength, to fall below the gross stress applied. At this point, fast fracture occurs, causing the crack to extend rapidly, which in turn overloads the second fastener and causes it to fail. As the crack rapidly extends, the rivets "unzip" all the way along the crack arresting stiffeners.

In the case of the circumferential crack, it can be seen that, although the strength of the panel is dictated by rivet strength, the skin fracture toughness criterion is almost of equal importance, and any reduction in fracture toughness will cause a reduction in panel strength. This fact weighed very heavily on the choice of 2024-T3 material for the DC-10 fuselage skin material.

## Minimum-Gauge Configuration for the DC-10

The final structural configuration for minimum-gauge areas of the fuselage is as shown in Figure 46. This configuration is very similar to the DC-8 configuration described in Figure 21. However, the use of 2024-T3 skin and frames with larger cross-sectional areas allowed a higher PR/t stress. At a nominal cabin pressure of 8.6 psi, the PR/t stress is 14,987 psi. The average stress across the bay, based on Equation 2, is 10,904 psi. It should be noted that the titanium crack stopper straps completely encircle the cabin so that protection exists against cracks initiating anywhere in a longitudinal direction.

## Material Developments

The minimum-gauge material for the DC-10 aircraft (Figure 46) is 2024-T3 sheet. This was also the material used for the DC-3 more than 50 years ago. A number of attempts have been made to consider new aluminum alloys for reduced weight. As mentioned earlier, 7075-T73 was considered as a candidate for the DC-10 and, while it might have been adequate for the longitudinal crack case, it could not meet the damage tolerance design goals established for circumferential damage. All aluminum alloys have about the same density. Therefore, weight savings can only be achieved by increasing stresses. Unless a higher strength alloy can be found with a fracture toughness approaching that of 2024-T3, difficulty will be experienced in meeting the established design goals for the aircraft.

In the early 1970s, after development of the DC-10 had been completed, a new attractive alloy, 7475, looked promising from a weight savings standpoint. This alloy was being proposed in two heat-treatment conditions, 7475-T61 and 7475-T761, with room temperature fracture toughness values of 136 ksi $\sqrt{\text{in.}}$ and 155 ksi $\sqrt{\text{in.}}$, respectively, for the LT direction. These values were obtained from tests of 48-inch-wide panels. Ultimate tension strengths were 72 ksi for the T61 condition and 68 ksi for the T761 condition with high-strength clad, compared to 62 ksi for 2024-T3. Therefore, it appeared that some weight savings might have been achievable by slightly increasing stress levels to satisfy static strength requirements providing the circumferential crack goals, established for the basic airplane, could still be realized. During the course of this development, however, it became evident that the fracture toughness of the 7475 material was reduced between 20 and 30 percent at a temperature of —65°F, the operating skin temperature of the fuselage, whereas the fracture toughness of 2024-T3 remained stable down to this temperature. This reduction in fracture toughness is discussed by Abelkis et al (20). From a skin fracture toughness standpoint, the circumferential crack condition is the most critical in areas of the fuselage shell subjected to high axial stresses produced by inertial bending and cabin pressure. The 2024-T3 material provided ample margin for the longitudinal crack case where residual strength was limited by stiffening element strength. For the circumferential crack case, however, skin fracture toughness played a more important role. A study was therefore conducted to establish residual strength for the circumferential crack case for a number of typical skin thickness/longeron area combinations. Both 7475-T61 and 7475-T761 were considered for the skin using fracture toughness values of 96.35 and 113 ksi $\sqrt{\text{in.}}$, respectively, obtained from 48-inch-wide panels tested at —65°F. The combinations considered were as follows:

| Longeron Area | Skin Thickness | Longeron Material |
|---|---|---|
| 0.214 | 0.063 | 7075-T6 Sheet |
| 0.024 | 0.071 | 7075-T6 Sheet |
| 0.312 | 0.071 | 7075-T6 Extrusion |
| 0.540 | 0.071 | 7075-T6 Extrusion |
| 0.312 | 0.080 | 7075-T6 Extrusion |

Longeron spacing was assumed to be 8 inches.

The finite-element analysis method described in Figure 34 was used to obtain crack tip stress intensity factor and stiffener bending stresses as a function of crack length for the two-bay circumferential crack condition with a broken central longeron. This analysis was based on a uniform stress applied to both skin and longeron. However, because of skin biaxial loading effects, the skin stress was higher in the pressurized shell than the longeron stress. This effect was accounted for as follows. Equation 2 from Reference 11 provides average hoop tension stress in the skin in the presence of biaxial loading. The same reference gives equations for axial skin and longeron stress as a function of gross axial loading due to both fuselage inertial loading and cabin pressure.

Skin axial stress:

$$\sigma_S = \frac{t_\phi N_x + \nu(t_x - t)\, N_\phi}{\left(1-\nu^2\right) t_\phi t_x + \nu^2 t\left(t_\phi + t_x - t\right)} \tag{7}$$

Longeron stress:

$$\sigma_L = \frac{\left[\left(1-\nu^2\right) t_\phi + \nu^2 t\right] N_x - \nu t N_\phi}{\left(1-\nu^2\right) t_\phi t_x + \nu^2 t\left(t_\phi + t_x - t\right)} \tag{8}$$

With longeron spacing assumed to be 8 inches, gross stress is given as follows:

$$\sigma_g = 8N_x/\left(8t + A_L\right)$$

Equation 7 can now be rearranged in terms of $\sigma_g$:

$$\sigma_g = 8/\left[t_\phi\left(8t + A_L\right)\right]\left[\sigma_S\left\{\left(1-\nu^2\right)t_\phi t_x + \nu^2 t\left(t_\phi + t_x - t\right)\right\} - \nu\left(t_x - t\right)N_\phi\right] \tag{9}$$

$N_x$ = axial load pounds/inch
$N_\phi$ = radial load PR pounds/inch

Other terms are the same as for Equation 2. The residual strength from a skin fracture viewpoint in terms of gross stress accounting for distribution of skin/longeron stress due to biaxial effects can now be determined by substituting Equation 6 for $\sigma_S$ in Equation 9. The values of $\beta$ are obtained from the finite-element analysis for each crack length and longeron/skin combination.

The correction for longeron stress due to biaxial effects can be accomplished as follows:

Let the increase in longeron stress due to the skin crack = $\Delta\sigma_{LC}$ psi/psi of gross skin stress $\sigma_S$. Then the total longeron stress $\sigma_{LT}$ with skin crack is as follows:

$$\sigma_{LT} = \sigma_L + \sigma_S\left(\Delta\sigma_{LC}\right) \tag{10}$$

where $\sigma_S$ is given by Equation 7 and $\sigma_L$ is given by Equation 8. The term $\Delta\sigma_{LC} = \sigma_{LC} - 1$ where, $\sigma_{LC}$ is the longeron stress concentration factor, which is a function of crack length obtained from the finite-element analysis for unit gross stress.

Substituting 7 and 8 into 10 gives:

$$\sigma_{LT} = \frac{\left[(1-\nu^2)t_\phi + \nu^2 t\right]N_x - \nu t N_\phi + \left[t_\phi N_x + \nu(t_x - t)N_\phi\right]\Delta\sigma_{LC}}{(1-\nu^2)\,t_\phi t_x + \nu^2 t(t_\phi + t_x - t)} \tag{11}$$

Values of $t_x$ and $t_\phi$ for the various combinations of skin and longeron with an average circumferential frame plus crack stopper area of 0.6077 square inch can be substituted into Equation 11. The allowable value of gross axial loading, $N_x$, can be obtained as a function of crack length by substituting the ultimate tension strength of the longeron material for $\sigma_{LT}$ in Equation 11 and rearranging in terms of $N_x$. These ultimate strength values were 74 ksi for the 7075-T6 rolled "hat" longerons and 82 ksi for the extruded "hat" longerons.

The results of this analysis are summarized in Figure 47. The curve on the left shows one example for a 0.071-inch-thick 7475-T761 panel stiffened by 7075-T6 extruded longerons, each with an area of 0.312 square inch. The allowable for a two-bay crack with a broken central longeron is given by the intersection of the outer intact stiffener strength curve and the skin fracture curve represented by point A. A skin fast fracture lower than 27.75 ksi will be arrested. A skin fast fracture at a stress higher than 27.75 ksi will cause failure precipitated by outer intact stiffener failure. Allowables for other configurations are shown by the table in Figure 47. The curve in Figure 47 is plotted as a function of gross area stress. The actual skin stress, higher because of biaxial hoop stress at a cabin pressure of 9.1 psi, is shown by the dotted line.

Figure 48 illustrates the relationship of allowable gross area stress to actual applied stress at the crown of the fuselage. Applied stresses will be higher than allowable stresses from point A to B using 7475-T761 material and from point C to D using 7475-T61 material. The applied stresses are based on 2024-T3 material. Using 7475 to save weight in the forward fuselage will, of course, increase applied stresses. It may be possible to save a little weight in the forward fuselage, although much of this is already considered to be minimum gauge. On the whole, little advantage is gained using 7475 material, mainly because of the attendant increase in stress to save weight.

Perhaps the most encouraging development in recent years, as far as potential replacement for pressure cabin skins is concerned, is the renewed interest in aluminum-lithium alloys. Unlike all previous aluminum alloy developments, where increases in stress level were required to save weight, a 10-percent weight decrease can be achieved while maintaining current operating stress levels. Aluminum-lithium was first used in the late 1950s on the Navy's RA-5C Vigilante aircraft. The lower density and higher modulus of the alloy were accompanied by reduced ductility and fracture toughness. These facts combined with manufacturing difficulties caused use of the alloy to be discontinued. In recent years, a number of aluminum companies have been conducting research into alloy chemistry and processing for aluminum-lithium. Two such alloys, Lital C (being developed by Alcan in the United Kingdom) and 2091-CP 274 (developed by Pechiney in France), appear to be very promising replacements for 2024-T3. Some plane stress fracture toughness testing has been accomplished on these alloys, but unfortunately the tests have been conducted on very narrow panels (400 mm) probably because of the limited widths available in the early phases of development. Until test data on wider panels become available, it is difficult to decide whether require fracture toughness values, suitable for pressurized fuselage damage tolerance evaluation, are being achieved.

The effect of panel width on critical stress intensity factor is illustrated for 2024-T3 in Figure 49a. These data are obtained from References 21 and 22 for the TL direction. It can be seen that panel widths greater than 48 inches are required to obtain valid plane stress fracture toughness values unlimited by net section yielding. As mentioned earlier, the most critical condition for the pressure cabin is the circumferential crack case shown in Figure 32. In this case, the load/crack orientation is LT. Figure 49b shows critical stress intensity factor plotted as a function of test panel width for 2024-T3 with load/crack orientation LT. Aluminum-lithium test data obtained from 400-mm-wide panels are plotted on this curve. The Lital C and 2091-CP 274 T8x data were obtained from References 23 and 24, respectively. Although these data were obtained from narrow panels, it can be seen that the results are very encouraging compared to 2024-T3. However, wide panel test data at both room temperature and −65°F are needed to be sure that the trend compares to the 2024-T3 curve of Figure 49b. An item worth mentioning is that the point in Figure 49b at 60 inches wide was obtained from fast fracture of a stiffened panel, where yielding in the uncracked ligament may have been delayed by the 7075-T6 stiffening (19).

## MULTIPLE-SITE DAMAGE

The advantage of designing pressurized cabins to sustain extremely large damage is obvious from an inspection standpoint. This design goal can be achieved by maintaining reasonable stress levels, choosing materials with high fracture toughness, and providing geometric detail design consistent with good crack arresting capability. This philosophy should adequately protect the safety of the aircraft for single-site inadvertent damage either accidentally induced in service or during initial manufacture where fatigue cracking may initiate at one location and propagate into a lead crack within the projected life of the aircraft. However, this philosophy alone may be inadequate from the viewpoint of multiple-site damage (MSD), a condition where small cracks may initiate at both sides of each hole in a row of fasteners and become critical because of net section yielding between fasteners before detection in service. The probability that this condition will lead to failure prior to discovery appears to be remote because of variations in stress level and manufacturing quality. It may be argued, from a probabalistic standpoint, that cracking will always occur in one place and grow to a detectable size before MSD joins into a long critical crack. However, MSD has occurred with catastrophic results and therefore cannot be ignored in the opinion of this author.

The difficulties associated with MSD are briefly illustrated in Figure 50. Figure 50a shows residual strength as a function of multicrack size, a, and rivet spacing for 2024-T3-clad sheet, where strength in the presence of cracking is limited to yield strength between adjacent crack tips. Critical crack sizes at limit load are very small for this condition. Figure 50b illustrates that, in order to establish a reasonable inspection frequency, it is necessary to find extremely small cracks. These cracks very possibly may be buried under the rivet heads. Although nondestructive inspection (NDI) techniques are available to detect damage of this type, it appears economically unfeasible, in service, to completely rely on this approach for the vast expanse of basic structure existing in wide-bodied aircraft. However, some changes can be made in detail design to improve this situation. Figure 50c shows the difficulty that would exist in establishing inspections for MSD in simple lap splices at critical row B. This would normally require inspection from the inside, which is always difficult in the commercial aircraft maintenance environment since interior linings must be removed. Inspection of row A, which is equally critical, would be much easier from the outside. Figure 50d shows a typical DC-10 longitudinal butt splice in the fuselage. This splice was designed so that if fatigue cracking occurred in the splice it would always be in the skin at the end of the fingers and therefore would be detectable externally. More than 100 development tests of the type shown in Figure 29 were conducted for each of the longitudinal and circumferential configurations to perfect this design concept. Finger doubler geometric configurations, thicknesses, and fastener patterns, were varied to achieve the desired results. At the most sensitive rivet row in the finger doubler, the rivet spacing is twice as great as through the external splice plate area. The advantages of this are illustrated in Figure 50a, which shows that critical crack size is increased by a factor of 2.5 at an average hoop stress of 11,000 psi when fastener spacing is doubled from 0.8 to 1.6 inches.

Although improvements can be made in design philosophy, as described above, it must be ensured that MSD will never occur during the operational life of the aircraft. In the opinion of this author, this is only possible for the pressure cabin by full-scale fatigue testing of large representative sections of the cabin for a minimum of two service lifetimes. For completely circular fuselages, perhaps this could be accomplished by testing curved biaxially loaded panels such as those illustrated in Figure 38. For out-of-round fuselages, however, the calculation of accurate skin stresses is extremely difficult. Figure 51 describes some of the effects that are not reliably simulated by simple uniaxially loaded specimens. It appears that the only reliable way to ensure that multisite damage will not occur within the service life of an aircraft is to test for this condition to at least two lives and to perform teardown inspection of critical splices. In the absence of this testing on aircraft that are exceeding their test life in service, the only alternative may be to perform teardown inspection of high-time aircraft.

Effect of MSD on Critical Crack Size

In the absence of at least two lifetimes of testing, it would appear that MSD may affect the critical crack sizes. Figure 52a shows an infinitely wide unstiffened panel whose critical crack size would normally be predicted by Equation 6 with $\beta = 1.0$. If, however, the crack were propagating along a row of holes, where MSD existed in the holes ahead of the lead crack tip as shown in Figure 52b, then the residual strength should be affected. As mentioned earlier, the residual strength in the presence of multisite damage in 2024-T3 is limited by net section yielding in the ligament between the crack tips, as indicated in Figure 52a. It would appear from this that instability of the lead crack, shown in Figure 52b, would occur when the ligament stress between the lead crack tip and the small crack in the hole ahead of the lead crack reached the material yield strength. Referring to Figure 52c, the stress $\sigma_y$ at a distance, r, ahead of the lead crack is normally expressed as:

$$\sigma_y = K/\sqrt{2\pi r} = \sigma\sqrt{\pi a} \,/\, \sqrt{2\pi r} \tag{12}$$

If the crack were propagating along a row of holes, the net stress between holes would simply be p/(p-d). In the presence of the holes, as shown in Figure 52c, it would appear that the stress at a distance, r, ahead of the lead crack would be:

$$\sigma_y = \sigma\sqrt{\pi a} \,/\, \sqrt{2\pi r} - \sigma + \sigma P/(P-d) \tag{13}$$

Let $\sigma_y = \sigma_{yld}$, the yield strength of the material. Now, assuming the plastic zone R extends to the boundary of the hole ahead of the lead crack tip (i.e., r = p-d), Equation 13 can now be rearranged in terms of half-crack length, a, as follows:

$$a = \left\{\sqrt{2(P-d)} \,/\, \sigma\left[\sigma_{yld} - \sigma d/(P-d)\right]\right\}^2 \tag{14}$$

This of course is not a rigorous solution and is only included here to convey an idea. It does not, for example, account for the concentration provided by the hole. However, it does indicate that the critical crack size may be much smaller than when calculated using Equation 6, for example. The upper curve of Figure 52e shows the residual strength for a 2024-T3 infinitely wide panel, obtained from Equation 6 with $\beta = 1.0$, where the crack tips are in parent material not influenced by holes. Plane stress fracture toughness, $K_c$, in the TL direction was obtained from Equation 13 with material yield strength equal to 42 ksi. The hole diameter and spacing were assumed to be 0.19 and 1.0 inch, respectively. The resulting crack size was such that the ligament between the lead crack tip and the adjacent hole were completely yielded (not accounting for concentration effects from the hole). It would appear, then, that if a small crack existed in the hole, then the lead crack tip would extend into the hole and continue if a crack existed on the opposite side of the hole. It can be seen that a three-to-one difference exists in critical crack size under these circumstances.

## Controlled Decompression by Flapping

A phenomenon exists in thin cylindrical pressurized shells containing longitudinal cracks that may prevent complete failure of the shell. This phenomenon, which causes longitudinal cracks to turn in a circumferential direction, may ensure pressure relief before catastrophic failure.

Any element in a cylindrical shell subjected to internal pressure is normally in equilibrium under hoop tension stress $\sigma_{hoop}$, given by $PR_s/t$, as shown in Figure 53. However, in the presence of a longitudinal crack of length 2a, any element along the crack edge has lost one component of $\sigma_{hoop}$, as illustrated. Since equilibrium of the element must be maintained, the shell bulges with radius $R_b$, and the element is placed in equilibrium along the crack edge by a stress approximately equal to $PR_{b/t}$ and in a direction parallel to the crack. When the crack is short, the radius $R_b$ is smaller than $R_s$, and thus $\sigma_{hoop}$ is larger than $\sigma_{bulge}$. Under these conditions, the crack will propagate in a longitudinal direction. However, as the crack length increases, $R_b$ becomes larger than $R_s$ and $\sigma_{bulge}$ exceeds $\sigma_{hoop}$. In this case, the crack changes direction normal to $\sigma_{bulge}$. The crack length at the change of direction is a function of shell radius and becomes very long for shells of a radius similar to wide-bodied jet aircraft. This phenomenon is illustrated in Figure 54, which shows a 24-inch-diameter unstiffened cylinder after pressure relief due to "flapping." A 4-inch-long fatigue crack was generated by cyclic pressure loading starting with a longitudinal sawcut. Pressure was then increased until fast fracture occurred. The crack path turned as illustrated. This is an ideal situation since pressure is relieved and the damage may not be catastrophic. This test program on 24-inch-diameter cylinders was described in more detail by Swift (18). In the case of stiffened curved shells, such as typical fuselage structure, a longitudinal crack can be made to change direction at shorter lengths than would normally be expected in unstiffened shells of similar radius. This is particularly true of shells stiffened by circumferential crack stopper straps. The reason for this is the reduced hoop stress locally near the crack stopper straps (Figure 55). Thus, in the presence of a longitudinal skin crack, $\sigma_{bulge}$ may be higher than

$\sigma_{hoop}$ at a frame location because of a reduction of $\sigma_{hoop}$ caused by the frame and crack stopper. Under these circumstances, the weakest failure path would be OA as shown in Figure 55. Figure 56a illustrates this phenomenon on a curved stiffened panel made from 0.063-inch-thick 2024-T3 sheet. Figure 56b shows the failure in more detail normal to the longitudinal crack. Figure 26 also shows this type of cracking after penetration of a DC-8 forward fuselage fatigue test specimen by a harpoon blade. In that case the material was 0.05-inch-thick 2014-T6. This type of failure is very desirable from an inspection standpoint. There would be no necessity to inspect in detail since the damage, illustrated by Figures 26 and 56a, would relieve pressure and would be immediately obvious prior to catastrophic failure.

Dependence on flapping to eliminate the need for detailed inspection should be treated with caution. For example, in shells of a radius similar to wide-bodied jet transports, flapping within two bays will not occur when skin gauges are thicker than 0.063 inch. In these cases the longitudinal crack will tend to follow the axis of the shell. Flapping may not always be depended upon for a number of other reasons related to stress level, material, and geometrical configuration. In cases where the fuselage is not circular, frame bending due to pressure may cause the skin stress locally near the frame to be higher than midway between the frames, as illustrated by Figure 57. Under these circumstances, $\sigma_{bulge}$ is less likely to be higher than $\sigma_{hoop}$, especially in cases of high hoop stress. When this situation exists, the crack is less likely to turn in a circumferential direction. Another situation where flapping is less likely to occur is in the presence of multisite damage. This is illustrated in Figure 57, where MSD may be present ahead of the lead crack. In this case, even though $\sigma_{bulge}$ may be higher than $\sigma_{hoop}$ in the vicinity of the frame, the fracture path along OB may be weaker than along OA. This is another reason for ensuring that MSD does not exist by conducting a fatigue test to at least two lifetimes.

## Full-Scale Fatigue Testing of the Pressure Cabin

As mentioned earlier, the most reliable way to handle multiple-site damage is to make sure it never occurs within the projected life of the aircraft. The difficulties associated with predicting this condition analytically without substantiation testing are obvious, as illustrated by Figure 51. For this reason, curved development panel tests have been completed in some cases to as many as nine lifetimes for DC-8, DC-9, and DC-10 aircraft. These tests have been followed by further substantiation tests, in the case of DC-8 and DC-9, by testing representative sections of the forward fuselage, including cockpit, to 140,400 and 120,600 simulated pressurized flights, respectively. This represents over five and a half initially anticipated lives for the DC-8 and three lives for the DC-9. The DC-10 aircraft was tested in three major sections (Figure 58) to the equivalent of 120,000 hours and 84,000 pressurized flights, representing two initially anticipated lifetimes. At the time of this test, the anticipated average flight length was 1.43 hours per flight. On an average, after more than 15 years of successful service the average flight length exceeds 2 hours so that the test of the pressure cabin more realistically represents 2.8 lifetimes. As indicated by Table 1, the DC-10 current high time is low compared to this number.

The DC-9 fleet has successfully doubled its initially anticipated life of 40,000 flights, as indicated by Table 1. In order to aid the development of a supplemental inspection document (SID) in support of continued safe operation of the DC-9 fleet, the third aircraft was purchased for continued fatigue testing of the fuselage. This aircraft (Figure 59) had accumulated 66,500 in-service flights. The fuselage has now been subjected to additional pressure cycles simulating a total of 208,000 flights. The test aircraft has been inspected and maintained on a regular schedule representing normal service, and the results have been recorded for use in developing improved in-service maintenance programs. This aircraft is currently being subjected to an extensive teardown inspection program.

## CONCLUSIONS

This paper has attempted to describe the development of fracture technology related to the design of pressurized fuselage structure capable of sustaining large, easily detectable damage. The importance of stress level, geometry, and material choice has been emphasized. An attempt has been made to evaluate design details that led to the inability to sustain large detectable damage in early pressurized cabins and, in particular, the Comet I aircraft. A historical development of detail design concepts that has led to the achievement of extremely large damage capability in current commercial transport aircraft has been included. In particular, development of the minimum-gauge structure for DC-8, DC-9, and DC-10 aircraft has been included along with descriptions of the DC-6 and DC-7. The following conclusions, which are opinions of the author, are included as lessons learned and guidance in the development of pressure cabins for long life and large damage tolerance capability:

1. Analysis indicates that the weak link that prevented the Comet I type fuselage configuration from sustaining large detectable damage appears to be the frame cutout, which allows axial stiffening material to remain continuous.

2. Frame section properties, normally supported by effective skin material, are drastically reduced in the presence of longitudinal skin cracking, which results in high frame bending stresses at the notch.

3. The cutout in the frame, unreinforced by crack stopper straps, creates a severe stress concentration factor in the skin, as illustrated in Figure 6.

4. The stress concentration factor in the skin at the frame notch was apparently hindered by additional concentration provided by the automatic direction finding window, as shown in Figure 6.

5. Design should account for out-of-plane secondary bending stresses caused by shell curvature near cutouts such as windows and door corners (Figures 3, 4, and 5).

6. It appears that large damage tolerance capability is achievable in a Comet I type design provided longitudinal crack tips are located midway between notches in the frame. However, this cannot be relied upon.

7. It is recommended that the notched frames (Figures 6b, 13, and 41d) be excluded from pressurized aircraft design.

8. It is recommended that the notch for axial stiffening material continuity be placed in a separate shear clip as shown in Figures 21, 27, 31b, and 46.

9. Unless PR/t stress levels are very low, as in the case of the DC-9, it is recommended that the concentration provided by the notch in the shear clip (Figure 31b) be reduced by providing a crack stopper strap, as shown in Figures 21 and 46.

10. Currently, 2024-T3 is the only skin material suitable for large transport aircraft fuselage shells.

11. Out of the two damage scenarios considered in the design of pressurized fuselages (circumferential and longitudinal), the circumferential two-bay cracking with a broken central longeron is more critical.

12. Only 2024-T3 material is capable of achieving two bays of skin damage with a broken central longeron at limit stresses determined by static strength requirements in wide-bodied aircraft.

13. Other skin materials such as 7075-T73 and 7475-T761 have been considered as replacements for 2024-T3 but, although they may be adequate for the longitudinal cracking case, they are inadequate for the circumferential case.

14. The only metallic material that may be a replacement for 2024-T3 as a fuselage skin material is aluminum-lithium. This alloy offers reduced weight without increasing stress levels, which has been the case for all previous candidates.

15. Wide panel fracture testing at both room and reduced temperature is needed before a decision can be made on the use of aluminum-lithium for a fuselage skin replacement.

16. In order to account for the possibility of multiple-site damage occurring within one projected lifetime, at least two lifetimes of testing should be accomplished on a full-scale representative section of the pressure cabin.

17. Flapping should not be completely relied upon to eliminate the need for inspection unless at least two lifetimes of testing have verified that multisite damage will not be present ahead of the lead crack.

18. Flapping cannot be relied upon on skin gauges thicker than 0.063 inch in conventional fuselage shells.

19. Finally, for long-life pressurized fuselage structure with large damage tolerance capability:

    - Keep PR/t stresses low (15 ksi).
    - Be careful about geometrical details such as cutouts in skin shear clips.
    - Use crack stopper straps around the entire circumference (titanium).
    - Account for out-of-plane bending stresses due to curvature.
    - Use damage-resistant materials (2024-T3).

## ACKNOWLEDGEMENT

The author is indebted to Douglas Aircraft Company and in particular to Dale Warren and Jean McGrew for allowing him to present this paper, which he committed to when employed by the Federal Aviation Administration. He is also indebted to Bob Eastin and his group for teaching him how to use a TSO terminal so that he could perform analysis that 5 years ago he submitted on punched cards.

## REFERENCES

1. Boggs, B. C., et al, "Digital and Analog Computer Equipment and Its Application to In-House Testing," paper in ASTM STP-613, 1975.

2. Mann, J. Y., "Aircraft Fatigue – With Particular Emphasis on Australian Operations and Research," The Ninth Plantema Memorial Lecture, presented to ICAF, Toulous, France, May 1983.

3. Gassner, E., "Fatigue Life of Structural Components Under Random Loading," The Fourth Plantema Memorial Lecture, presented to ICAF, London, England, July 1973.

4. Report of the Court of Inquiry into the Accidents to Comet G-ALYP on 10th January 1954 and Comet G-ALYY on 8th April 1954, Ministry of Transport and Civil Aviation Report CAP 127, 1955.

5. Report on Comet Accident Investigation Part 3, "Fatigue Tests on the Pressure Cabin and Wings," Royal Aircraft Establishment Accident Note No. 263, September 1954.

6. Stone, M., "Airworthiness Philosophy Developed from Full-Scale Testing," Douglas Paper 6099, presented to the 7th ICAF Symposium, London, England, 18-20 July 1973, published in RAE TR 73183, March 1974.

7. Report on Comet Accident Investigation Part 2 "Wreckage Investigation," Royal Aircraft Establishment Accident Note No. 260.

8. Williams, D., "An Experimental Verification of the Theoretical Conclusions of RAE Technical Note No. Structures 156 (ARC CP No. 286)," ARC Technical Report CP No. 357, May 1957.

9. Williams. D., "A Constructional Method for Minimizing the Hazard of Catastrophic Failure in a Pressure Cabin," ARC Technical Report CP No. 286, March 1955.

10. Swift, T., "The Effects of Fastener Flexibility and Stiffener Geometry on the Stress Intensity in Stiffened Cracked Sheet," published in Prospects of Fracture Mechanics, Noordhoff International, Leydon, Netherlands, 1974.

11. Flugge, W., "Stress Problems in Pressurized Cabins," NACA TN 2612, February 1952.

12. Swift, T., "Design of Redundant Structures," published in Fracture Mechanics Design Methodology, AGARD-LS-97, 1979.

13. Kuhn, P., "Notch Effects on Fatigue and Static Strength," published in Current Aeronautical Fatigue Problems, Proceedings of ICAF Symposium, Rome, 1963.

14. Walker, P. B., "Destructive Energy in Aircraft Pressure Cabins," Journal of the Royal Aeronautical Society, Volume 54, April 1954.

15. Christensen, R. H. and Denke, P. H., "Crack Strength and Crack Propagation Characteristics of High-Strength Materials," Douglas Aircraft Company/Aeronautical Systems Division, ASD-TR-61-207, May 1961.

16. Hunt, R. T., et al, "Crack Propagation and Residual Strength of Stiffened and Unstiffened Sheet," presented at the Third ICAF Symposium in Rome, Italy, 22-26 April 1963.

17. Swift, T. and Wang, D. Y., "Damage Tolerant Design – Analysis Methods and Test Verification of Fuselage Structure," presented to Air Force Conference on Fatigue and Fracture of Aircraft Structures and Materials, Miami, Florida, 15-18 December 1969, published in AFFDL-TR-70-144, 1970.

18. Swift, T., "Application of Fracture Mechanics in the Development of the DC-10 Fuselage," published in AGARD-AG-176, 1974.

19. Swift, T., "Fracture Analysis of Stiffened Structure," published in Damage Tolerance of Metallic Structures, ASTM STP 842, July 1984.

20. Abelkis, P. R., et al, "Low Temperature and Loading Frequency Effects on Crack Growth and Fracture Toughness of 2024 and 7475 Aluminum," Douglas Paper 7317, presented to ASTM Symposium – Fatigue at Low Temperatures, Louisville, Kentucky, May 1983.

21. Liu, A. F., "Statistical Variation in Fracture Toughness Data of Airframe Materials," Proceedings of the Air Force Conference on Fatigue and Fracture of Aircraft Structures and Materials, published in AFFDL TR-70-144, 1970.

22. Wang, D. Y., "Plane Stress Fracture Toughness and Fatigue Crack Propagation of Aluminum Alloy Wide Panels," Douglas Paper 6054, published in ASTM STP 536, August 1972.

23. Private communication from Dr. W. S. Miller, Alcan International Ltd., Banbury Laboratories, Banbury Oxon, England.

24. LeRoy, G. and Meyer, P., "Status Report on the Development of Aluminum-Lithium at Pechiney," presented at Westec 86, 19 March 1986, Los Angeles, California.

## APPENDIX 1

### Development of Bulge Factor from Comet 1 Test

A number of tests were completed on a Comet 1 fuselage fitted with crack stopper straps. Test No. 6, reported by Williams (8), resulted in fast fracture and arrest of a simulated one-bay longitudinal crack. It is possible, making a number of assumptions, to estimate $K_c$ for the DTD 546 Comet fuselage skin material from this test.

A displacement compatibility analysis was performed for the configuration of Test 6 of Reference 8. The results are shown in Figure 7b in the form of a plot of $\beta$ versus crack length. It is necessary to determine the value of $\beta_B$, which accounts for bulging due to pressure and radius of shell curvature. The crack tip stress intensity factor is obtained from:

$$K = \sigma\sqrt{\pi a}\,\beta_B\beta \tag{A1}$$

At fast fracture, $a = a_F$, $\beta_B = \beta_{BF}$, and $\beta = \beta_F$. Therefore:

$$K_c = \sigma\sqrt{\pi a}\,\beta_{BF}\beta_F \tag{A2}$$

At crack arrest, $a = a_A$, $\beta_B = \beta_{BA}$, and $\beta = \beta_A$. Therefore:

$$K_c = \sigma\sqrt{\pi a}\,\beta_{BA}\beta_A \tag{A3}$$

We know $a_F$, $a_A$, $\beta_A$, and $\beta_F$, and we can equate A2 and A3. Therefore:

$$\beta_{BF}/\beta_{BA} = \sqrt{a_A}\,\beta_A/(\sqrt{a_F}\,\beta_F) \tag{A4}$$

The terms $\beta_F$ and $\beta_A$ are obtained for crack lengths at fast fracture and arrest, respectively, from Figure 7b.

As mentioned previously, it has been this author's experience that, when a crack tip is midway between frames or straps in a curved pressurized shell, maximum bulging occurs equivalently to an unstiffened shell. This bulging damps out to some value as the crack approaches the frame. The following expression provides a variation between 1.0, midway between straps, when x (Figure 7a) is zero to a value of F at x = L/2, where L is the distance between straps (Figure 7a).

$$\text{Damping term} = \frac{1}{2}(1 + \text{Cos } 2\pi x/L) + F/2(1 - \text{Cos } 2\pi x/L) \tag{A5}$$

A bulging expression for longitudinal cracks in unstiffened pressurized shells was obtained by Kuhn (13). This author has found that Kuhn's expression correlates with stiffened panel test results when the crack tip is midway between circumferential stiffeners. Using Kuhn's expression in conjunction with the cosinusoidal damping term of A5 results in an expression for $\beta_B$ as follows:

$$\beta_B = 1 + 5(L/2) \,/\, R\left[\frac{1}{2}(1 + \text{Cos } 2\pi x/L) + F/2(1 - \text{Cos } 2\pi x/L)\right] \tag{A6}$$

Where L = distance between stiffeners
R = shell radius
F = proportion of bulging at the stiffeners compared to full bulging between stiffeners
x = distance from center of bay to the crack tip (Figure 7a)

Consider Williams' Test 6:

$a_F$ = 4.125 inches
$a_A$ = (21-1.2)/2 = 9.9 inches

$$\left.\begin{array}{l}\beta_F = 0.97\\ \beta_A = 0.835\end{array}\right\} \text{Figure 7b}$$

Therefore $\beta_{BF}/\beta_{BA}$ = 1.3336 from Equation A4

and

$$\beta_{BA} = 0.7499\beta_{BF} \tag{A7}$$

At fast fracture $\beta_{BF}$ can be determined to be:

$$\beta_{BF} = 1.8027 + 0.05097F \tag{A8}$$

by substituting x = −1.65, L = 21, and R = 61.5 into Equation A6. At crack arrest $\beta_{BA}$ can be determined to be:

$$\beta_{BA} = 1.006829 + 0.8469F \tag{A9}$$

by substituting x = 9.9 into Equation A6. Equations A7, A8, and A9 can now be solved simultaneously to give F = 0.4266. This means that according to the Williams Test 6, if we assume the displacement compatibility analysis is providing the correct effect of stiffening, 42.66 percent of the maximum bulging still exists near the strap.

At fast fracture, with x = −1.65 and $\beta_{BF}$ = 1.8245 from Equation A6, the value of $\beta_F$ from Figure 7b is 0.97, and the average stress from Equation 2 in the body of this report is 14.746.

Therefore, $K_c = 14.746\sqrt{4.125\,\pi}(1.8245)\,(0.97) = 93.946$ ksi $\sqrt{\text{in.}}$

## APPENDIX 2

### ICAF History

| Conference | Symposium | Date | Location | Plantema Lecture (1) | |
|---|---|---|---|---|---|
| | | | | No. | Author |
| 1 | | 1952 | Amsterdam | | |
| 2 | | 1953 | Stockholm | | |
| 3 | | 1955 | Cranfield | | |
| 4 | | 1956 | Zurich | | |
| 5 | | 1957 | Brussels | | |
| 6 | 1 | 1959 | Amsterdam | | |
| 7 | 2 | 1961 | Paris | | |
| 8 | 3 | 1963 | Rome | | |
| 9 | 4 | 1965 | Munich | | |
| 10 | 5 | 1967 | Melbourne | 1 | J. Branger |
| 11 | * | 1969 | Stockholm | 2 | J. Schijve |
| 12 | 6 | 1971 | Miami | 3 | E.L. Ripley |
| 13 | 7 | 1973 | London | 4 | E. Gassner |
| 14 | 8 | 1975 | Lausanne | 5 | S. Eggwertz |
| 15 | 9 | 1977 | Darmstadt | 6 | H.F. Hardrath |
| 16 | 10 | 1979 | Brussels | 7 | A.J. Troughton |
| 17 | 11 | 1981 | Noordwijkerhout | 8 | O. Buxbaum |
| 18 | 12 | 1983 | Toulous | 9 | J.Y. Mann |
| 19 | 13 | 1985 | Pisa | 10 | L. Jarfall |

* No symposium this year. Two-day technical session
(1) Frederik J. Plantema, 21 October 1911 - 13 November 1966

Previous Plantema Memorial Lectures

| Lecture | Author | Title |
|---|---|---|
| 1 | J. Branger | The International Committee on Aeronautical Fatigue (ICAF), Its Foundation, Growth, and Today's Philosophy |
| 2 | J. Schijve | Cumulative Damage Problems in Aircraft Structures and Materials |
| 3 | E.L. Ripley | The Philosophy of Structural Testing a Supersonic Transport Aircraft with Particular Reference to the Influence of the Thermal Cycle |
| 4 | E. Gassner | Fatigue Life of Structural Components Under Random Loading |
| 5 | S. Eggwertz | Reliability Analysis of Wing Panel Considering Test Results from Initiation of first and Subsequent Fatigue Cracks |
| 6 | H.F. Hardrath | Advanced Composites – The Structures of the Future |
| 7 | A.J. Troughton | 33 Years of Aircraft Fatigue |
| 8 | O. Buxbaum | Landing Gear Loads of Civil Transport Airplanes |
| 9 | J.Y. Mann | Aircraft Fatigue – With Particular Emphasis on Australian Operations and Research |
| 10 | L. Jarfall | Fatigue and Damage Tolerance Analysis in the Aircraft Design Process |

## TABLE 1
## DESIGN LIFE VERSUS HIGH TIME FOR COMMERCIAL TRANSPORTS

| AIRCRAFT | DESIGN LIFE | | HIGH TIME | | AS OF DATE |
|---|---|---|---|---|---|
| | HOURS | FLIGHTS | HOURS | FLIGHTS | |
| DC-8 | 50,000 | 25,000 | 74,050 | 43,604 | SEP 1986 |
| DC-9 | 30,000 | 40,000 | 58,512 | 83,798 | SEP 1986 |
| DC-10 | 60,000 | 42,000 | 55,686 | 20,109 | SEP 1986 |
| L-1011 | 60,000 | 36,000 | 37,001 | 21,249 | JUN 1986 |
| 707 | 60,000 | 30,000 (1) | 76,285 | 35,235 | SEP 1986 |
| 720 | 60,000 | 50,000 | 67,745 | 43,588 | SEP 1986 |
| 727 | 60,000 | 60,000 | 65,814 | 64,227 | SEP 1986 |
| 737 | 45,000 | 75,000 | 58,450 | 81,689 | SEP 1986 |
| 747 | 60,000 | 20,000 | 67,048 | 24,241 | SEP 1986 |

(1) 50,000 FOR SOME MODELS

**UNIT CONVERSION FACTORS**

1 INCH = 2.54 cm
1 KSI = 6.895 MPa
1 KSI $\sqrt{\text{IN.}}$ = 1.0989 MPa.m$^{1/2}$

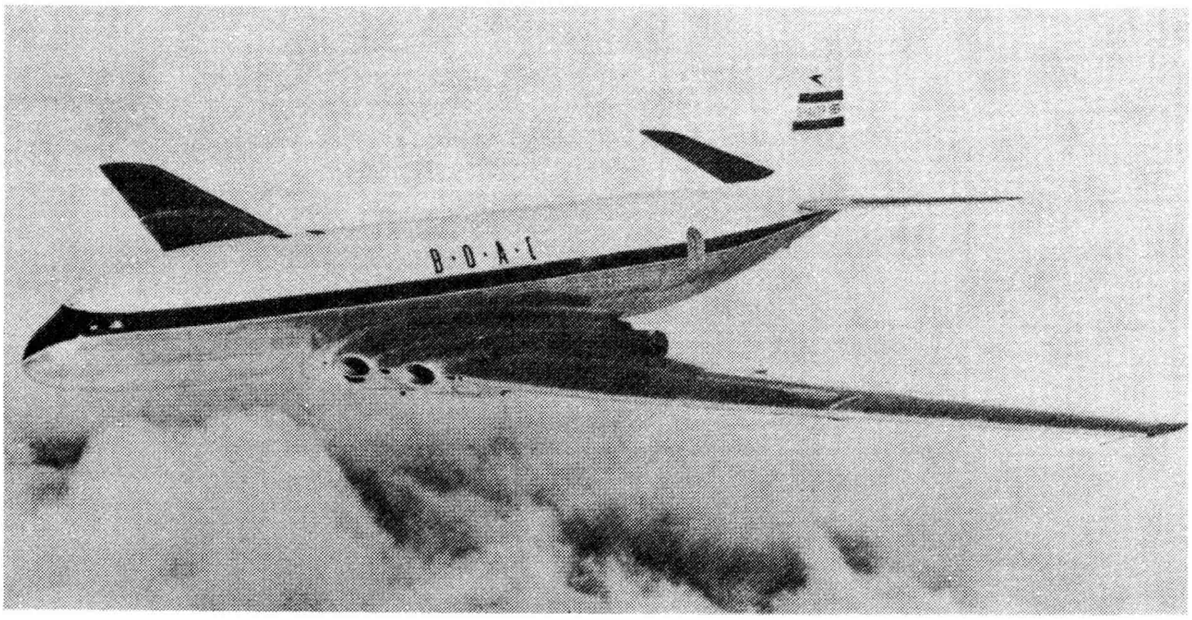


**FIGURE 1. COMET I YOKE PETER — FIRST JET TRANSPORT AIRCRAFT TO ENTER SCHEDULED AIRLINE SERVICE**

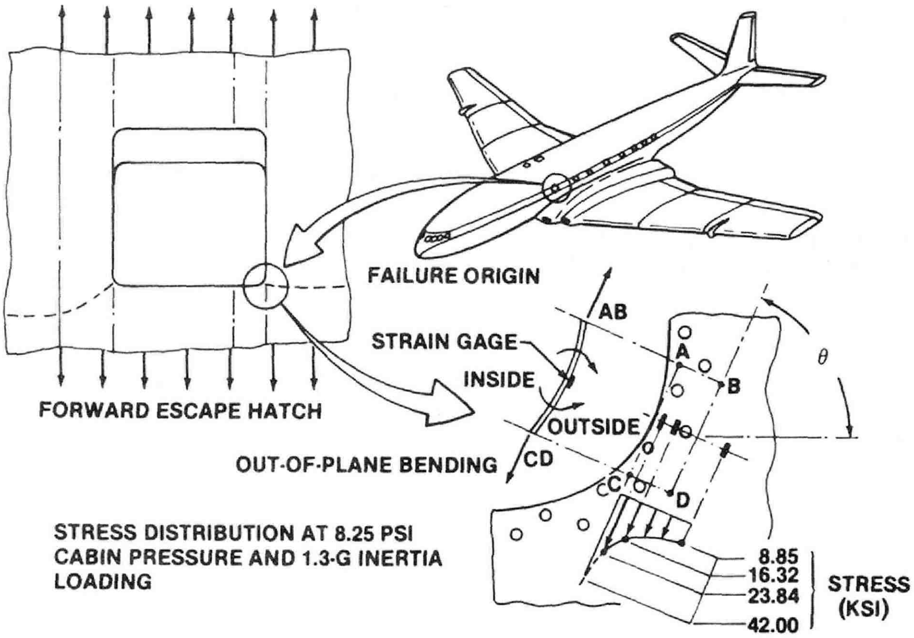


**FIGURE 2. PROBABLE FAILURE ORIGIN — COMET I YOKE UNCLE TEST AIRCRAFT**

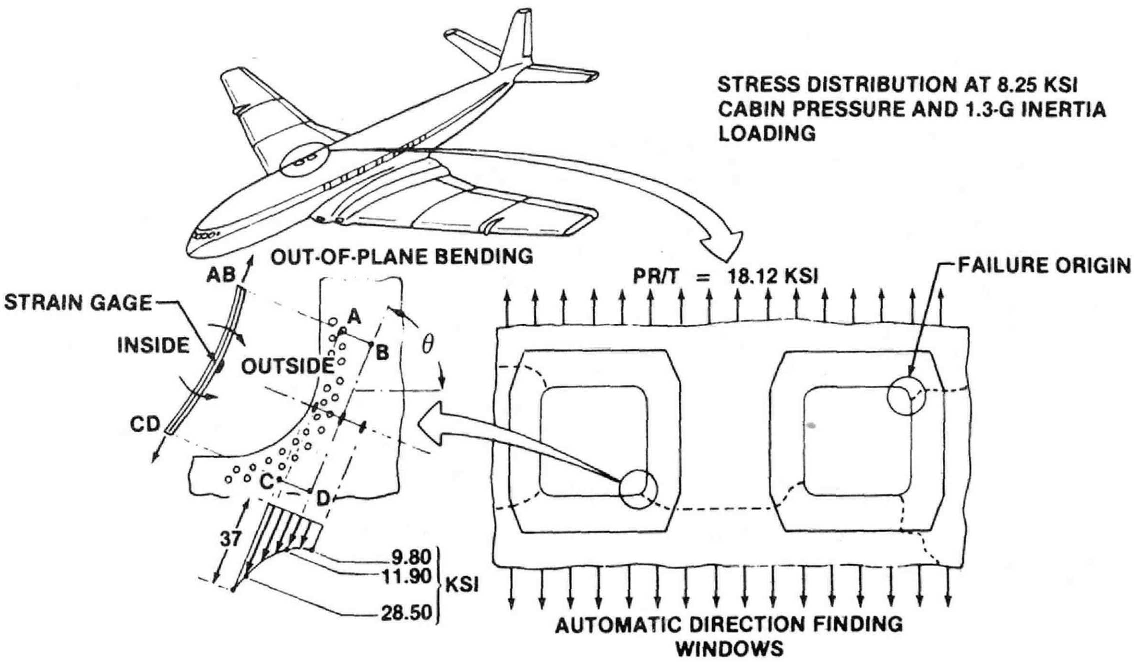


**FIGURE 3. PROBABLE FAILURE ORIGIN — COMET I YOKE PETER**

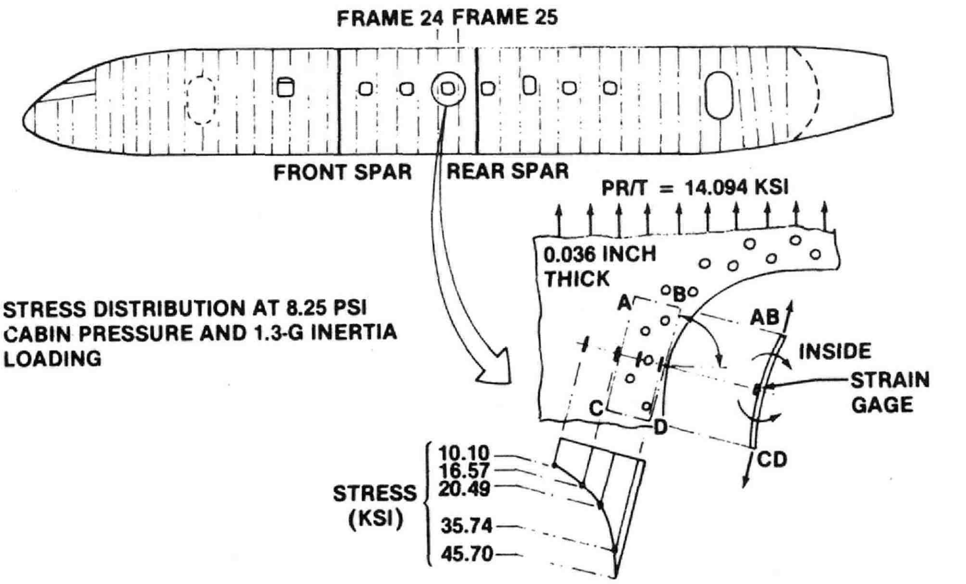


**FIGURE 4. TYPICAL WINDOW CORNER STRESSES**

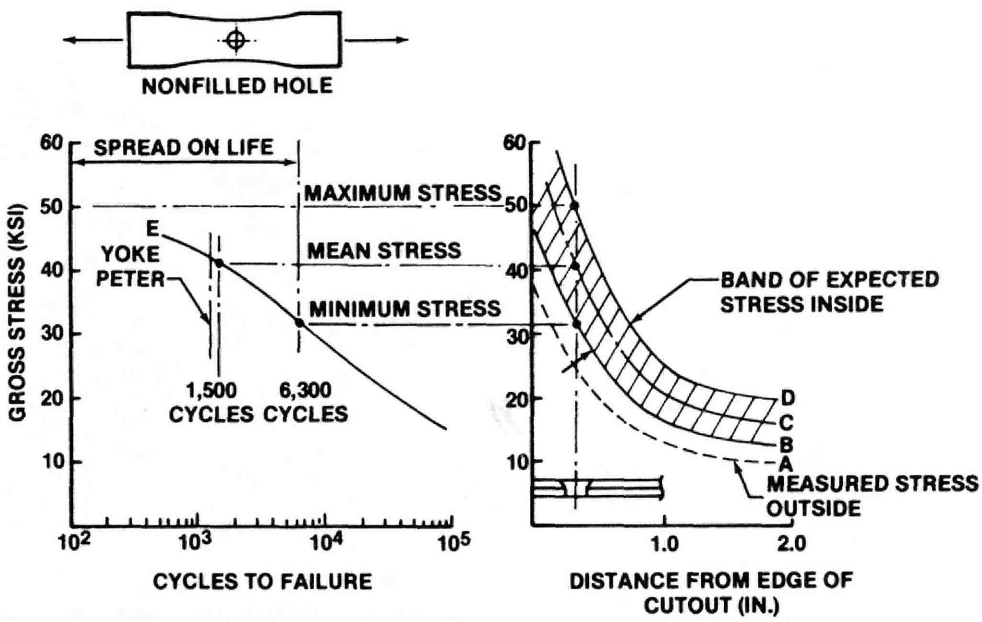


**FIGURE 5. COMET I ADF WINDOW STRESSES AND LIFE**

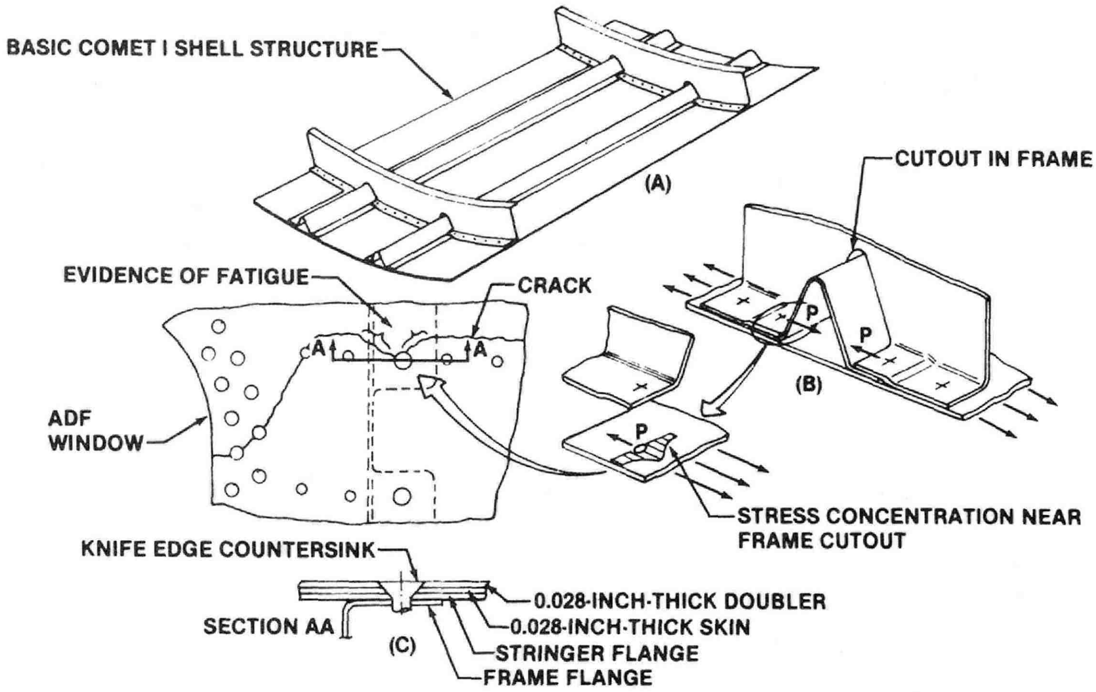


**FIGURE 6. BASIC COMET I SHELL CONFIGURATION PROBABLE FAILURE ORIGIN — YOKE PETER**

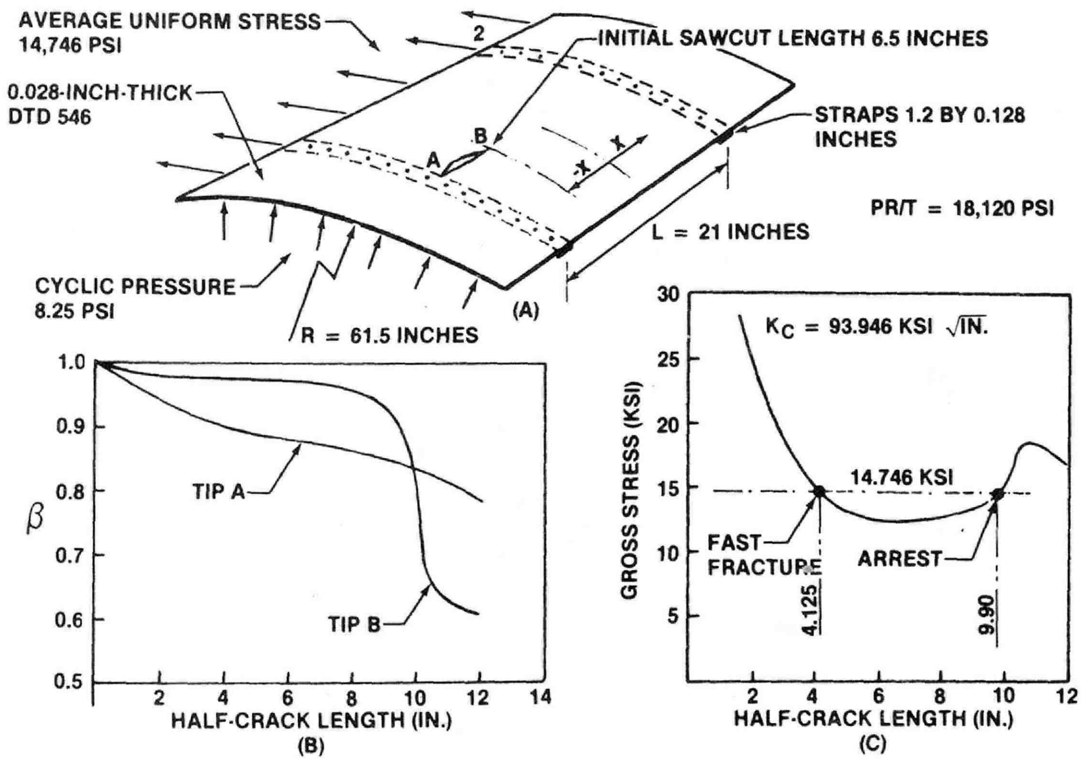


**FIGURE 7. RESIDUAL STRENGTH ANALYSIS AND TEST RESULTS ON COMET I FUSELAGE WITH CRACK STOPPER STRAPS (WILLIAMS TEST)**

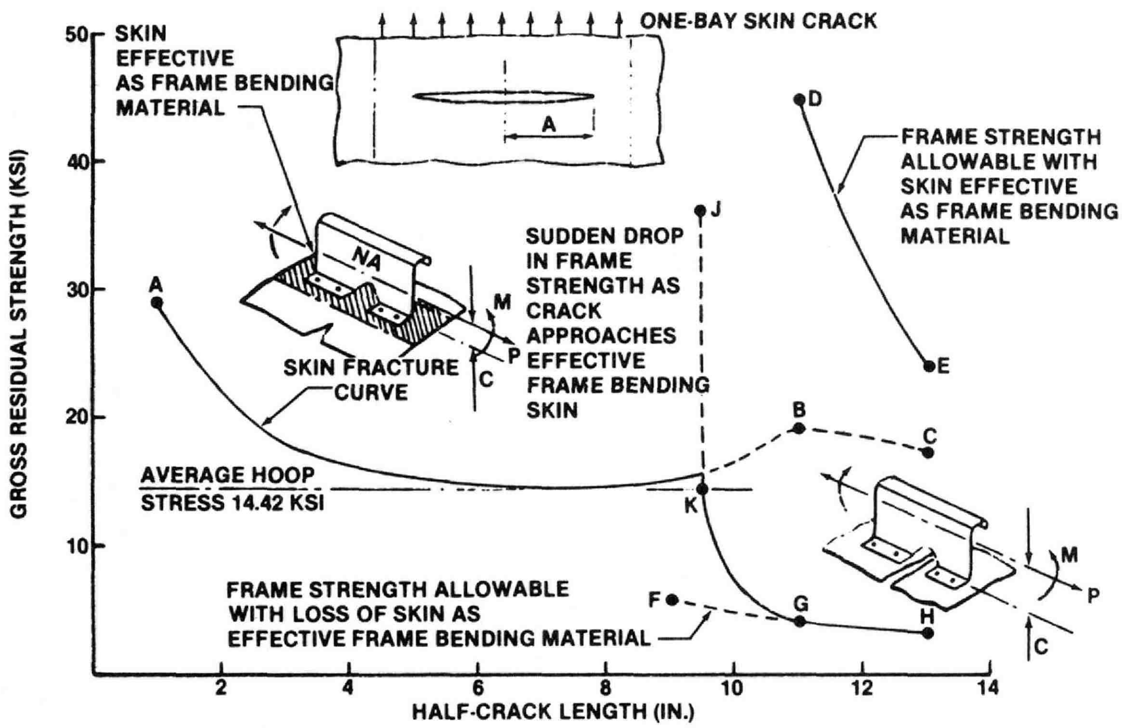


FIGURE 8. RESIDUAL STRENGTH DIAGRAM FOR ONE-BAY CRACK — CRACK HEADING TOWARD NOTCH (COMET I TYPE CONFIGURATION)

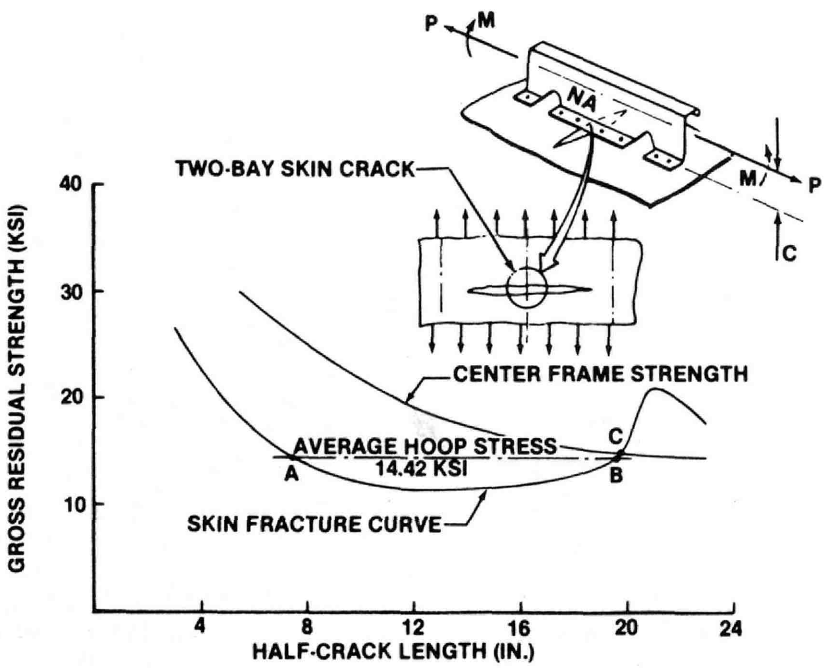


FIGURE 9. RESIDUAL STRENGTH DIAGRAM FOR TWO-BAY CRACK WITH CENTER FRAME INTACT — CRACK HEADING BETWEEN CUTOUTS (COMET I TYPE CONFIGURATION)

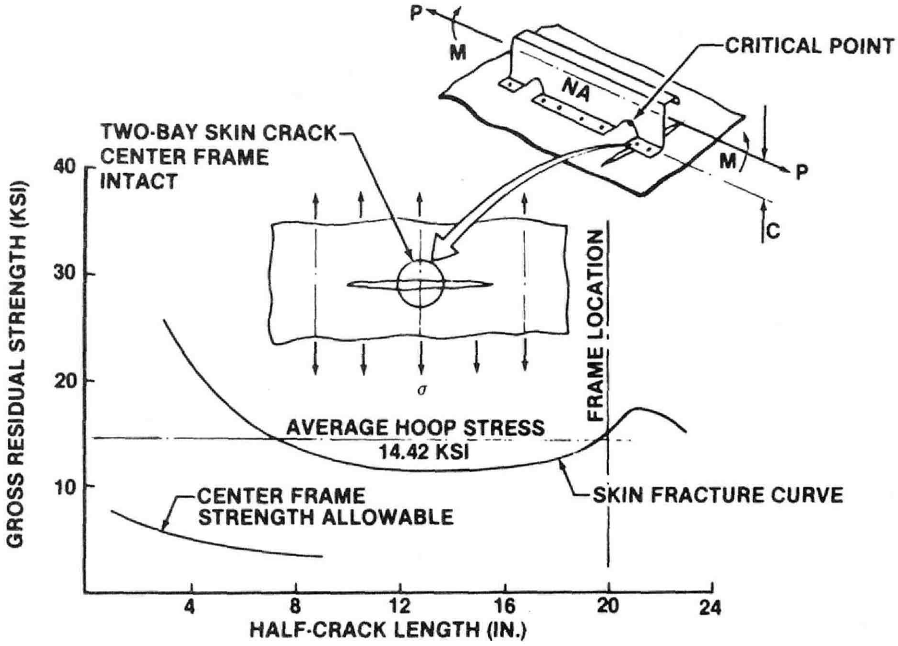


**FIGURE 10. RESIDUAL STRENGTH DIAGRAM FOR TWO-BAY CRACK WITH CENTER FRAME INTACT — CRACK HEADING TOWARD NOTCH (COMET I TYPE CONFIGURATION)**

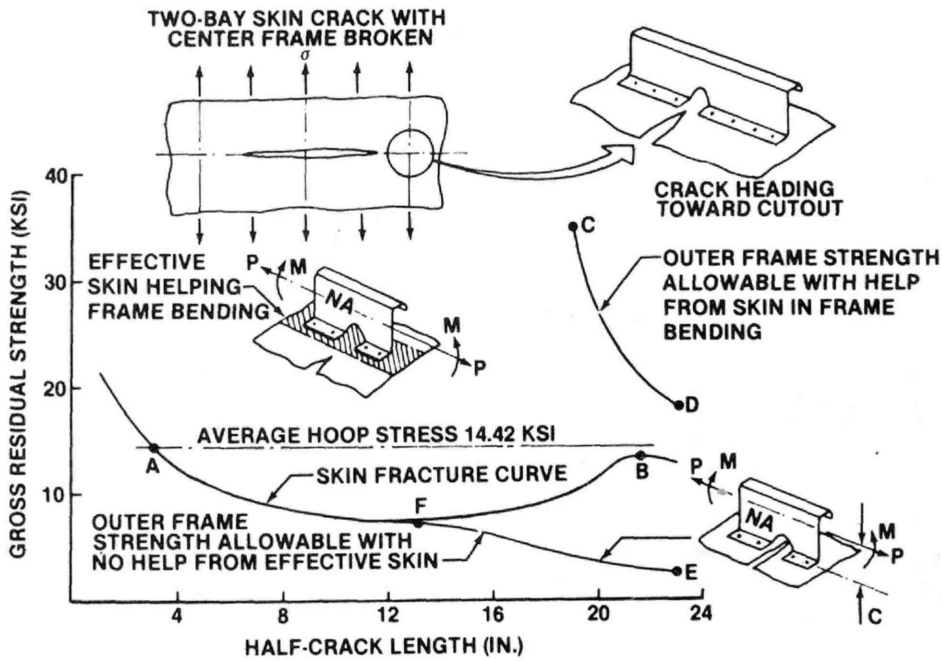


**FIGURE 11. RESIDUAL STRENGTH DIAGRAM FOR TWO-BAY CRACK WITH CENTER FRAME BROKEN — CRACK HEADING TOWARD NOTCH (COMET I TYPE CONFIGURATION)**

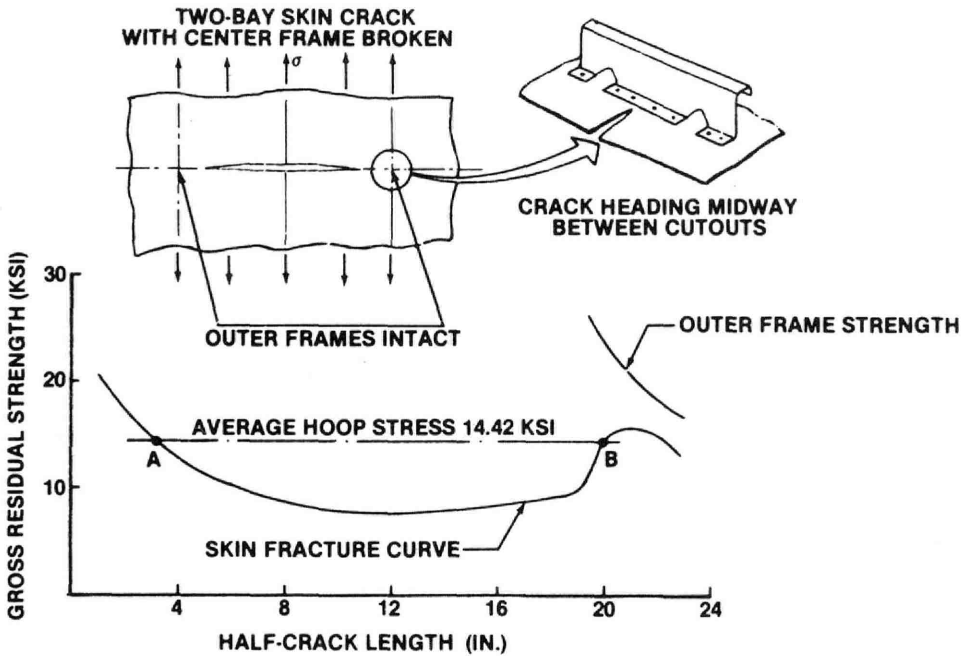


**FIGURE 12. RESIDUAL STRENGTH DIAGRAM FOR TWO-BAY CRACK WITH CENTER FRAME BROKEN — CRACK HEADING BETWEEN CUTOUTS (COMET I TYPE CONFIGURATION)**

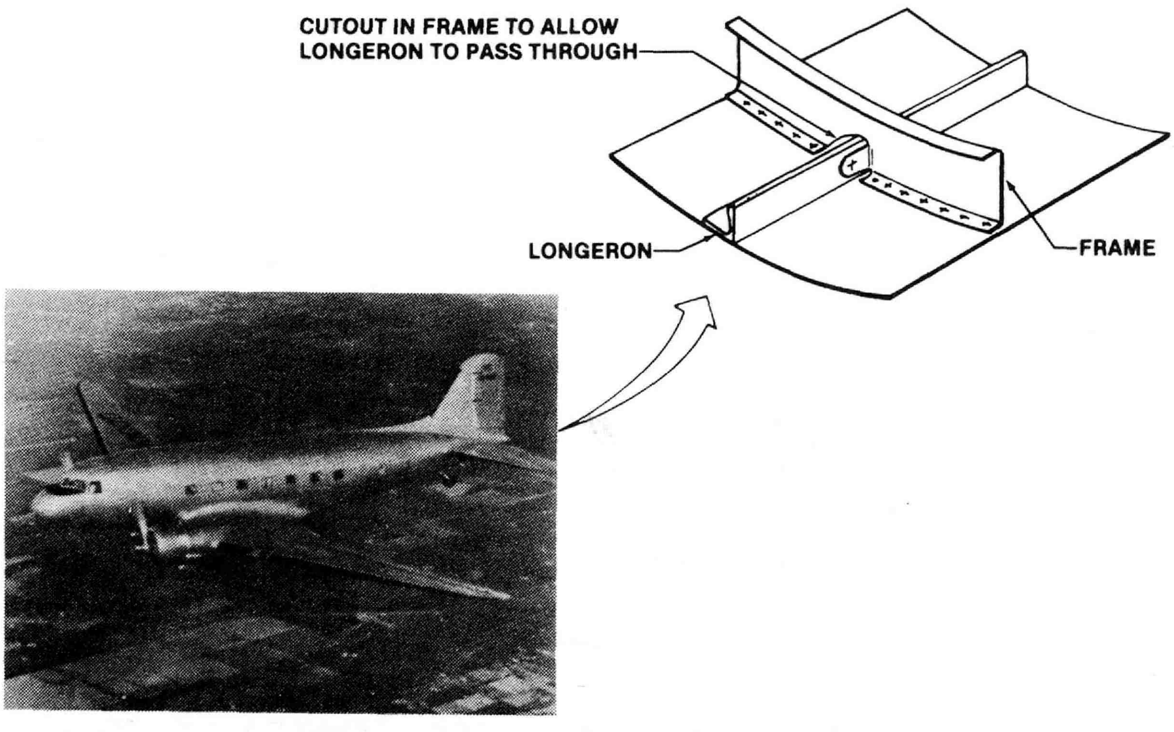


**FIGURE 13. DC-3 TYPICAL FUSELAGE CONSTRUCTION**

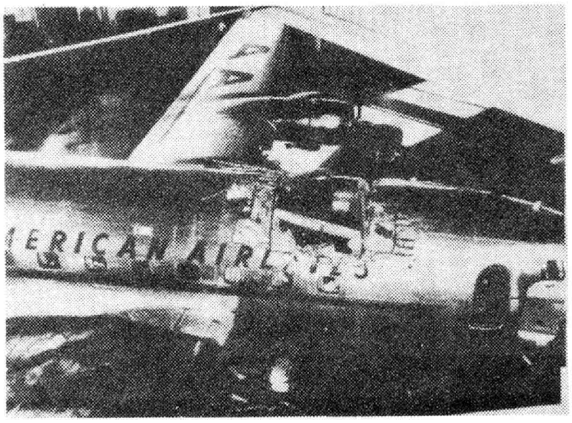

(A) PROPELLER BLADE DAMAGE, PRESSURIZED DC-6, NEAR DENVER, 22 AUGUST 1950

(B) PROPELLER DAMAGE, PRESSURIZED DC-7, NEAR MEMPHIS, 5 MARCH 1957

FIGURE 14. DC-6 AND DC-7 PROPELLER BLADE FAILURE INCIDENTS

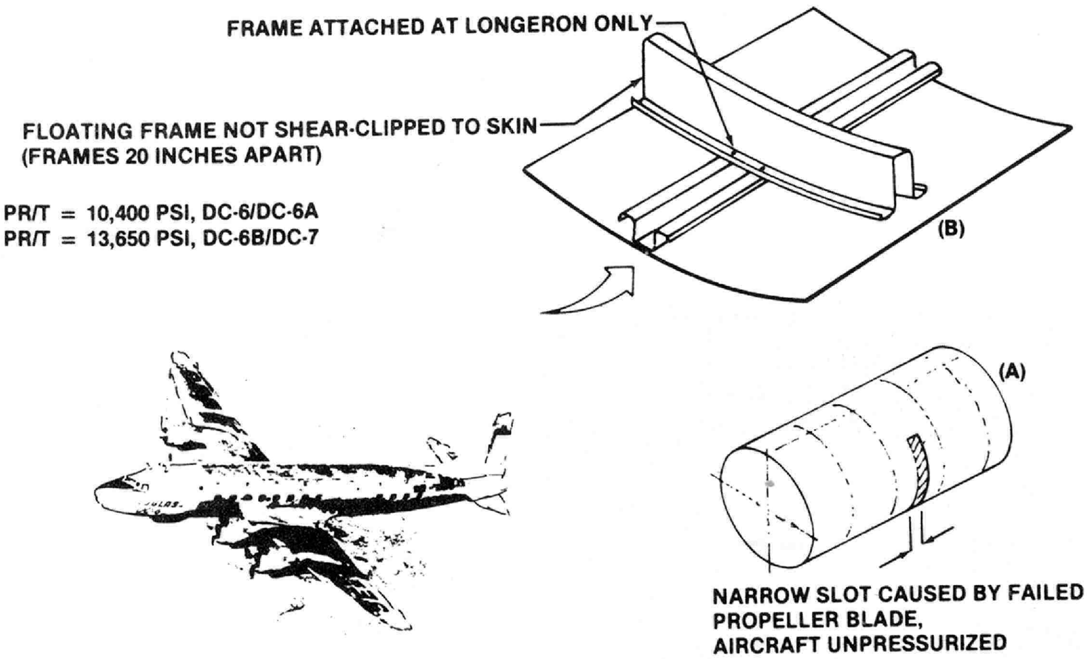


FIGURE 15. TYPICAL DC-6 AND DC-7 MINIMUM-GAUGE CONSTRUCTION

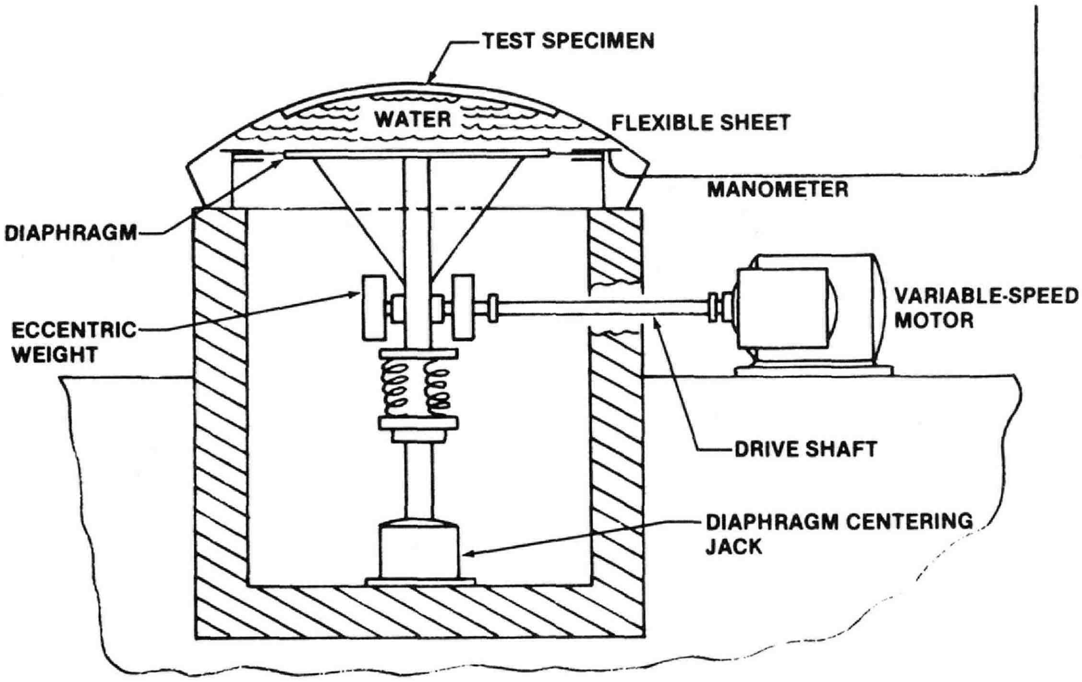


**FIGURE 16. WATER CYCLE TEST MACHINE**

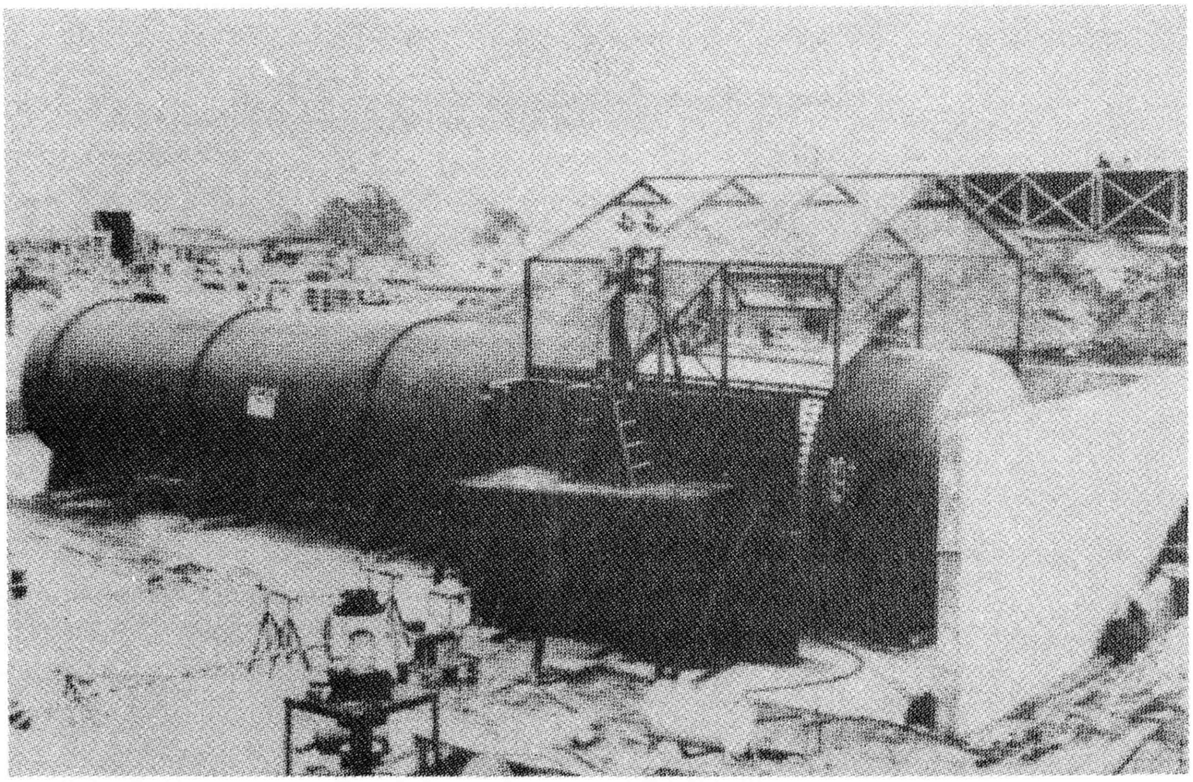

**FIGURE 17. DC-8 FUSELAGE PANEL AIR TANK TESTS**

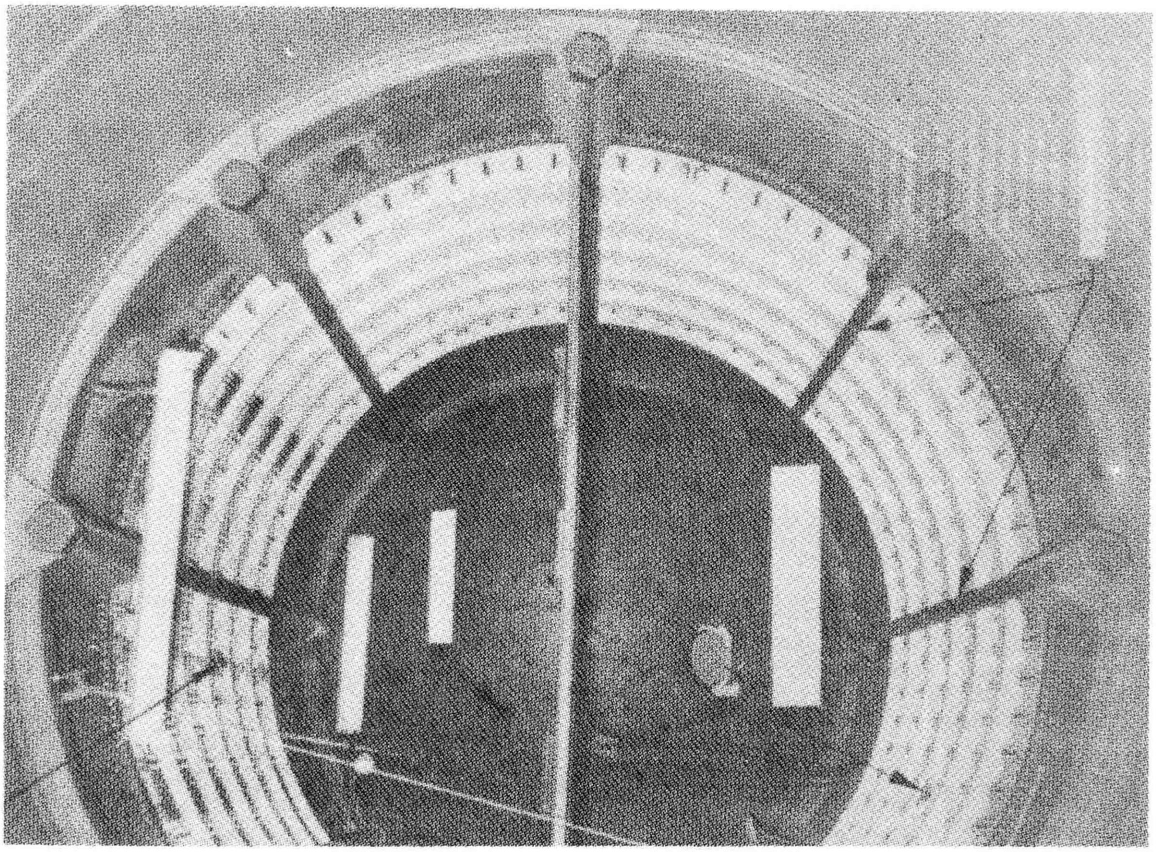

**FIGURE 18. VIEW INSIDE AIR TANK SHOWING SPECIMEN AND TIE BOLTS**

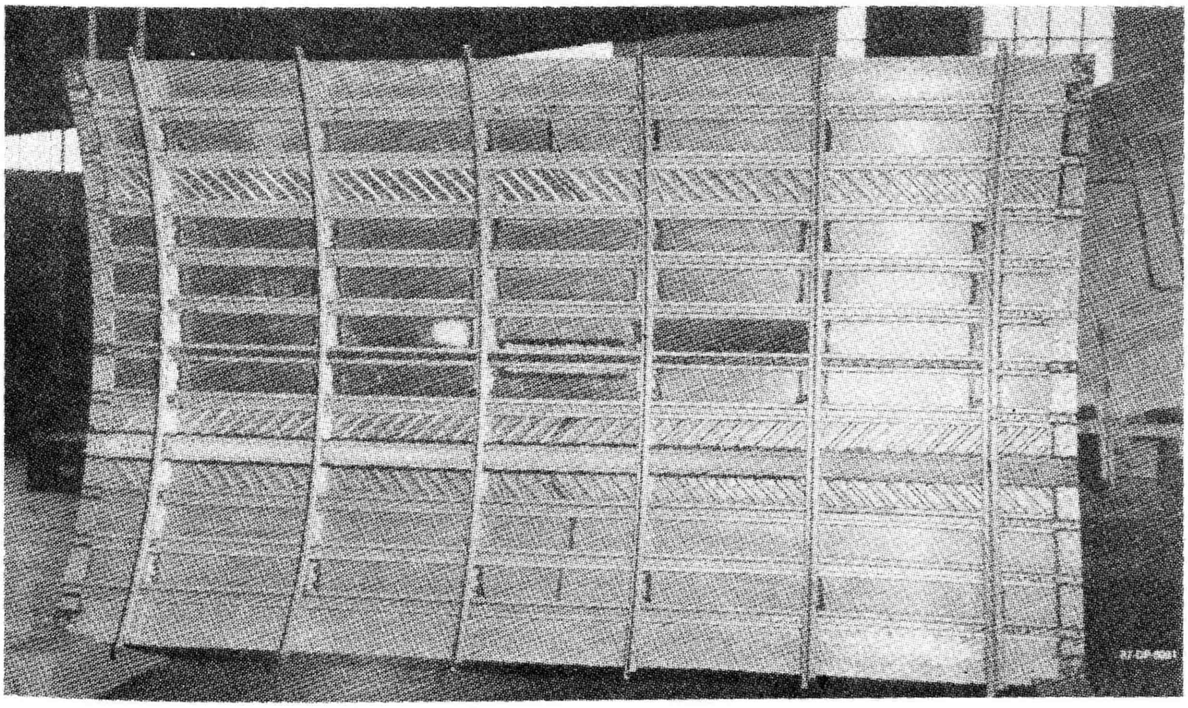

**FIGURE 19. TYPICAL CURVED PANEL TESTED IN WATER CYCLE AND AIR TANK FIXTURES**

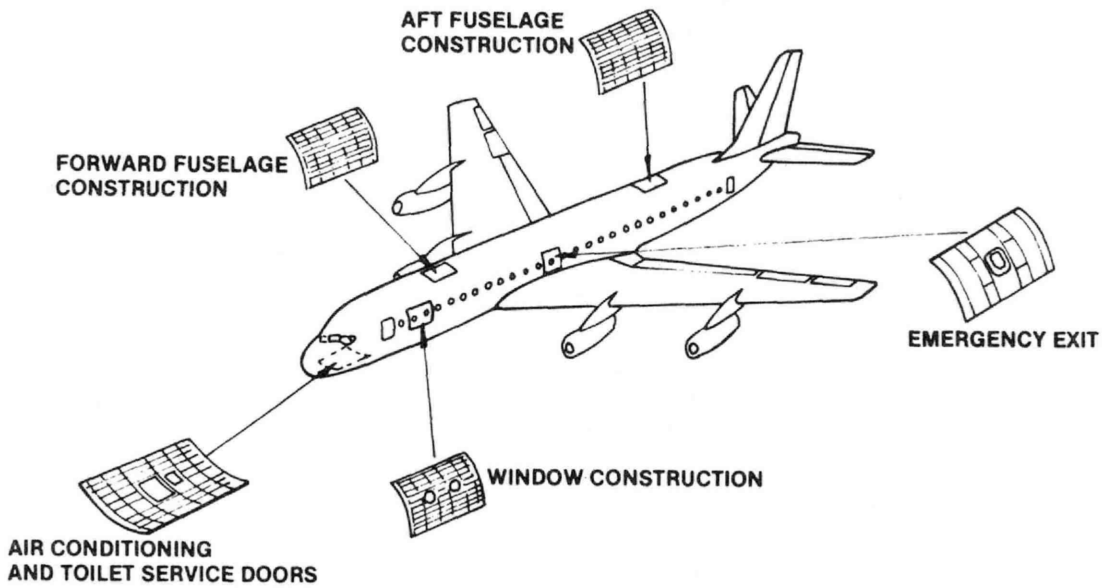


**FIGURE 20. DC-8 FUSELAGE FATIGUE TEST PANELS REPRESENTING VARIOUS AREAS OF THE AIRCRAFT**

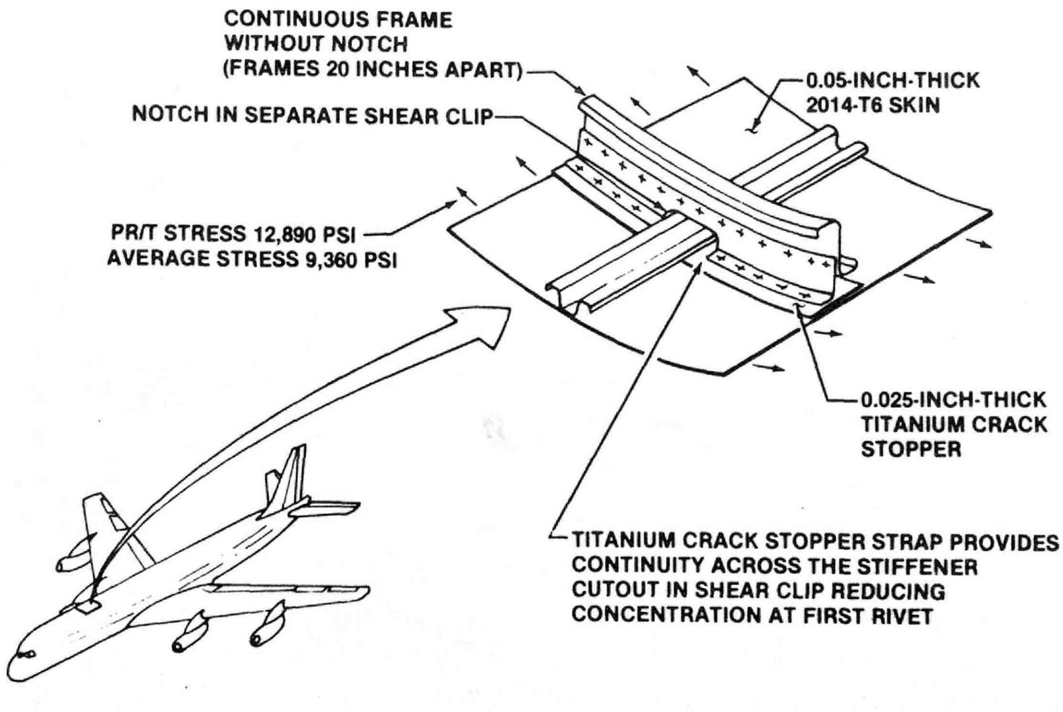


**FIGURE 21. MINIMUM-GAUGE CONSTRUCTION FOR DC-8 FUSELAGE**

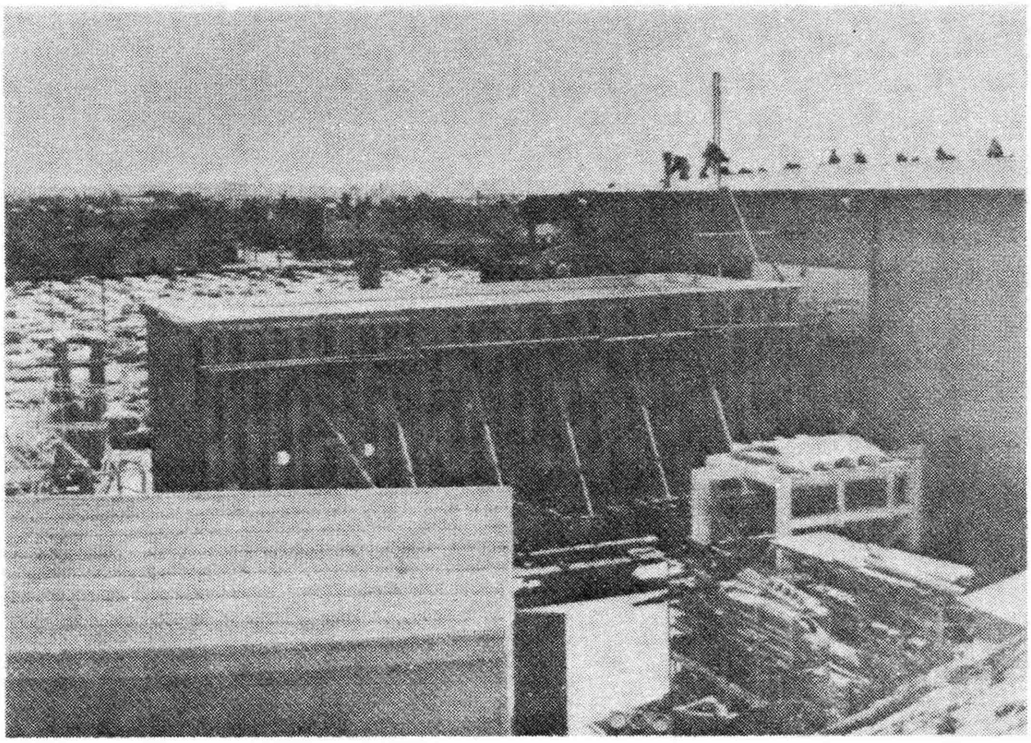

**FIGURE 22. DC-8 FORWARD FUSELAGE FULL-SCALE FATIGUE TEST WATER TANK**

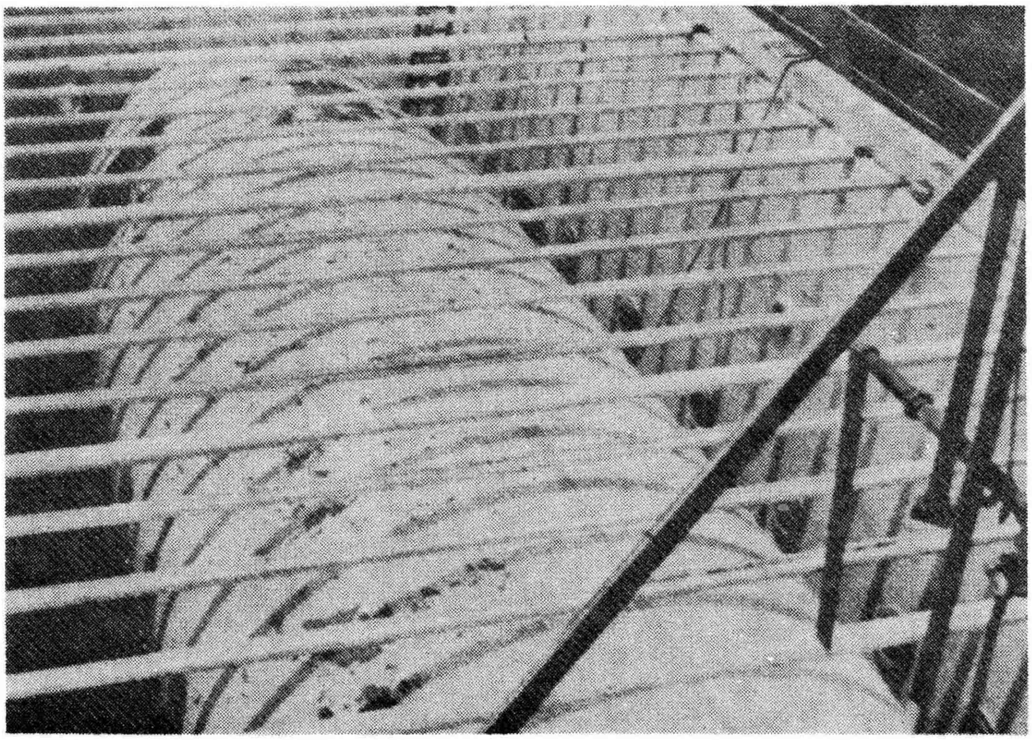

**FIGURE 23. DC-8 FORWARD FUSELAGE INSIDE THE TEST TANK**

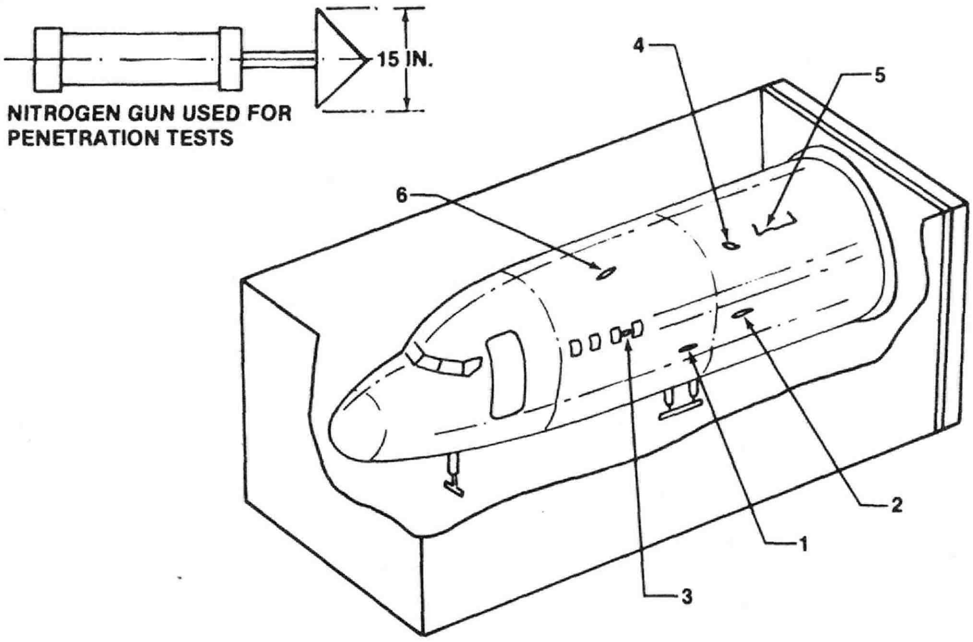


**FIGURE 24. DC-8 WEDGE PENETRATION TESTS**

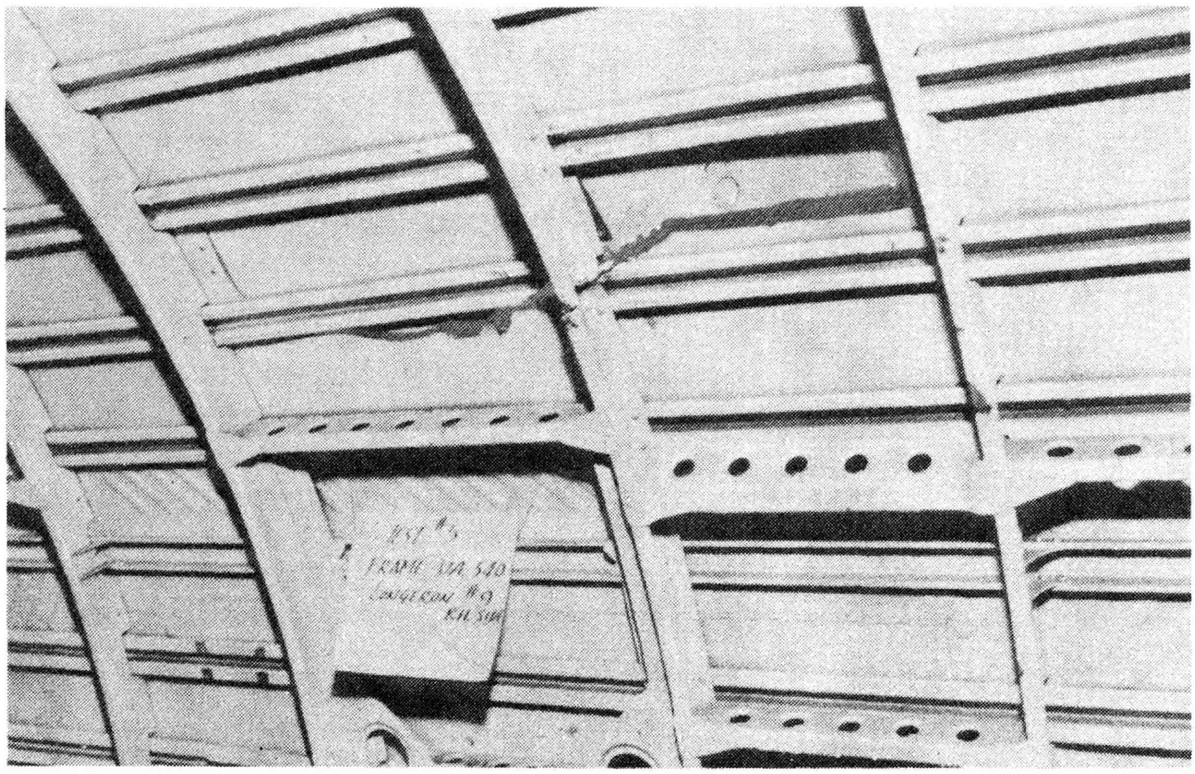

**FIGURE 25. TWO-BAY DAMAGE WITH BROKEN FRAME AND LONGERON (INSIDE VIEW)**

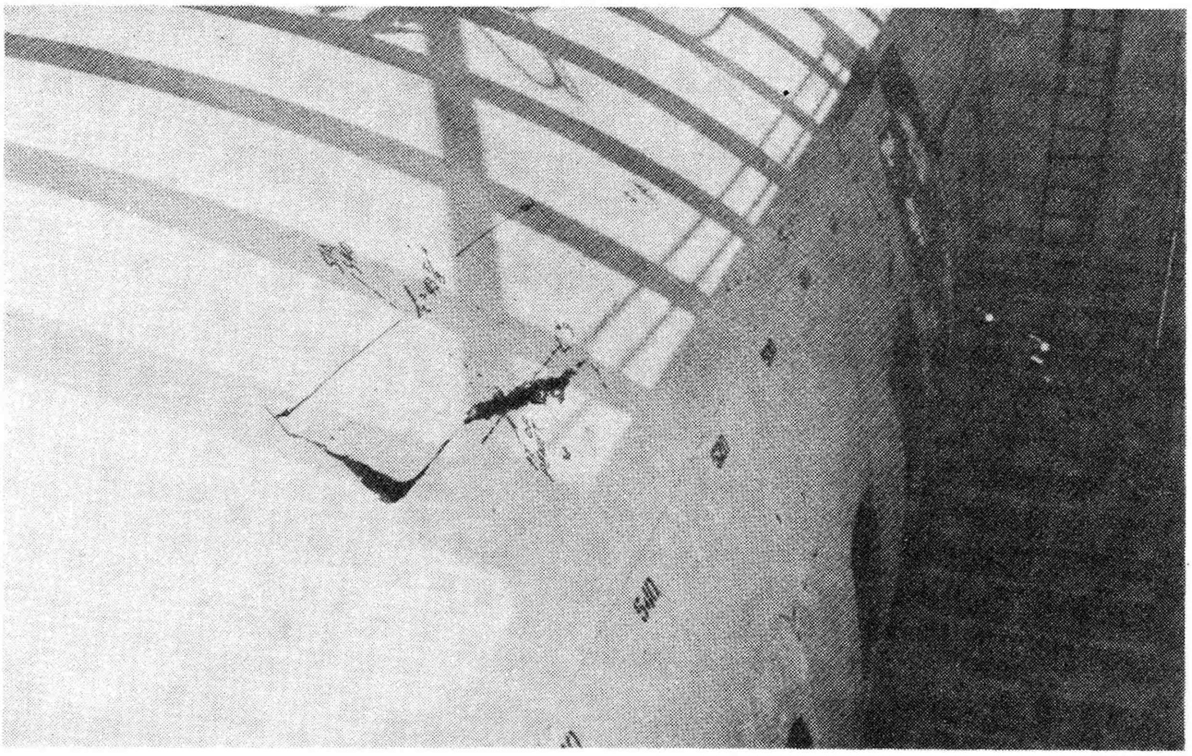

FIGURE 26. TWO-BAY SKIN CRACK SHOWING FLAPPING (EXTERNAL VIEW)

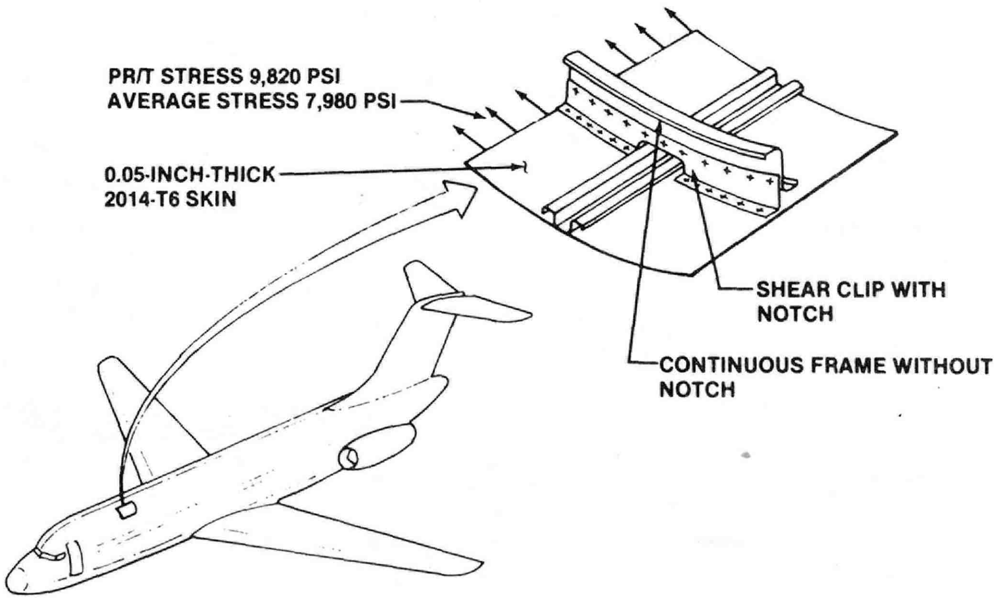


FIGURE 27. MINIMUM-GAUGE CONSTRUCTION FOR DC-9 FUSELAGE

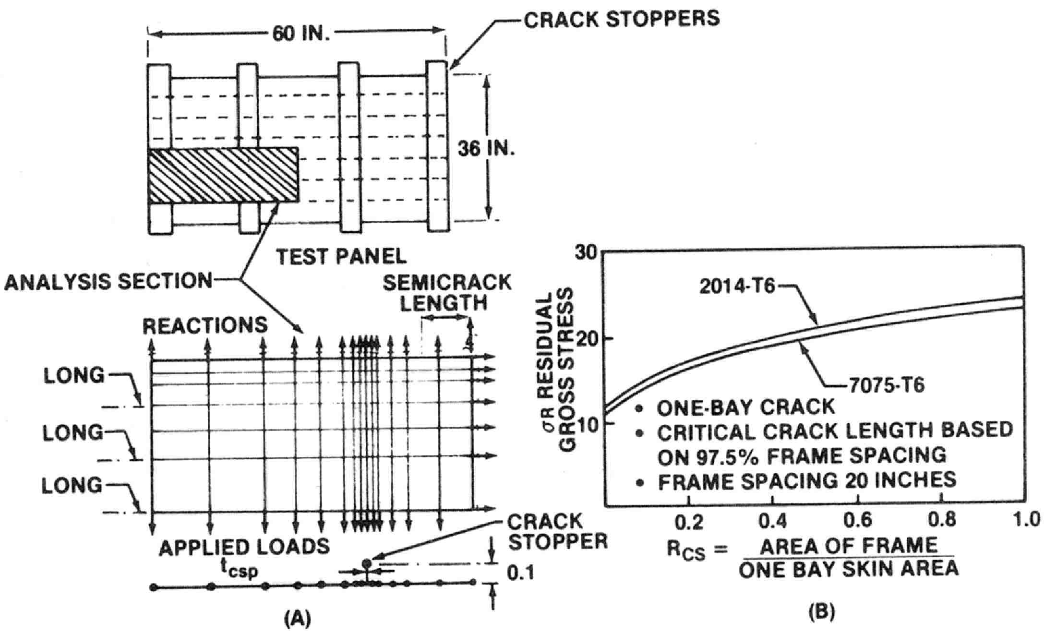


**FIGURE 28. TYPICAL IDEALIZATION AND RESIDUAL STRENGTH CURVE FROM LUMPED-PARAMETER FINITE-ELEMENT ANALYSIS**

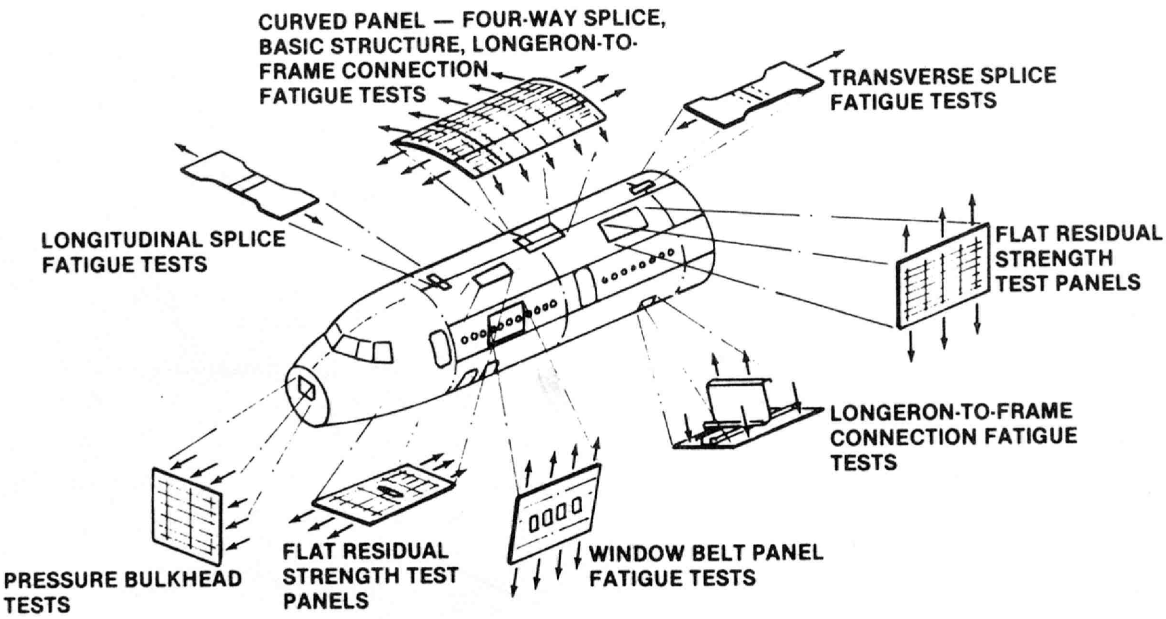


**FIGURE 29. EARLY DC-10 FUSELAGE FATIGUE DEVELOPMENT TESTS**

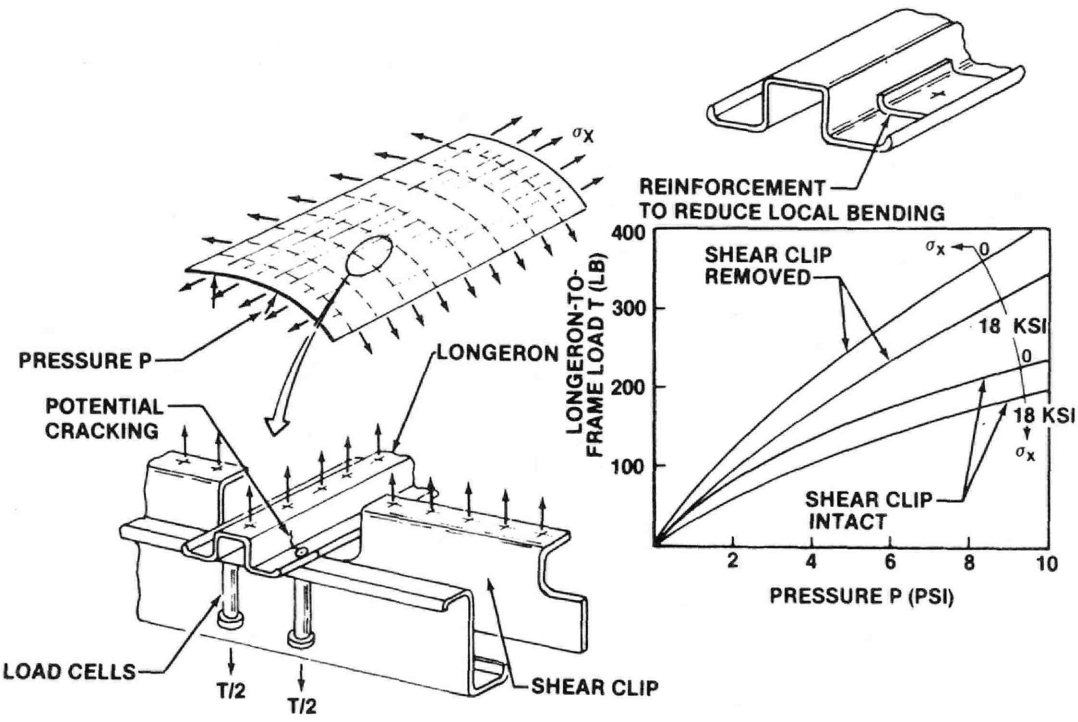


**FIGURE 30. FRAME-TO-LONGERON CONNECTION LOAD**

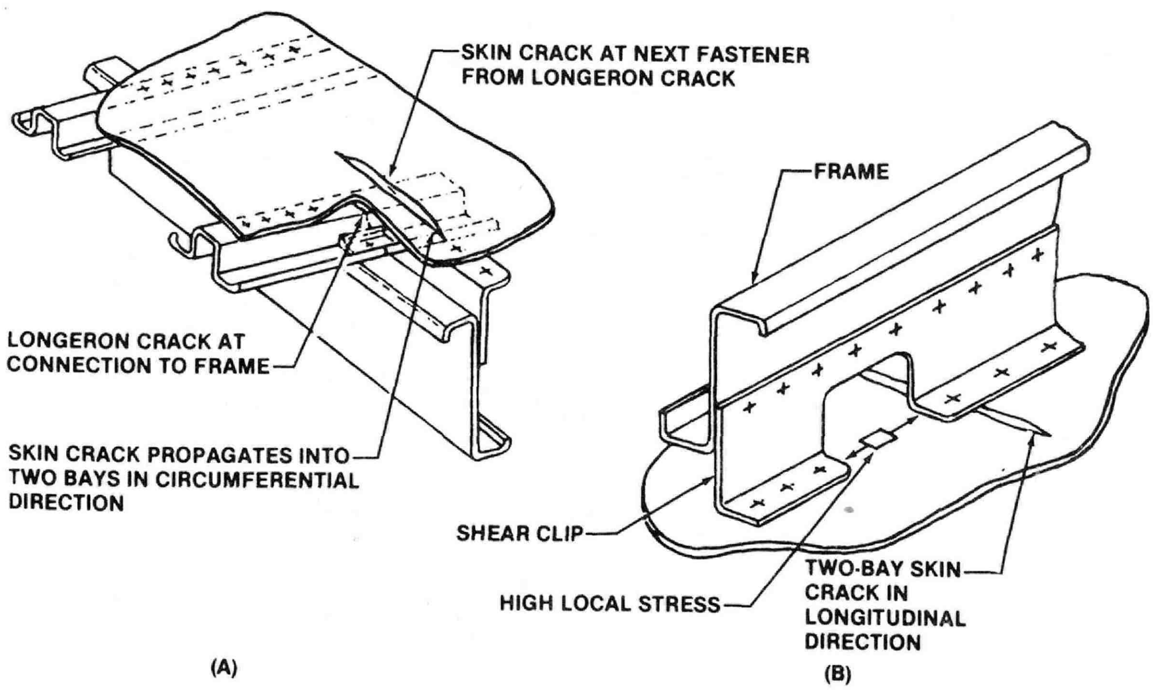


**FIGURE 31. POSSIBLE SKIN FATIGUE CRACKING SCENARIOS IN CIRCUMFERENTIAL AND LONGITUDINAL DIRECTIONS**

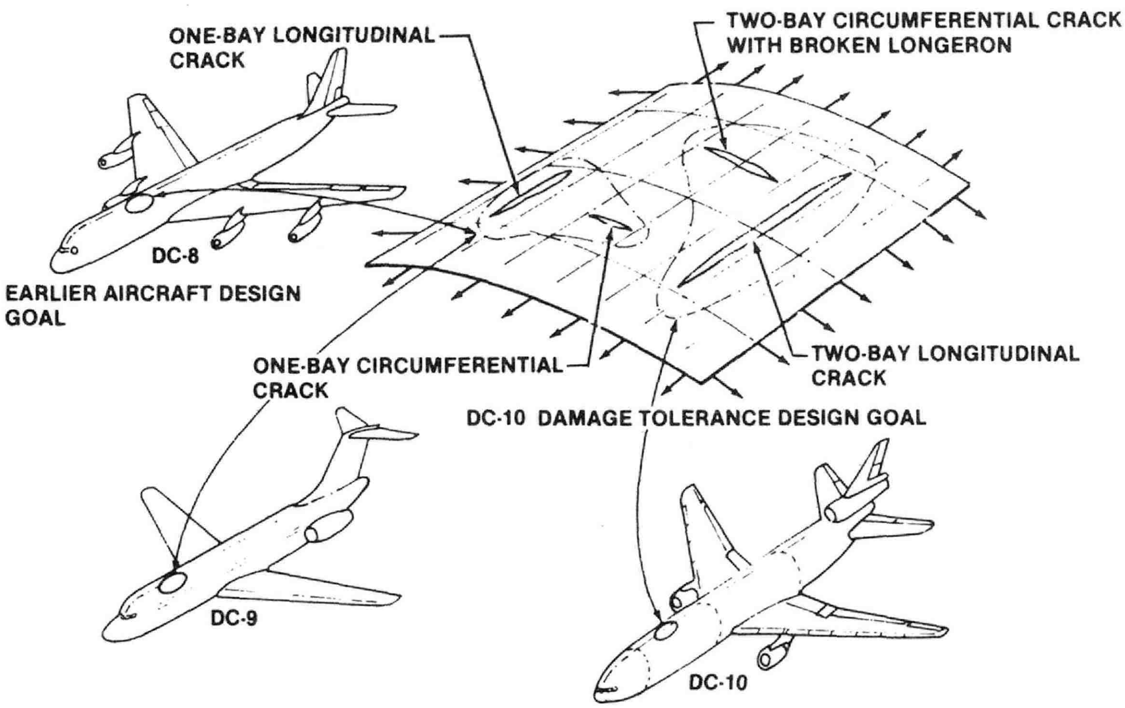


**FIGURE 32. DAMAGE TOLERANCE DESIGN GOALS FOR FUSELAGE SKIN**

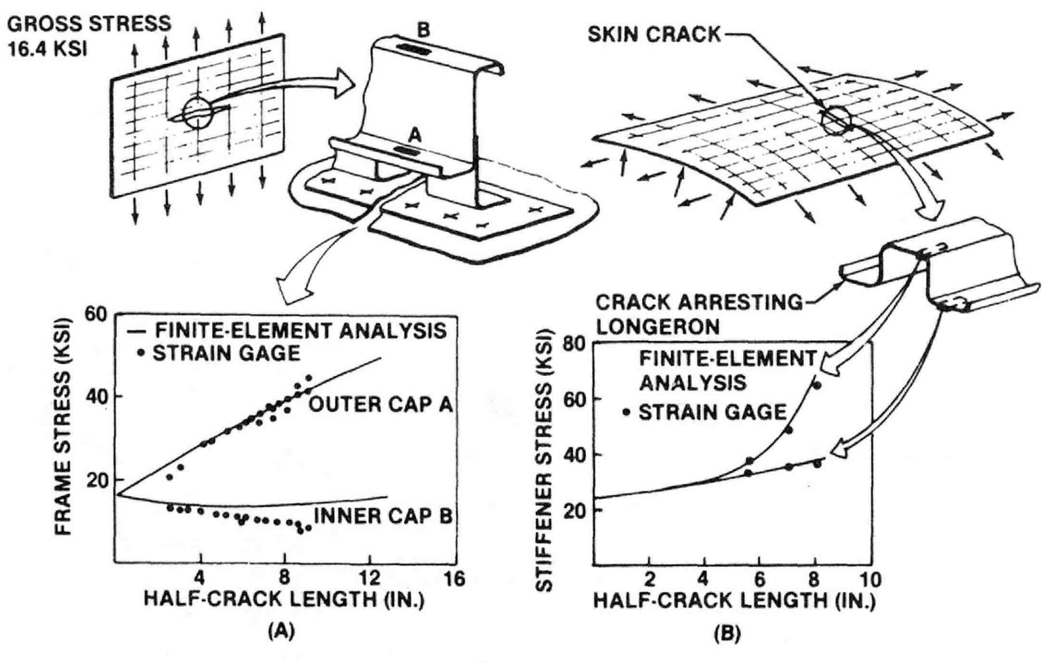


**FIGURE 33. STIFFENER ELEMENT BENDING IN THE PRESENCE OF LONGITUDINAL AND CIRCUMFERENTIAL SKIN CRACKING**

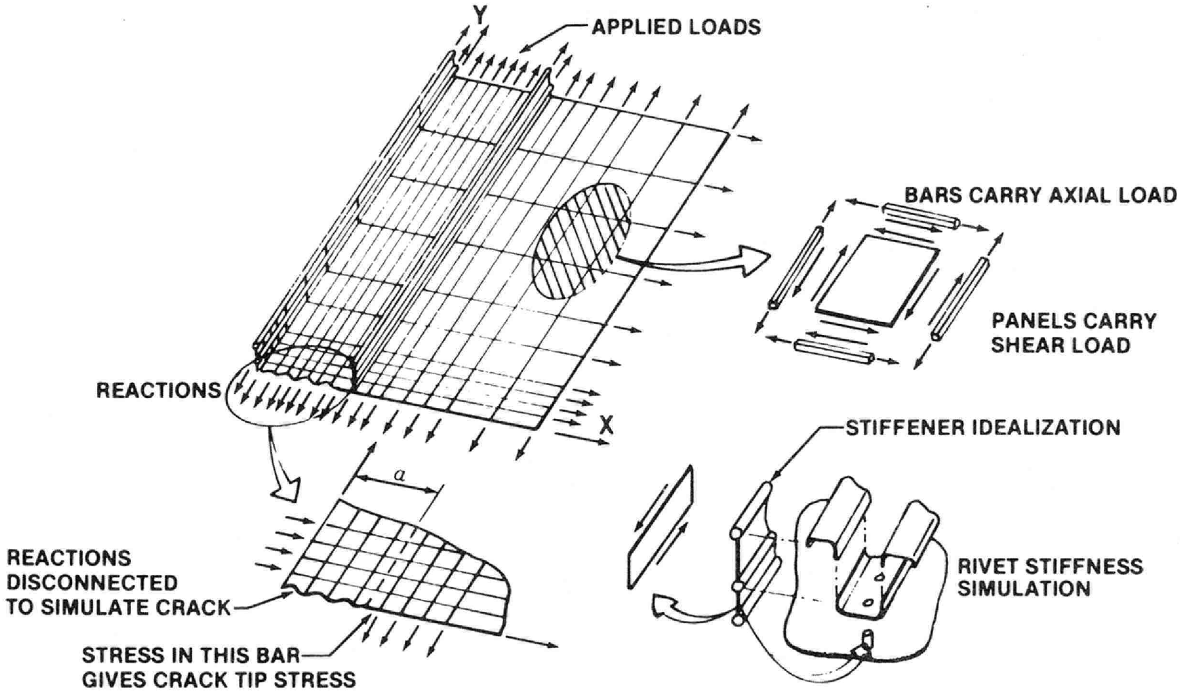


**FIGURE 34. PANEL IDEALIZATION FOR FINITE-ELEMENT ANALYSIS OF CRACKED PANEL FOR CIRCUMFERENTIAL CRACK**

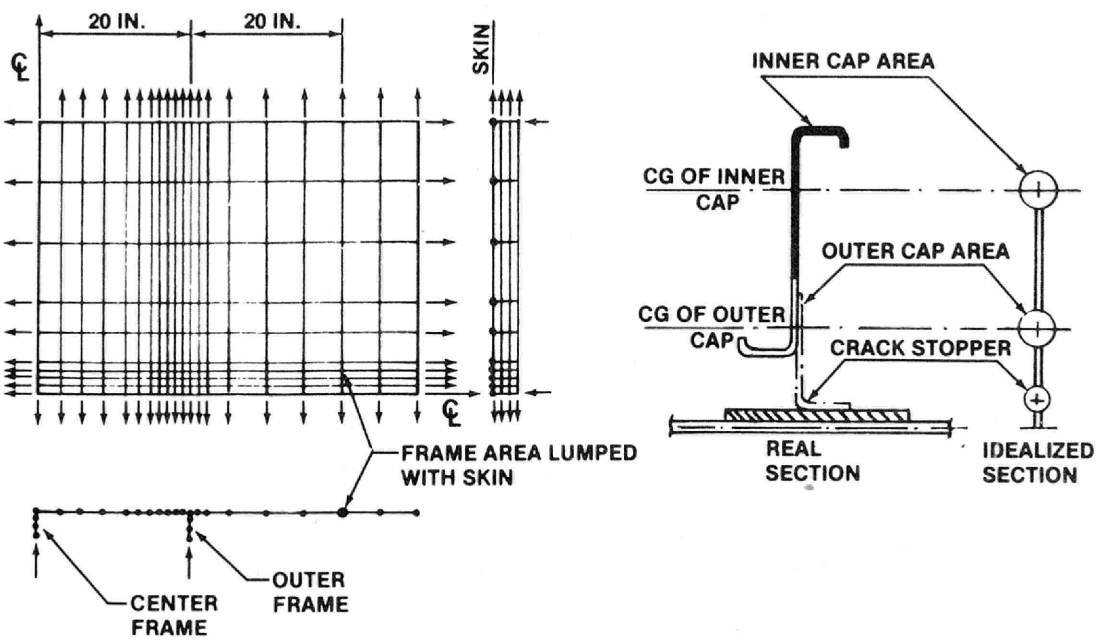


**FIGURE 35. PANEL IDEALIZATION FOR FINITE-ELEMENT ANALYSIS OF CRACKED PANEL FOR LONGITUDINAL CRACK**

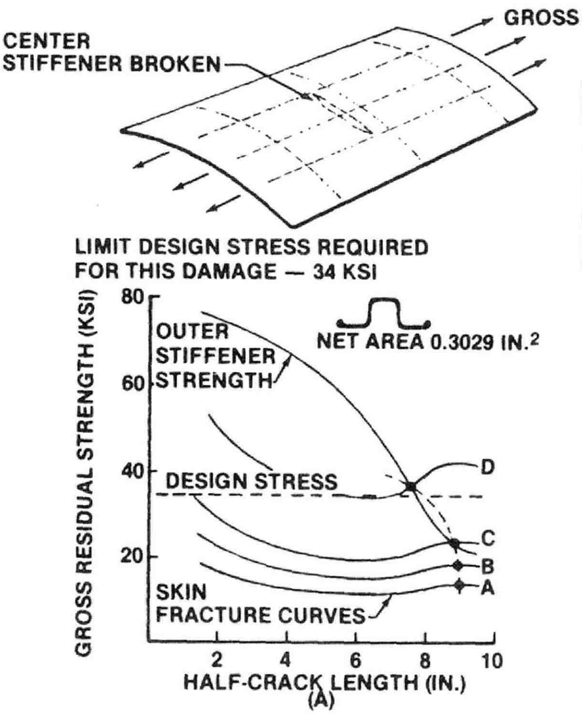


STIFFENER SPACING 8 INCHES

| MATERIAL | CALCULATED ALLOWABLE (KSI) | |
|---|---|---|
| | SMALL HAT | LARGE HAT |
| 7075-T6 | 13.60 | 14.72 |
| 2014-T6 | 18.40 | 19.52 |
| 7075-T73 | 23.52 | 25.28 |
| 2024-T3 | 36.48 | 38.72 |

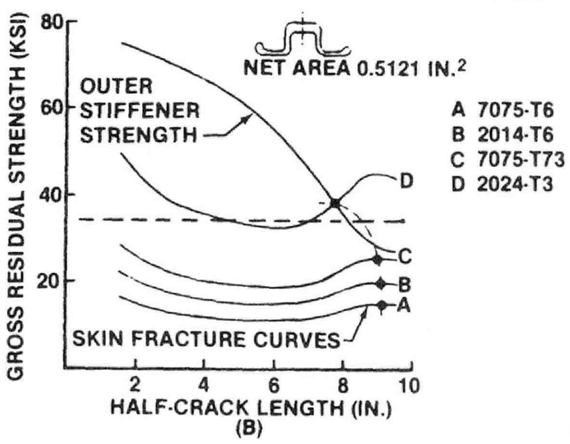


**FIGURE 36. RESULTS OF FINITE-ELEMENT ANALYSIS FOR CANDIDATE SKIN MATERIALS — TWO-BAY CRACK WITH BROKEN LONGERON**

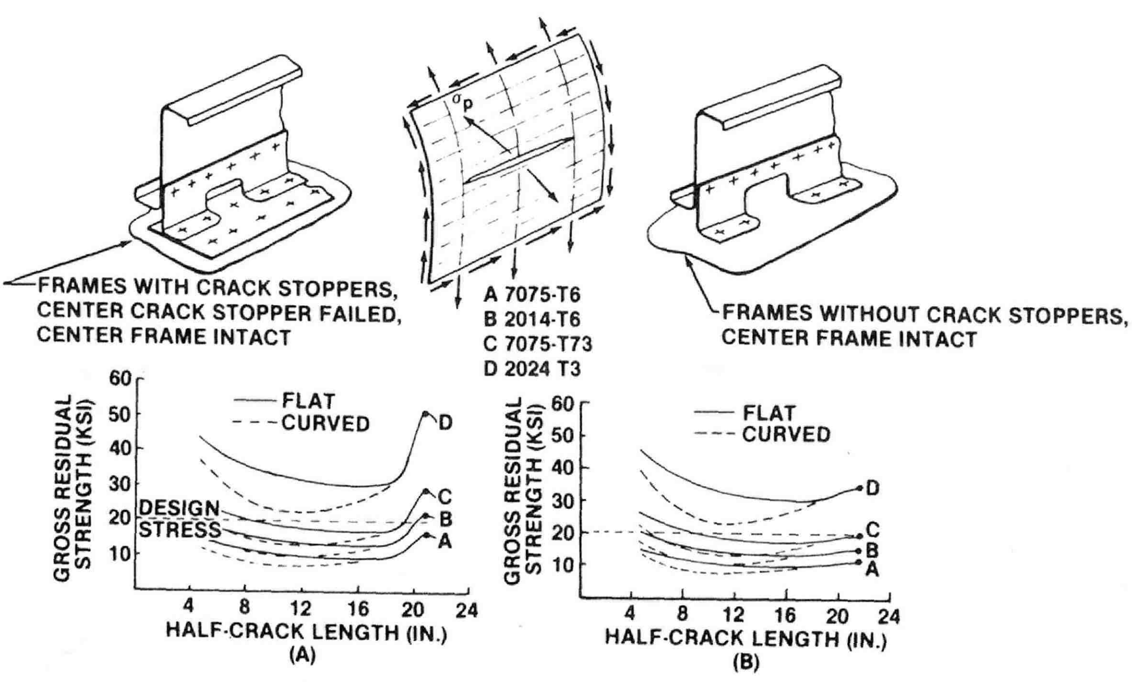


**FIGURE 37. FINITE-ELEMENT RESULTS — LONGITUDINAL CRACK CASE**

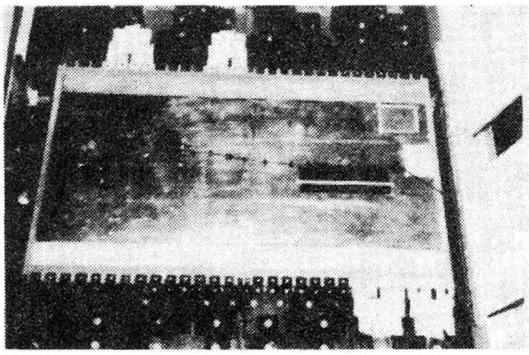

(A) FLAT PANELS — LONGITUDINAL CRACK

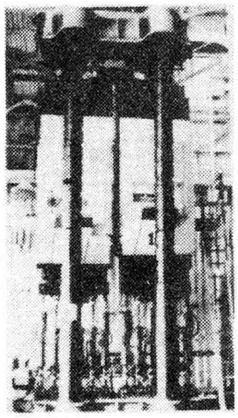

(B) FLAT PANELS — CIRCUMFERENTIAL CRACK

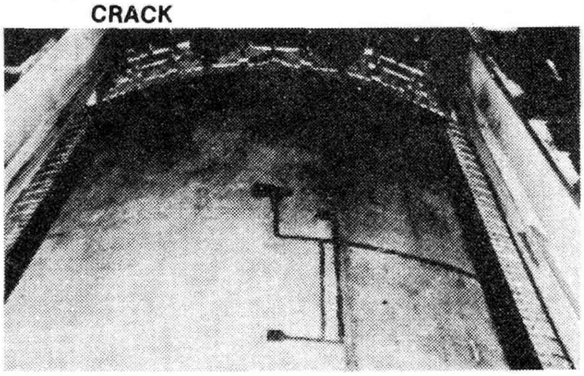

(C) CURVED PANELS

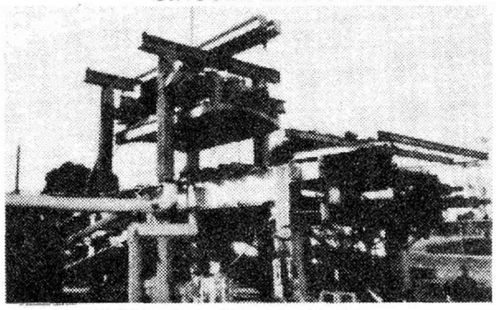

(D) VACUUM TEST MACHINE — CURVED PANELS

**FIGURE 38. DEVELOPMENT TEST PANELS FOR LARGE DAMAGE SIMULATION**

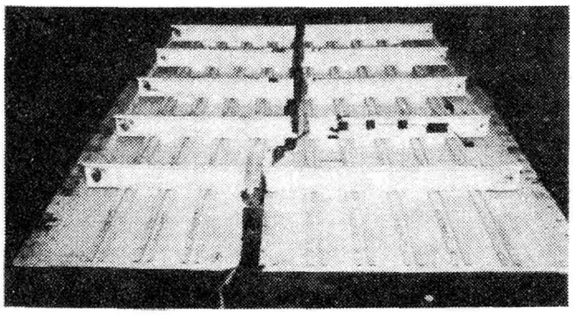

(A) FLAT PANEL SIMULATING LONGITUDINAL DAMAGE

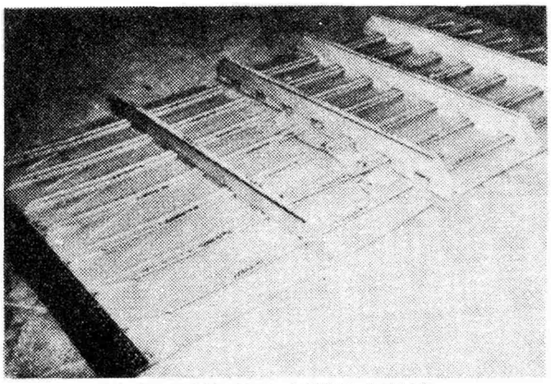

(B) FLAT PANEL SIMULATING CIRCUMFERENTIAL DAMAGE

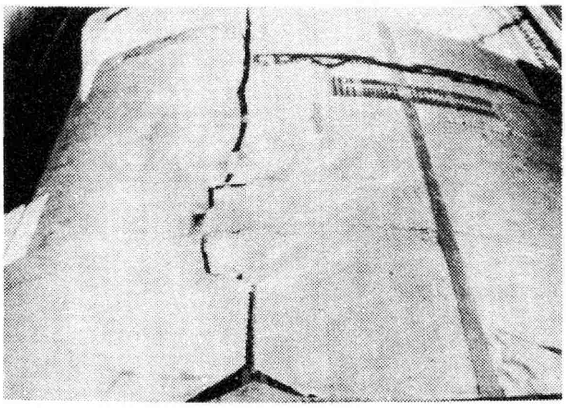

(C) CURVED PANEL AFTER FAILURE FROM LONGITUDINAL DAMAGE

**FIGURE 39. TYPICAL EXAMPLES OF PANELS CONTAINING LARGE DAMAGE LOADED TO FAILURE**

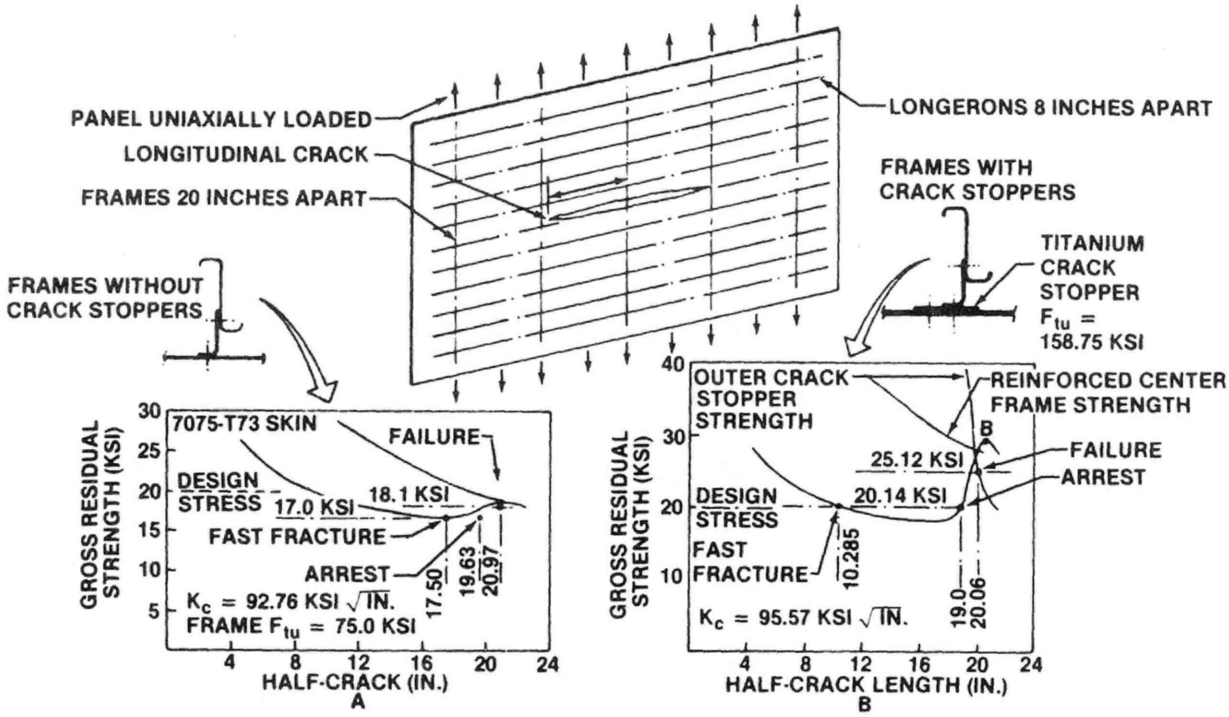


**FIGURE 40. FLAT PANEL RESIDUAL STRENGTH TEST RESULTS FOR LONGITUDINAL CRACK CASE**

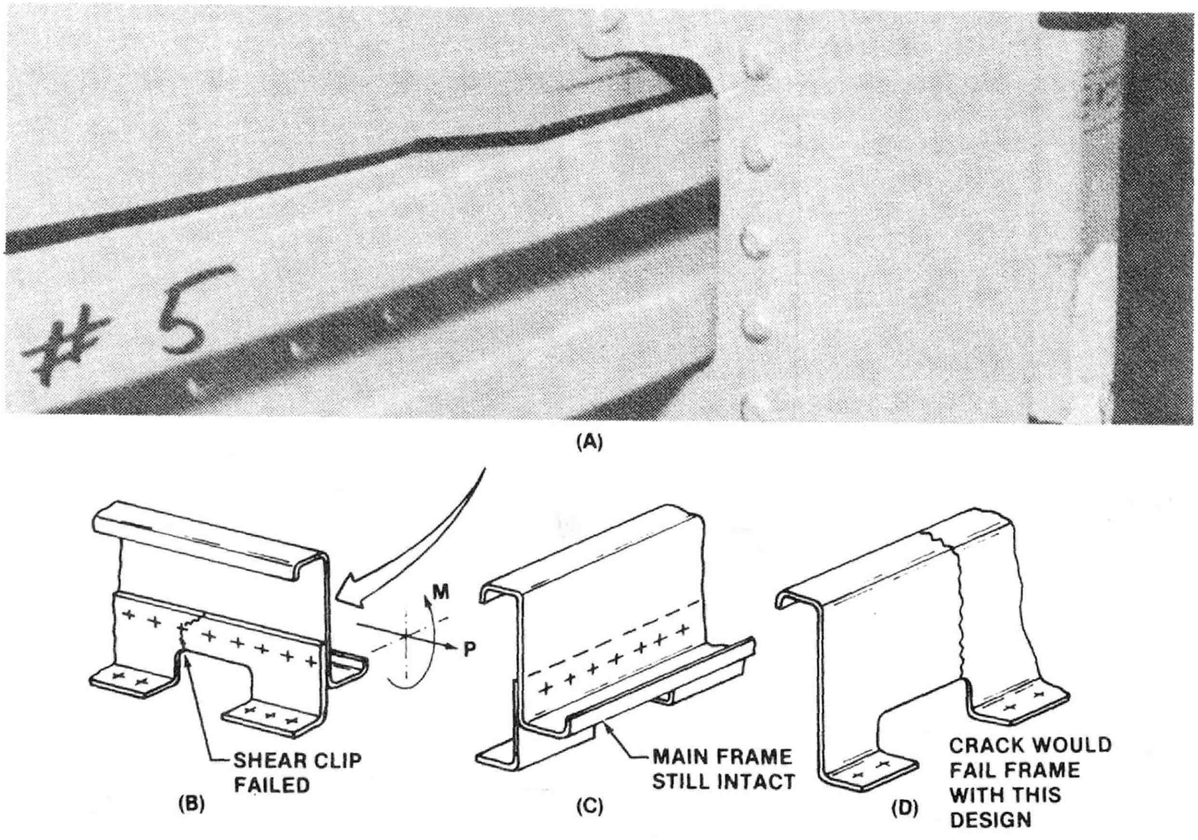


**FIGURE 41. FLAT PANEL AFTER ARREST OF TWO-BAY LONGITUDINAL CRACK**

| TEST NO. | DESCRIPTION OF DAMAGE STIFFENING ELEMENTS FAILED | SKIN CRACK LENGTH (IN.) | PRESSURE (PSI) | PR/t STRESS (KSI) | 0.82PR/t (KSI) |
|---|---|---|---|---|---|
| 1 | CENTER CRACK STOPPER | 17.22 | 14.34 | 23.934 | 19.626 |
| 2 | CENTER CRACK STOPPER | 19.10 | 14.44 | 24.101 | 19.762 |
| 3 | CENTER CRACK STOPPER | 25.28 | 14.49 | 24.184 | 19.831 |
| 4 | CENTER CRACK STOPPER PLUS CENTER FRAME | 34.98 | 14.59 | 24.351 | 19.968 |
| 5 | CENTER CRACK STOPPER, CENTER FRAME AND BOTH OUTER CRACK STOPPERS | 45.56 | 13.13 | 21.914 | 17.970 |

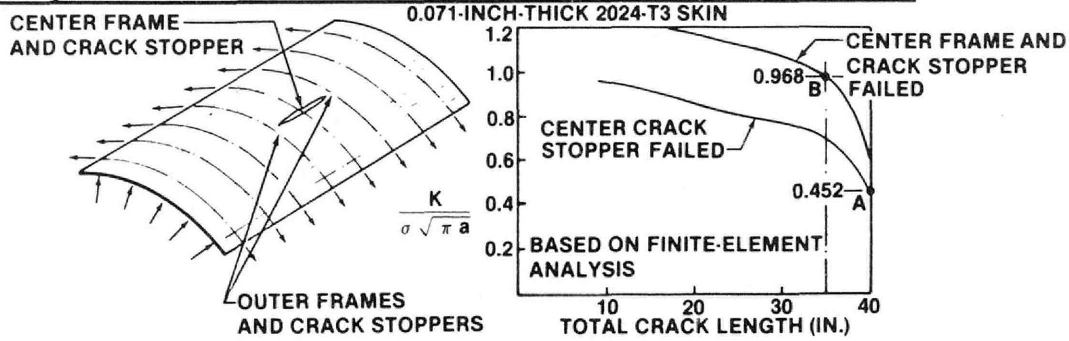


**FIGURE 42. RESULTS OF TESTS ON CURVED PANEL (TESTS 1-4 NOT LOADED TO FAILURE, TEST 5 LOADED TO FAILURE)**

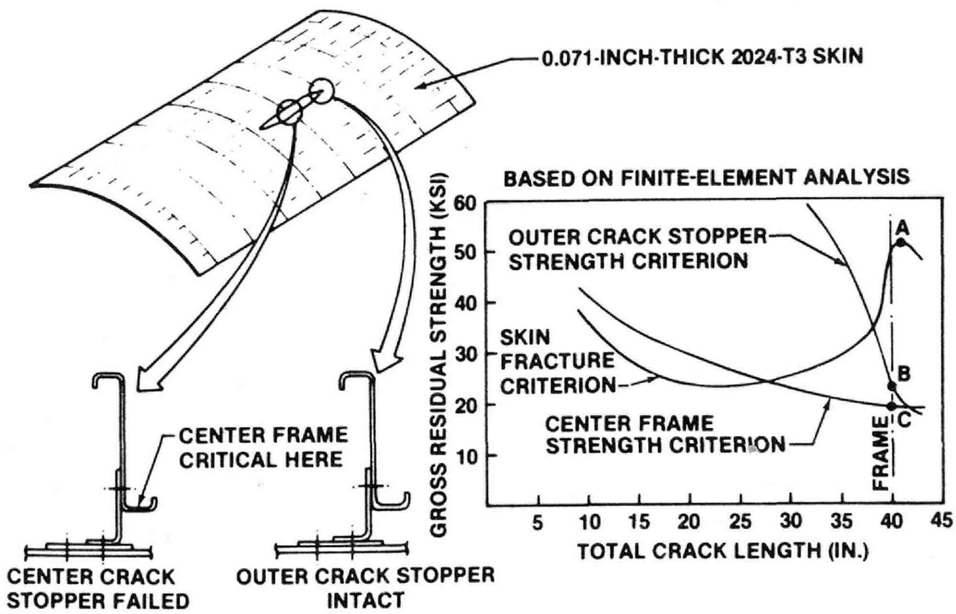


**FIGURE 43. RESIDUAL STRENGTH FOR LONGITUDINAL CRACK IS LIMITED BY STIFFENER STRENGTH**

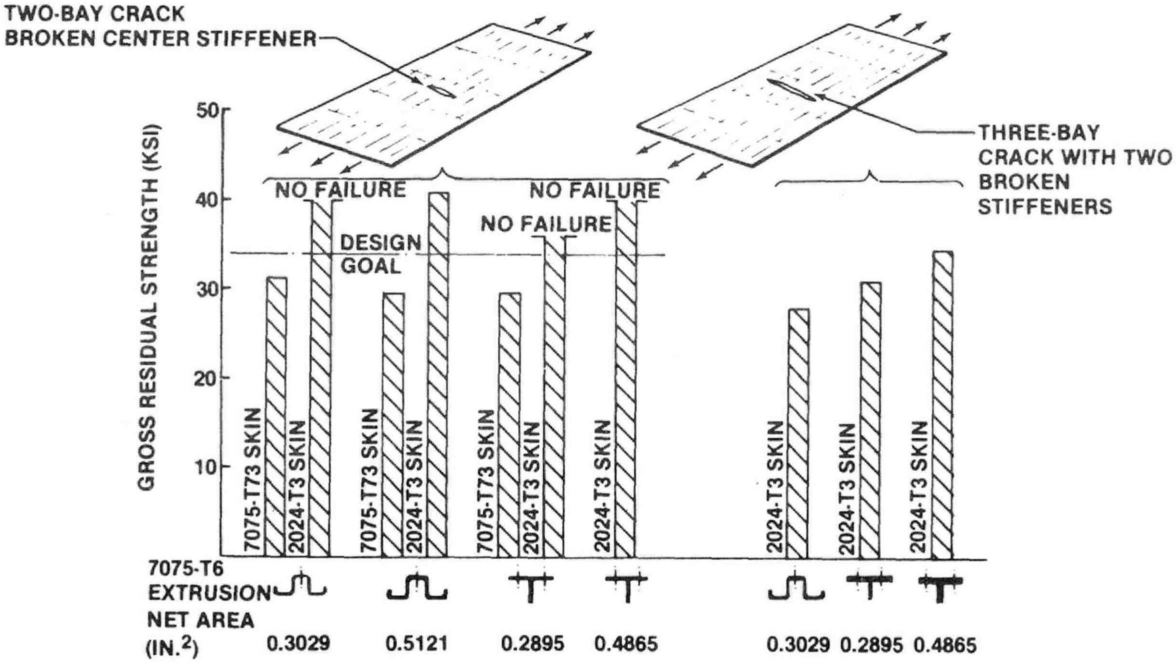


**FIGURE 44. TEST RESULTS FOR TWO-BAY CIRCUMFERENTIAL CRACK WITH BROKEN CENTRAL LONGERON**

| ANALYSIS | POINT | CRITERION | GROSS STRESS (KSI) |
|---|---|---|---|
| ELASTIC | A | SKIN FRACTURE | 53.60 |
| | B | STIFFENER STRENGTH | 32.50 |
| | C | FIRST RIVET FAILURE | 11.50 |
| PLASTIC | A' | SKIN FRACTURE | 41.25 |
| | B' | STIFFENER STRENGTH | 44.90 |
| | C' | FIRST RIVET FAILURE | 39.50 |

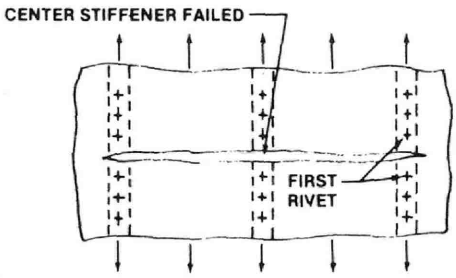


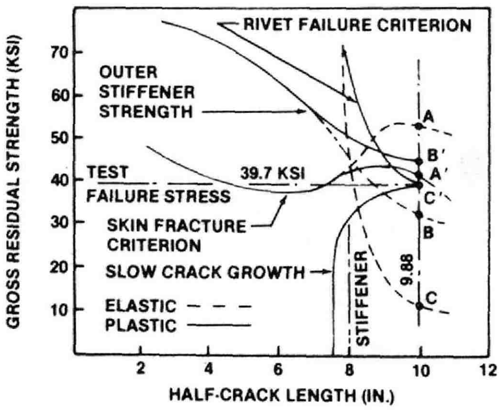


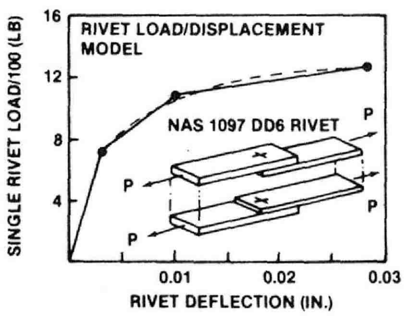


**FIGURE 45. ELASTIC-PLASTIC ANALYSIS RESULTS FOR TEST OF TWO-BAY CIRCUMFERENTIAL CRACK WITH BROKEN CENTRAL LONGERON**

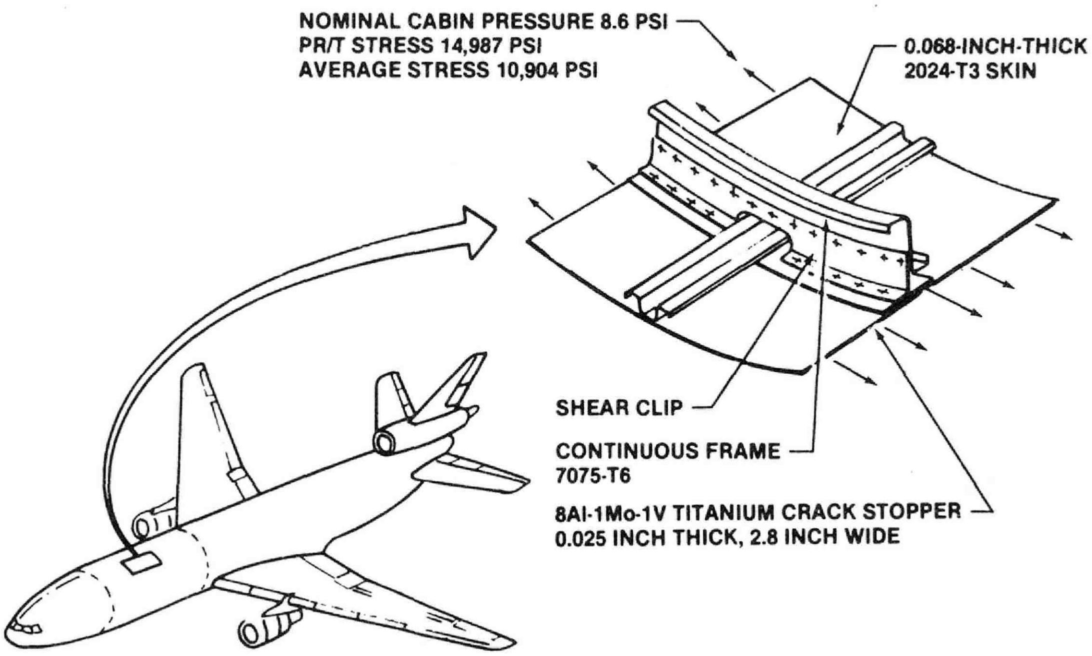


**FIGURE 46. MINIMUM-GAUGE CONSTRUCTION FOR DC-10 FUSELAGE**

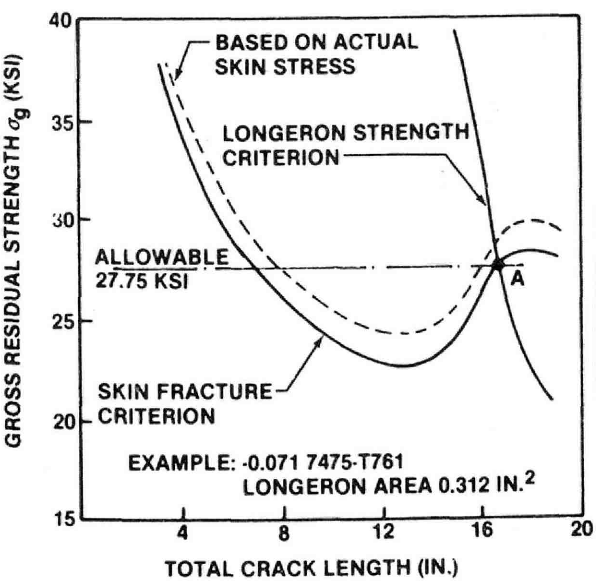


- ALLOWABLE GROSS STRENGTH
- TWO-BAY CIRCUMFERENTIAL SKIN CRACK WITH BROKEN LONGERON
- OPERATIONAL TEMPERATURE −65°F

| LONG. AREA (IN.$^2$) | SKIN THICKNESS (IN.) | ALLOWABLE GROSS STRESS (KSI) | |
|---|---|---|---|
| | | 7475-T761 | 7475-T61 |
| 0.214 | 0.063 | 26.00 | 22.80 |
| 0.214 | 0.071 | 25.60 | 22.50 |
| 0.312 | 0.071 | 27.75 | 24.00 |
| 0.540 | 0.071 | 29.75 | 25.00 |
| 0.312 | 0.080 | 26.80 | 23.50 |

**FIGURE 47. ANALYSIS RESULTS FOR CANDIDATE SKIN MATERIALS 7475-T761 AND 7475-T61**

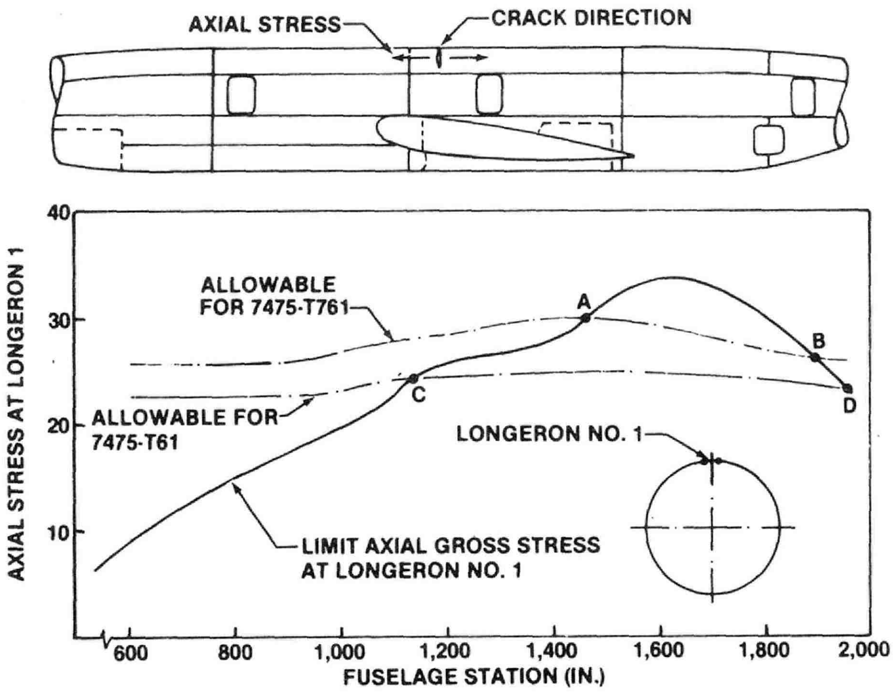


**FIGURE 48. LIMIT AXIAL GROSS STRESS VERSUS ALLOWABLE FOR TWO-BAY CIRCUMFERENTIAL DAMAGE REQUIREMENT**

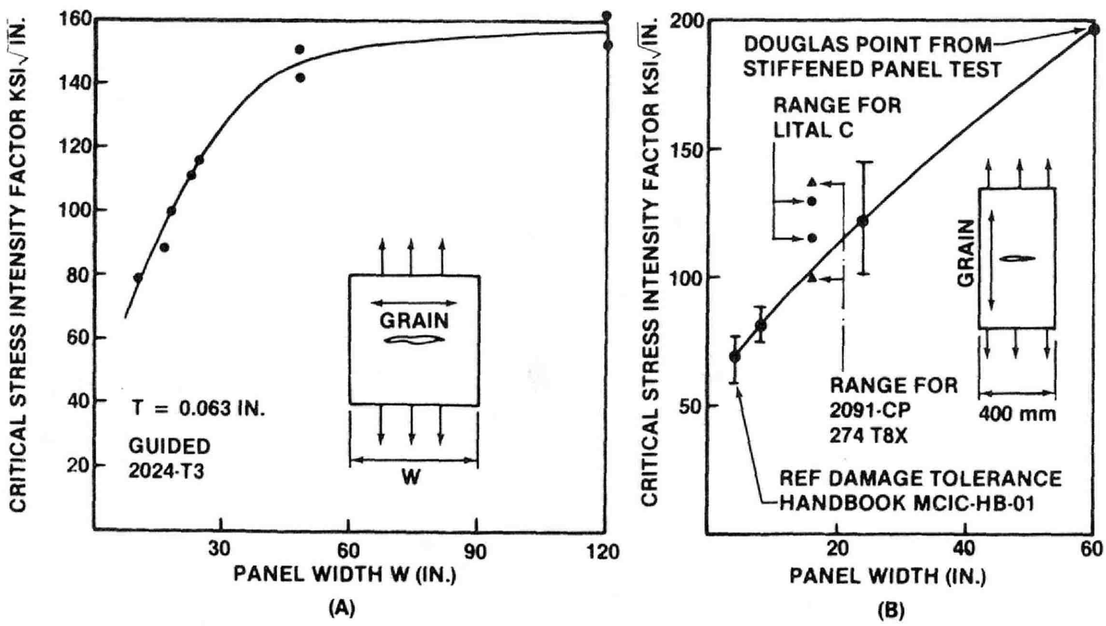


**FIGURE 49. CRITICAL STRESS INTENSITY FACTOR VERSUS PANEL WIDTH FOR 2024-T3 AND ALUMINUM-LITHIUM**

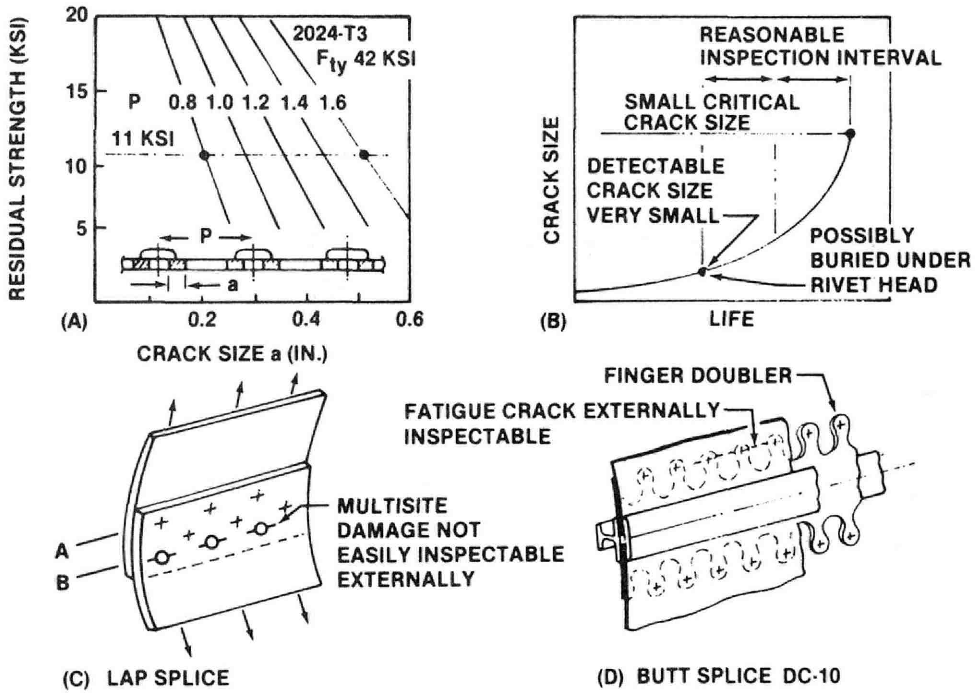


**FIGURE 50. MULTIPLE SITE DAMAGE (MSD)**

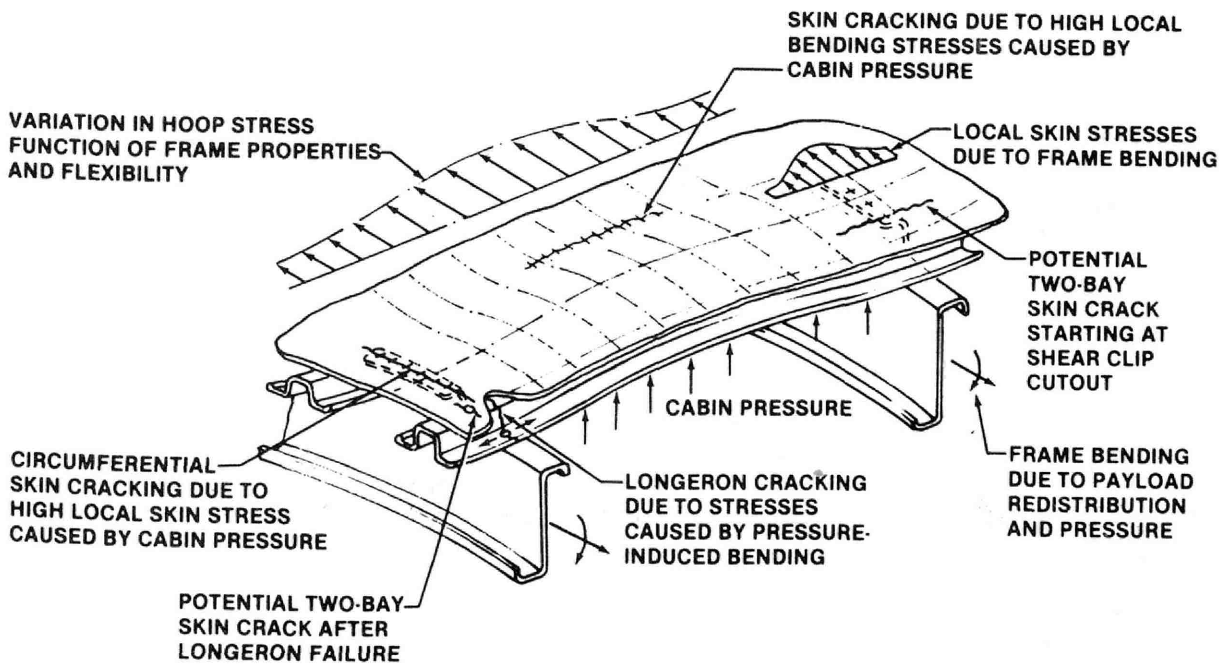


**FIGURE 51. FATIGUE-SENSITIVE AREAS IN FUSELAGE BASIC SHELL STRUCTURE**

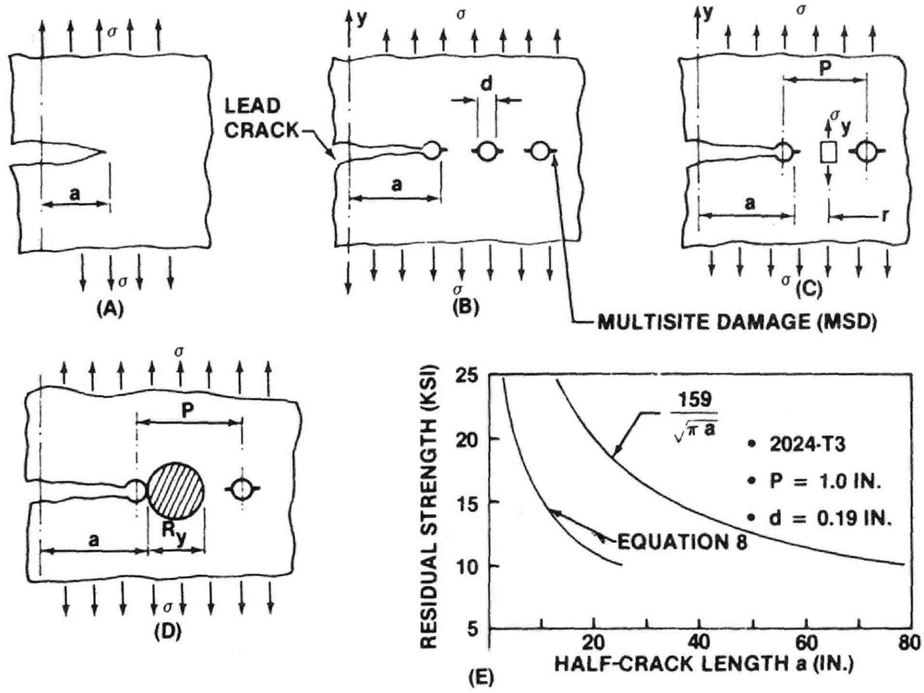


**FIGURE 52. EFFECT OF MULTISITE DAMAGE ON CRITICAL CRACK SIZE**

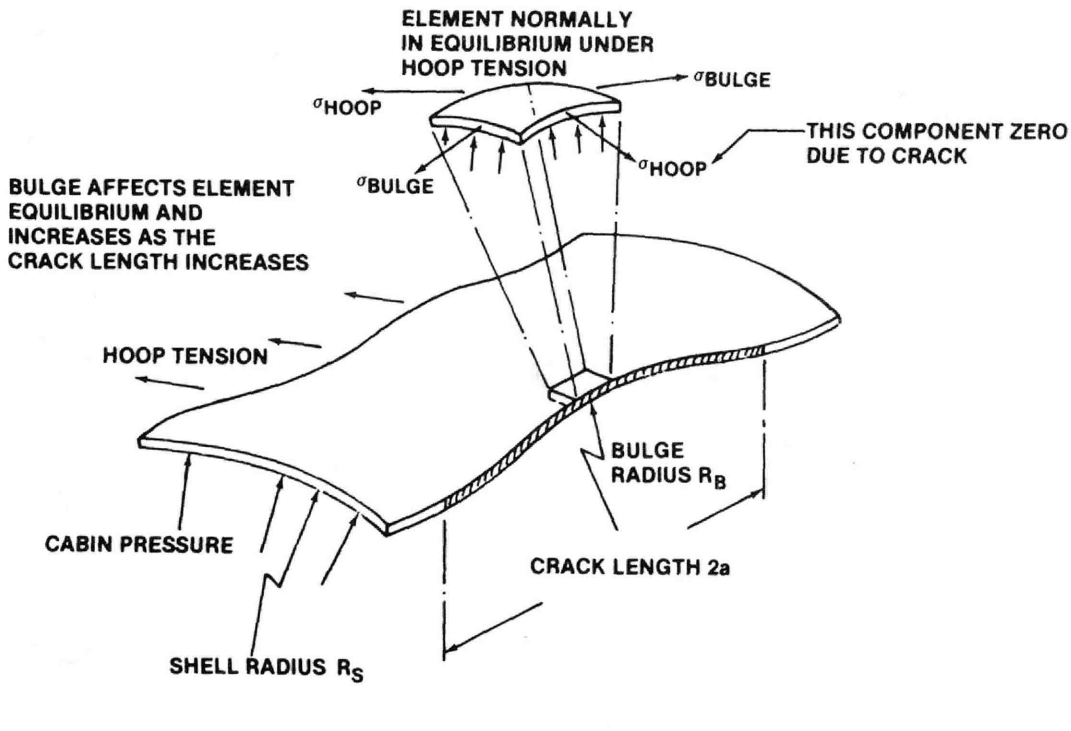


**FIGURE 53. BULGING IN A CRACKED CYLINDRICAL SHELL**

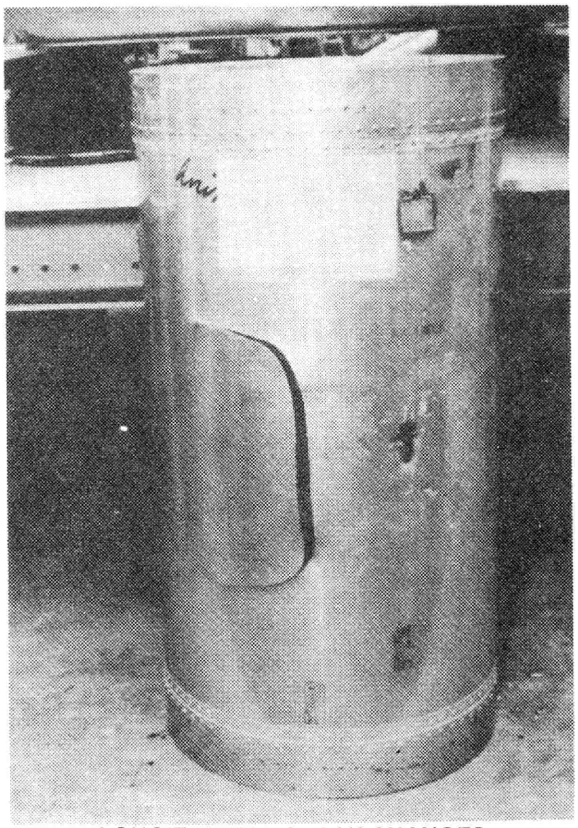

LONGITUDINAL CRACK CHANGES DIRECTION BECAUSE OF BULGING (FLAPPING)

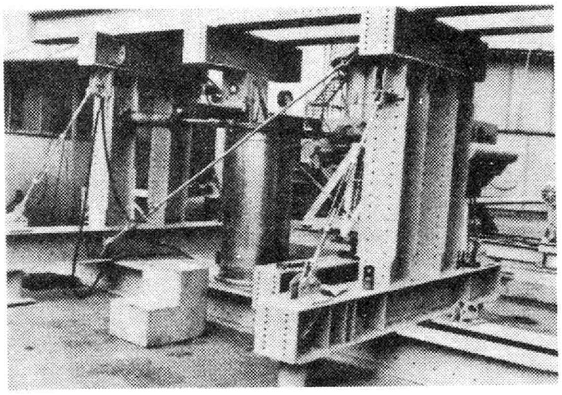

TEST FIXTURE FOR TESTING CRACKED CYLINDERS UNDER COMBINED PRESSURE AND TORQUE

**FIGURE 54. FLAPPING FAILURE IN UNSTIFFENED PRESSURIZED SHELL**

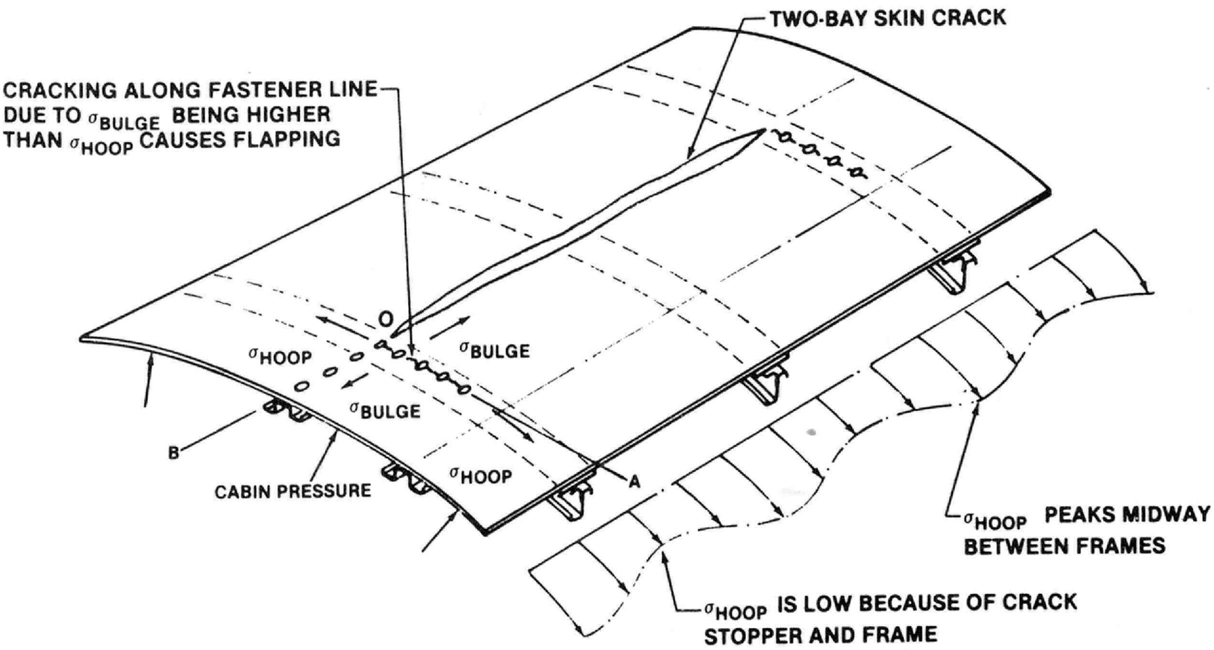


**FIGURE 55. EFFECT OF STIFFENING ON FLAPPING PHENOMENON**

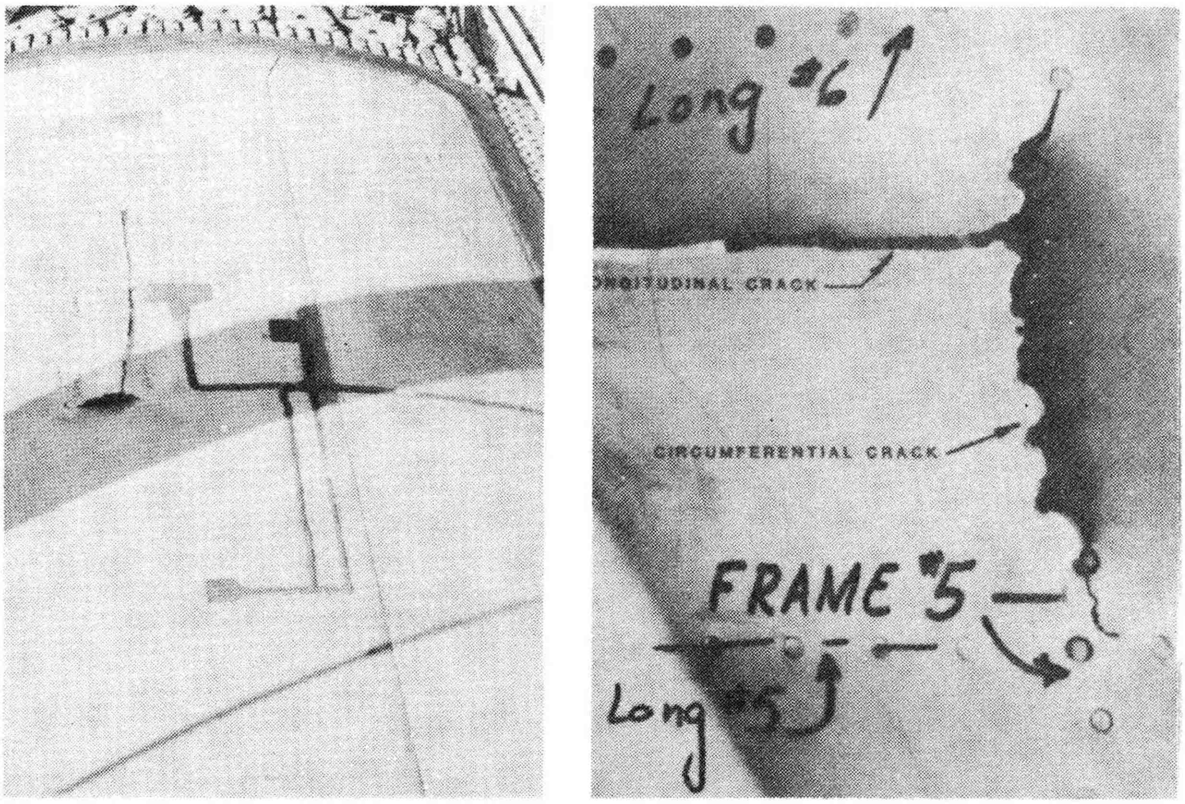


(A) (B)

**FIGURE 56. FLAPPING IN TYPICAL 0.063-INCH-THICK CURVED PANEL**

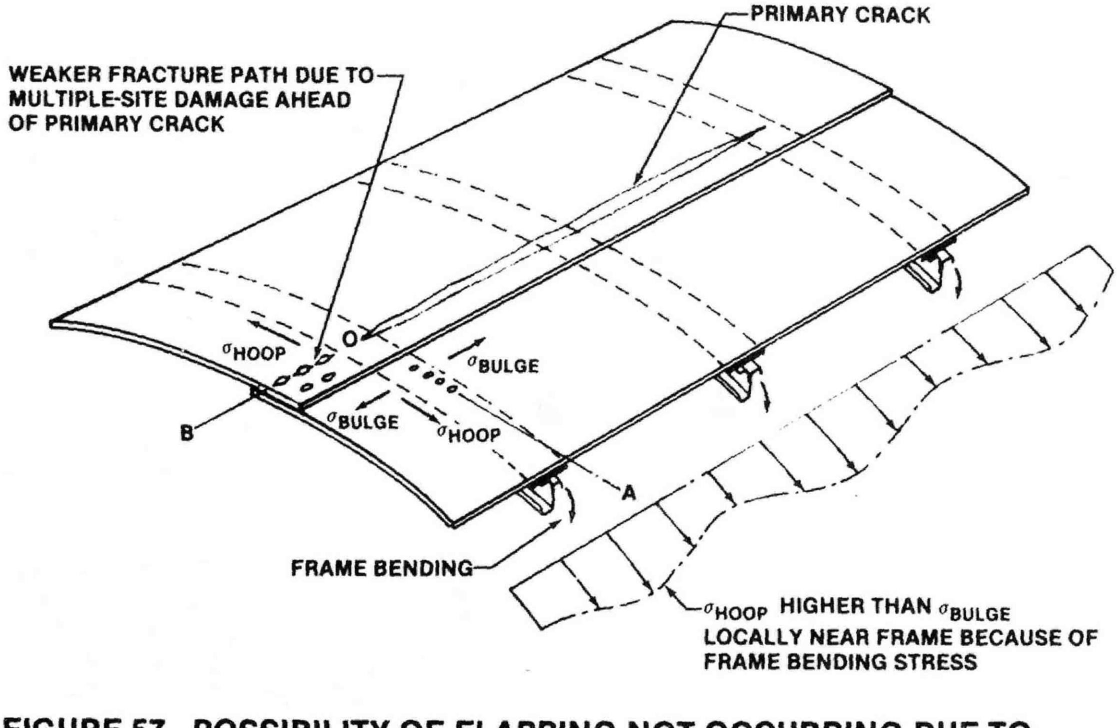


**FIGURE 57. POSSIBILITY OF FLAPPING NOT OCCURRING DUE TO MULTISITE CRACKING AHEAD OF LEAD CRACK AND HIGH STRESS DUE TO FRAME BENDING**

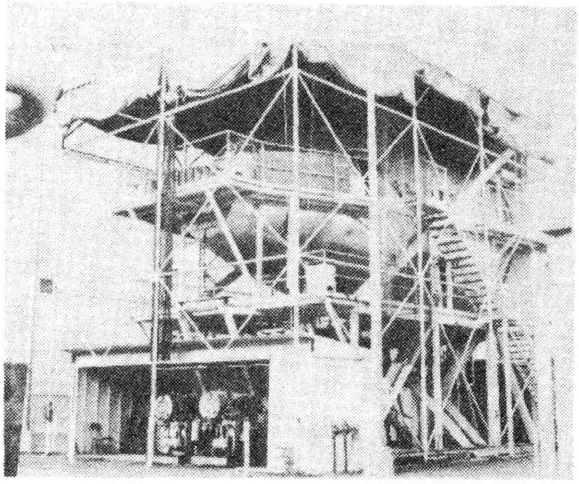

NOSE SECTION

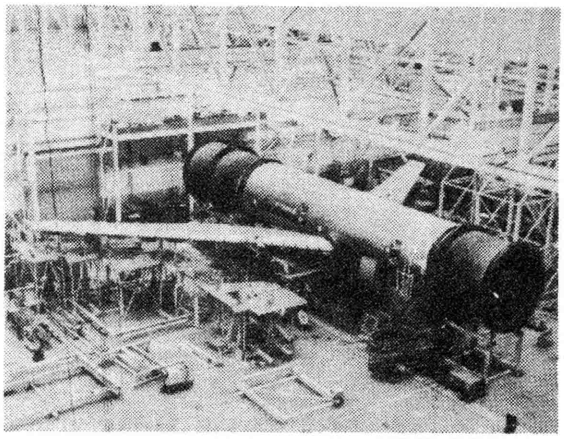

WING AND CENTER SECTION

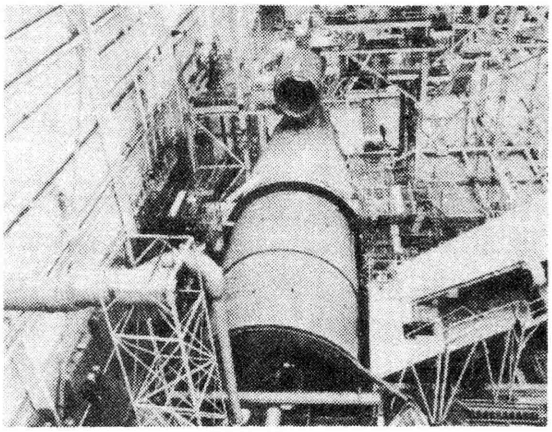

TAIL SECTION

**FIGURE 58. DC-10 FULL-SCALE FATIGUE TEST DURING SETUP**

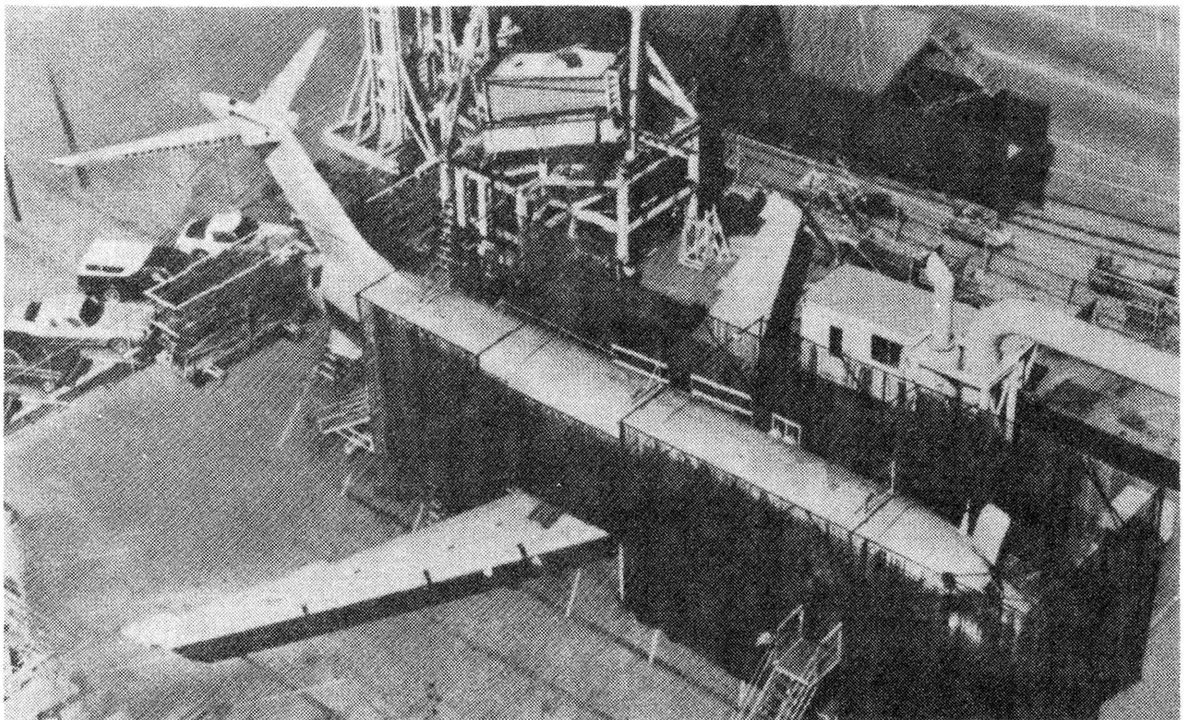

**FIGURE 59. DC-9 SHIP NO. 3 ON TEST PAD FOR CONTINUED FATIGUE TESTING**